Subduction zone dynamics and mantle flow

Thorsten W Becker

University of Southern California

Short course at Universita di Roma TRE

April 18 – 20, 2011

Revised syllabus

- Fundamentals of Earth Structure and Geophysical constraints for Subduction
- Fundamental of Fluid and Mantle Dynamics
- Regional Subduction Zone Modeling
  - From static to dynamic
- Global Mantle Flow Modeling
- Geological Constraints for Subduction
- Trench Migration and Upper Mantle Convection

Subduction I
Earth Structure and geophysical subduction zone constraints

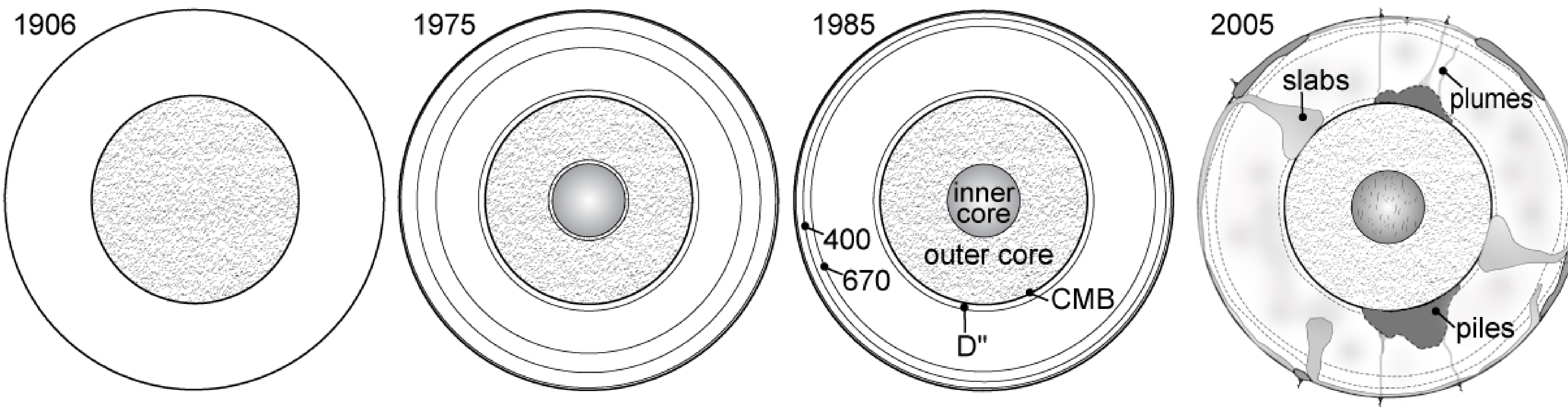

Figure courtesy Ed Garnero

Rocky planets

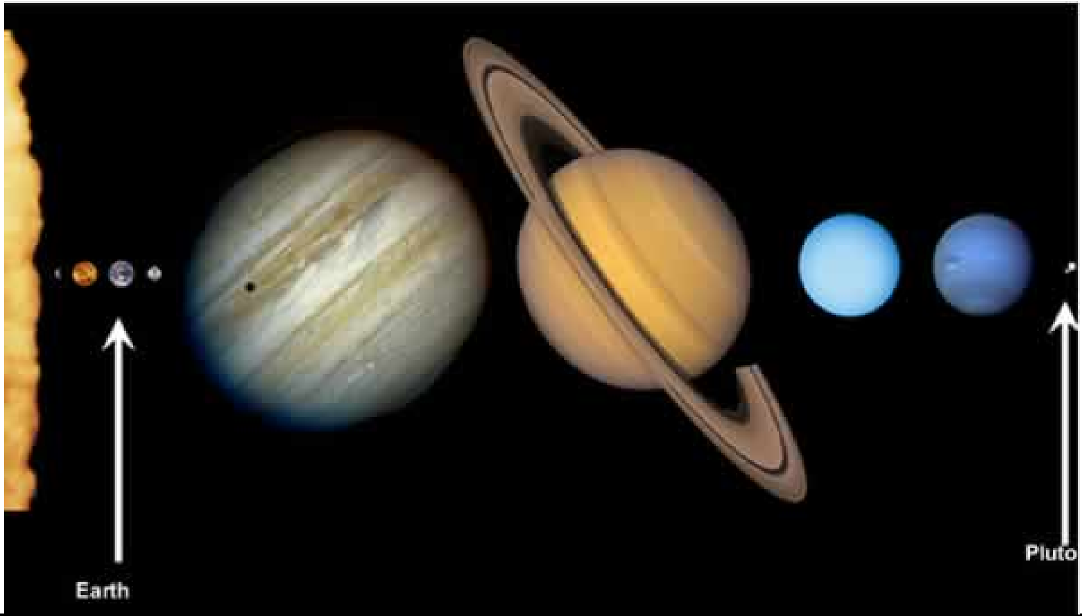

Lithosphere (plate tectonics) =
Top, cold boundary layer

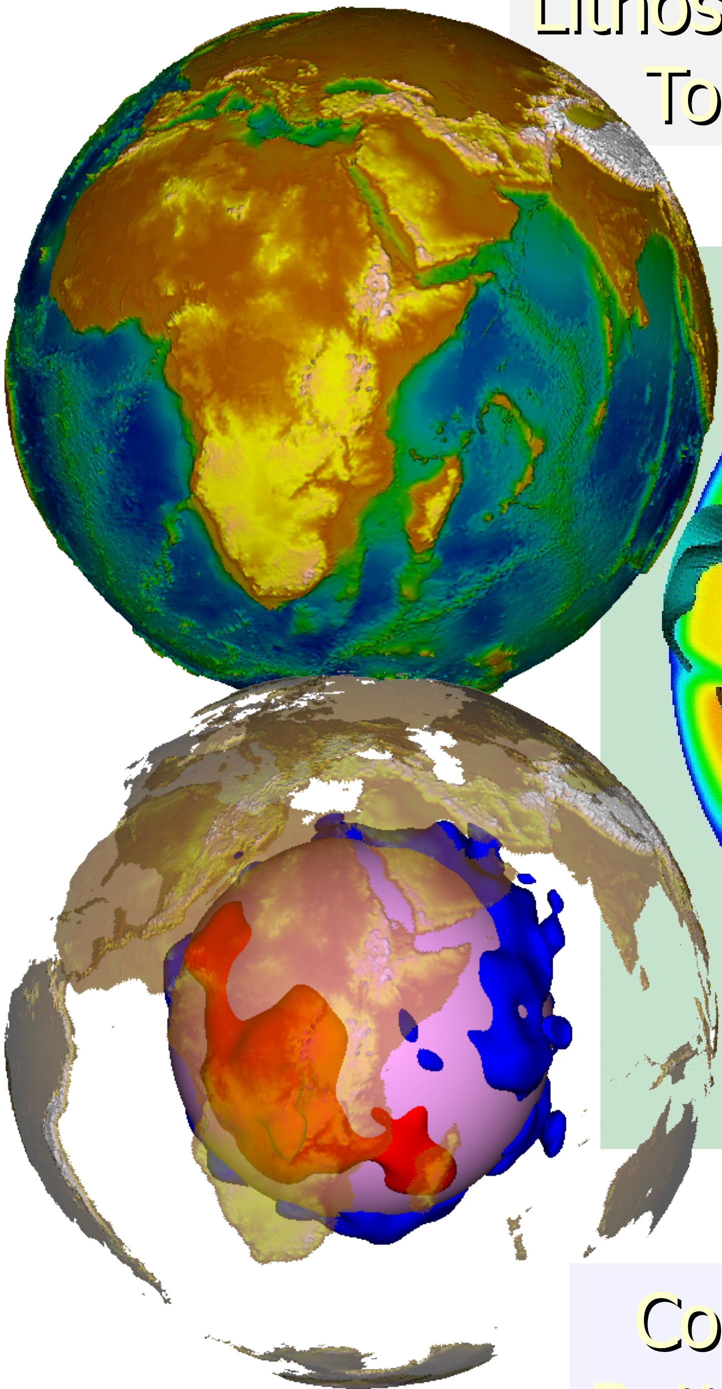

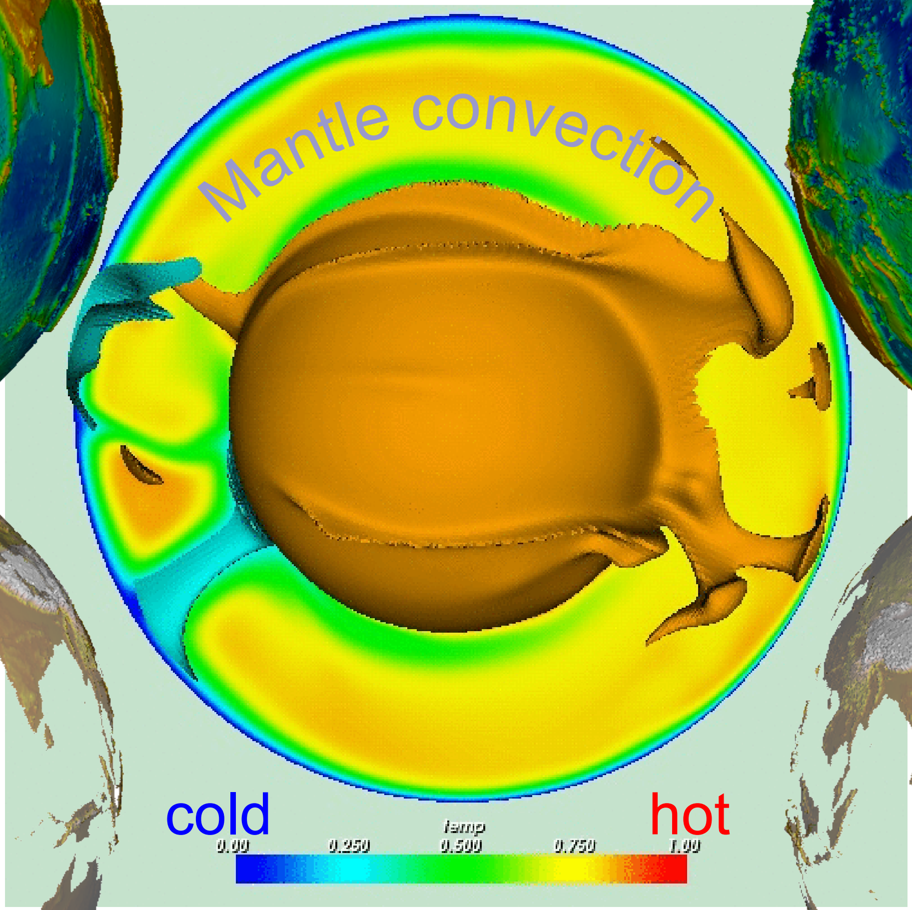

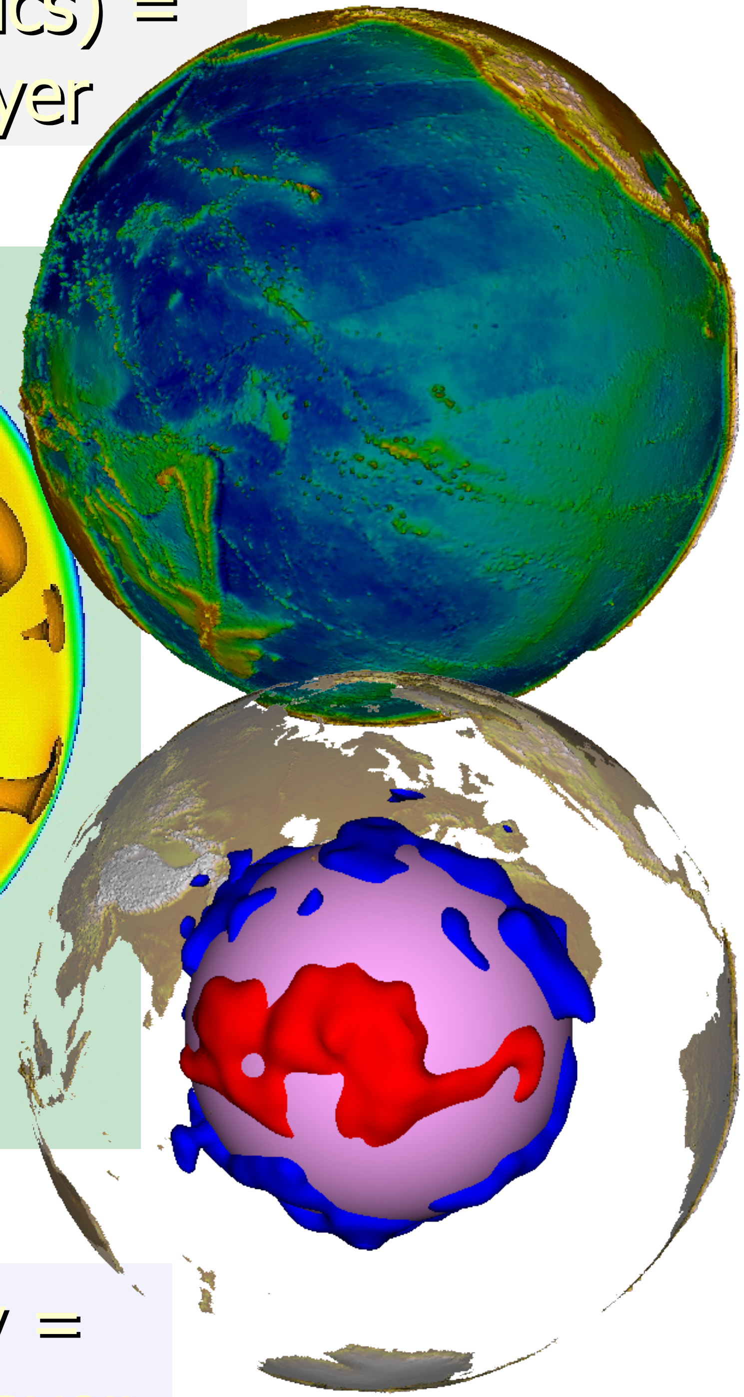

Core-mantle boundary =
Bottom, hot boundary layer

The mantle system

- **Dynamics of mantle largely thermally driven**

  Lithosphere:

  top thermal boundary layer of the mantle

  rheology(*p,T,C*) →

  strong, elastic with yielding (brittle/plastic)

  plate tectonics

  Heat sources

  loss of accretional heat of mantle and core

  radioactive heat production in mantle and core

- **Role of composition?**

  melting → compositional variations (crust)

  affects geochemistry? mantle dynamics?

  solidifying inner core → chemical source of energy

Some issues: 1) Plate generation

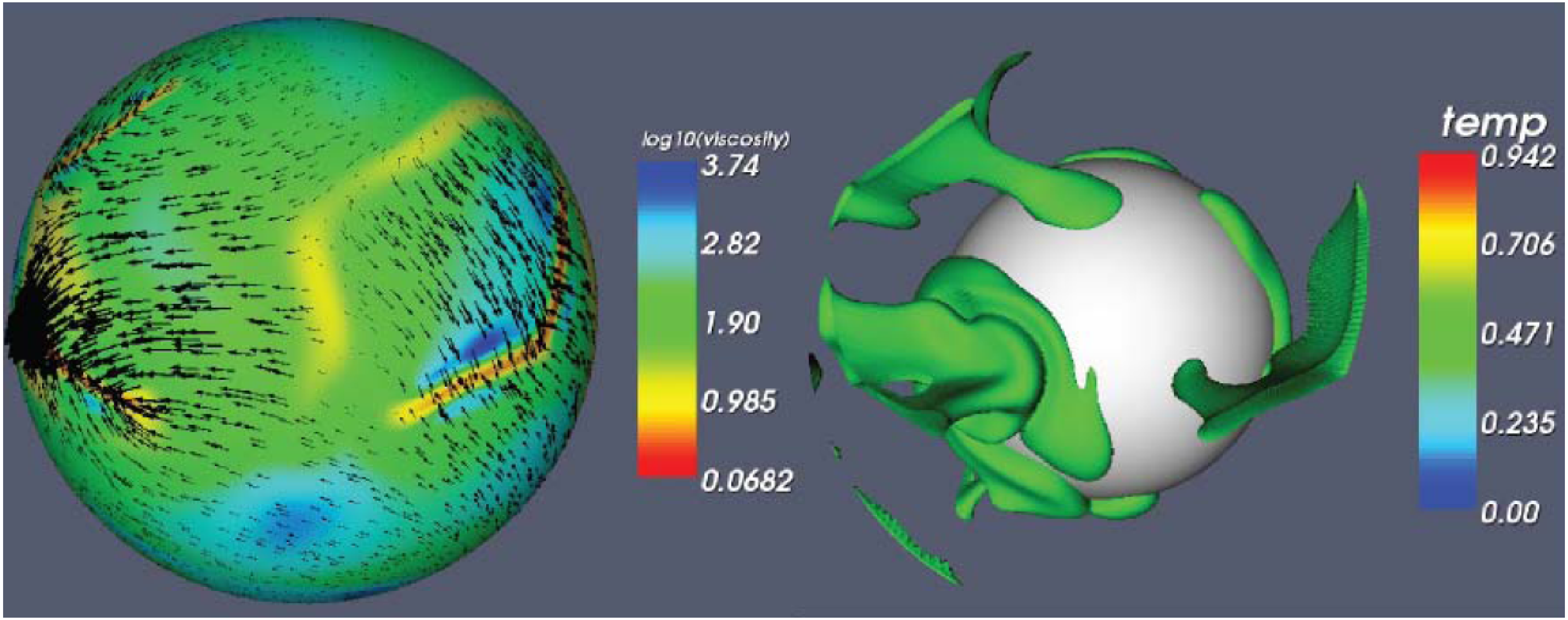

Foley & Becker (2009)

2) Thermo-chemical mantle structure

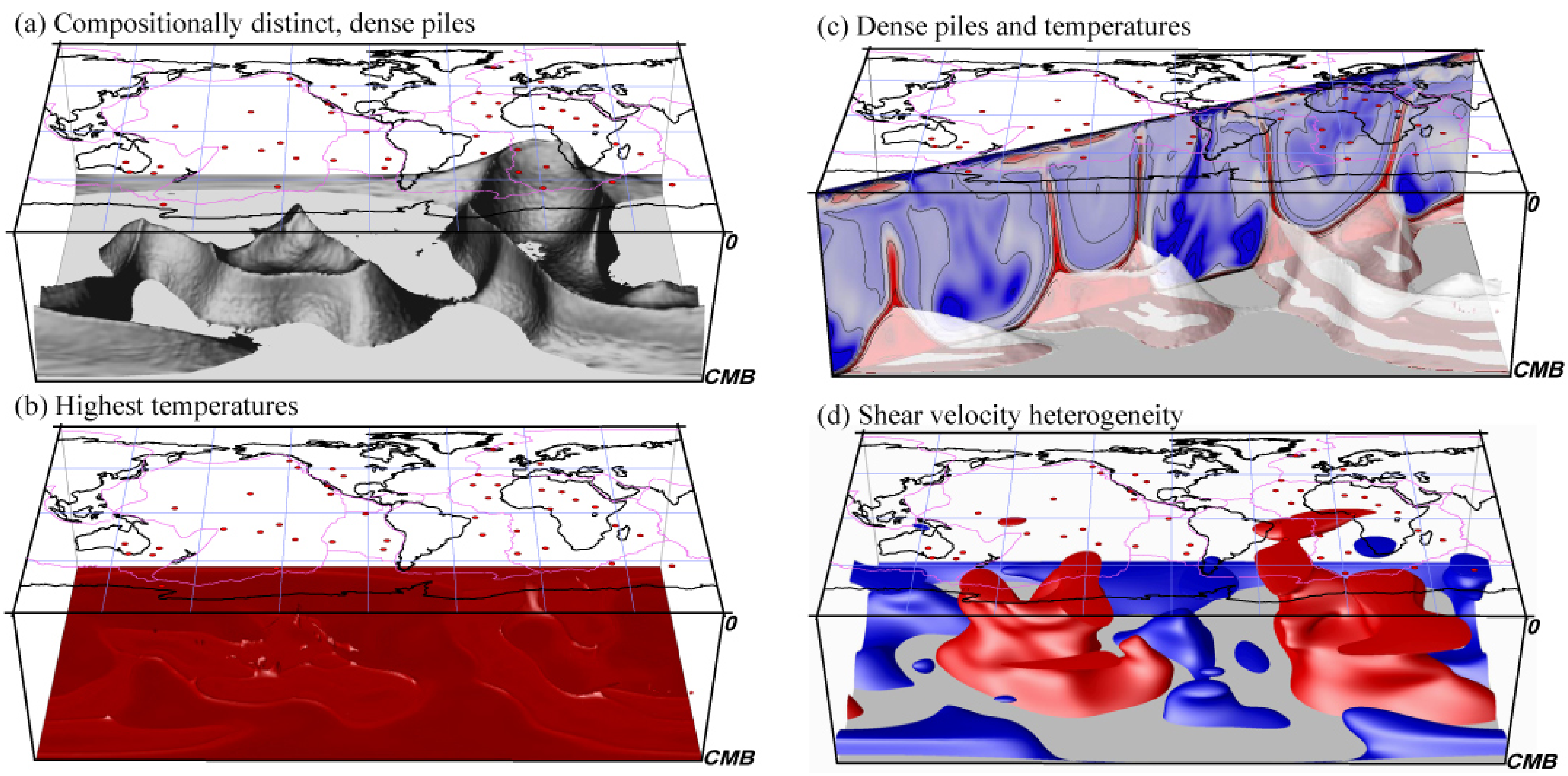

Figure courtesy Ed Garnero

3) Post-perovskite and ULVZs

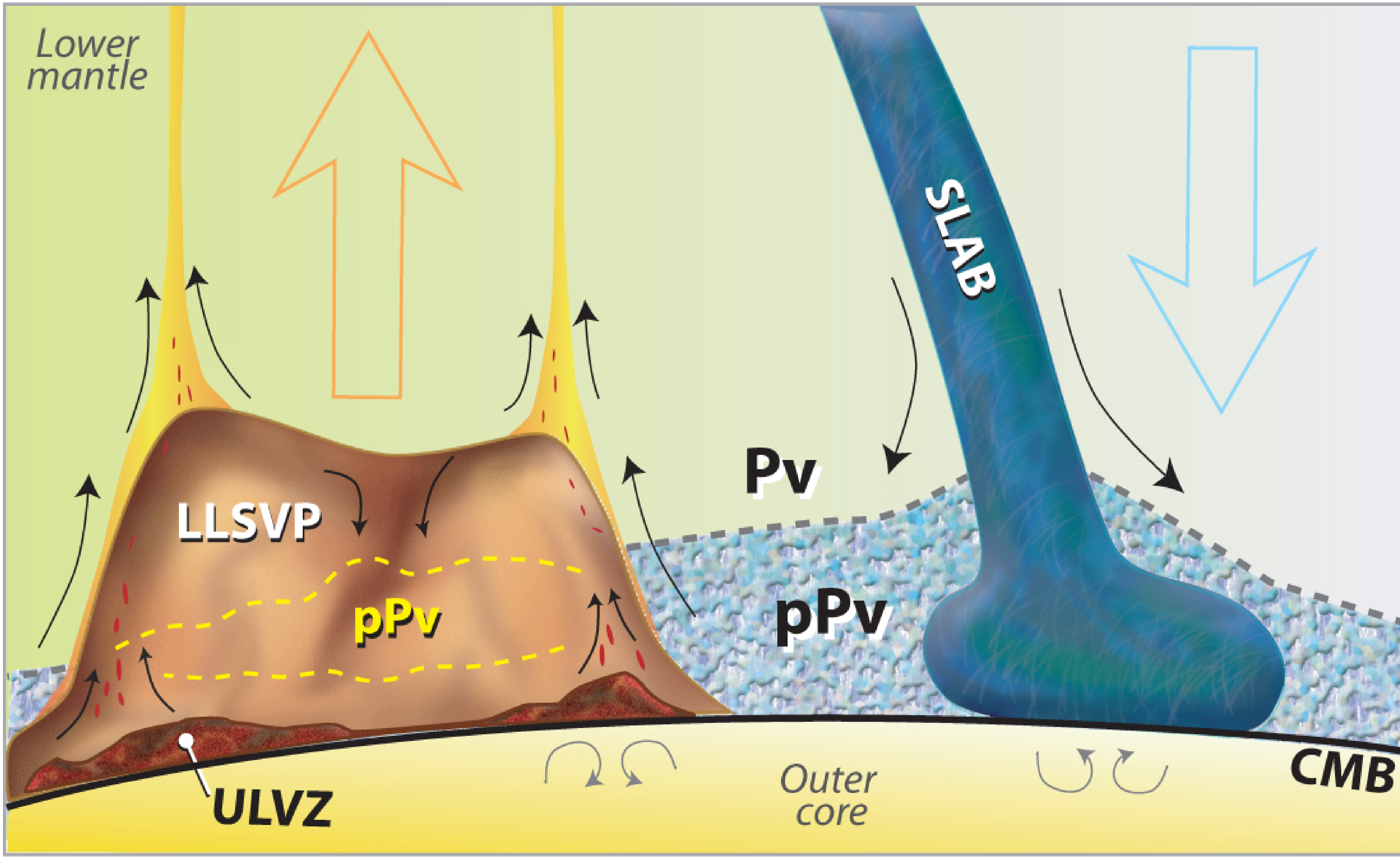

Figure courtesy Ed Garnero

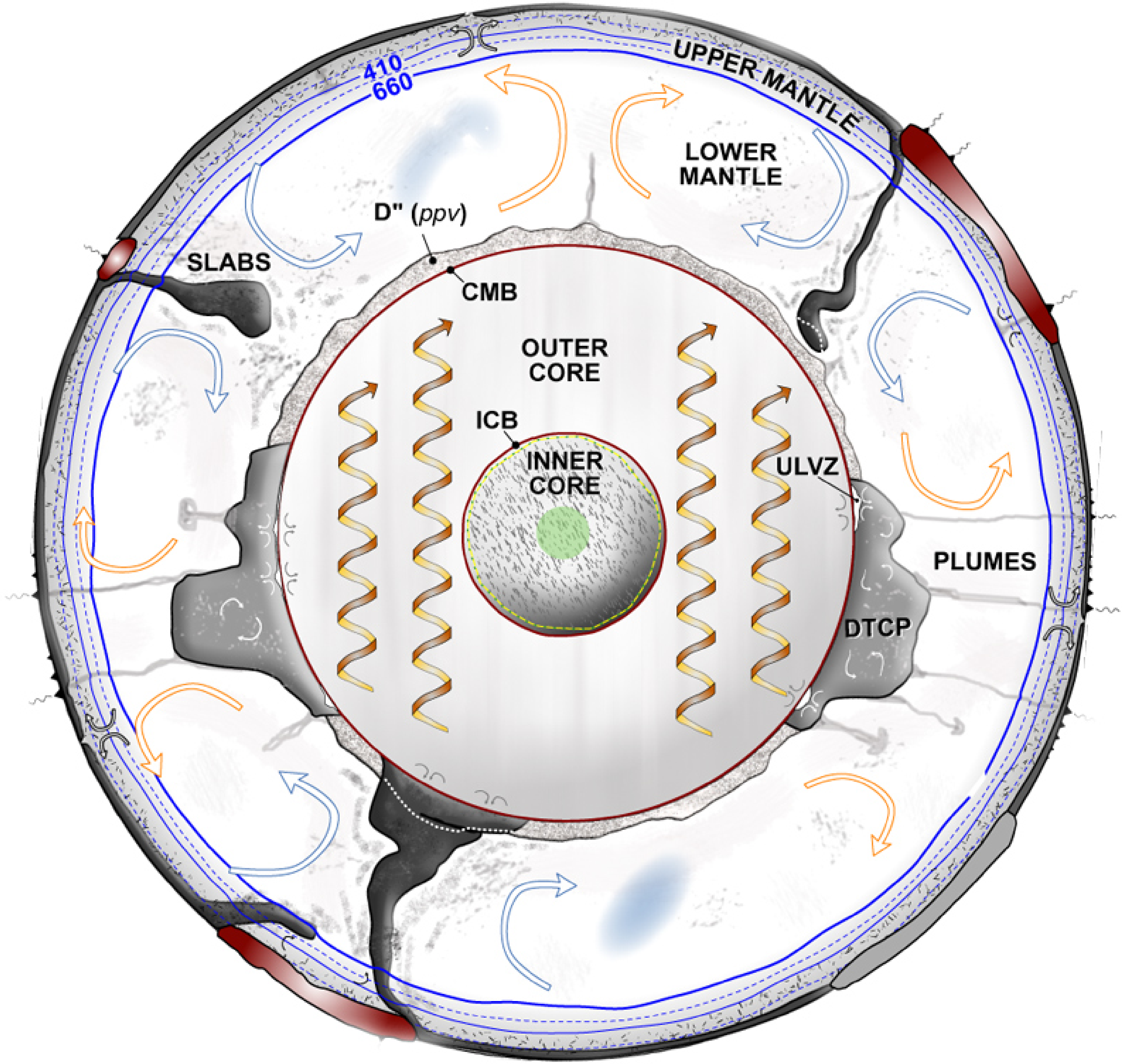

Figure courtesy Ed Garnero

Plate tectonics

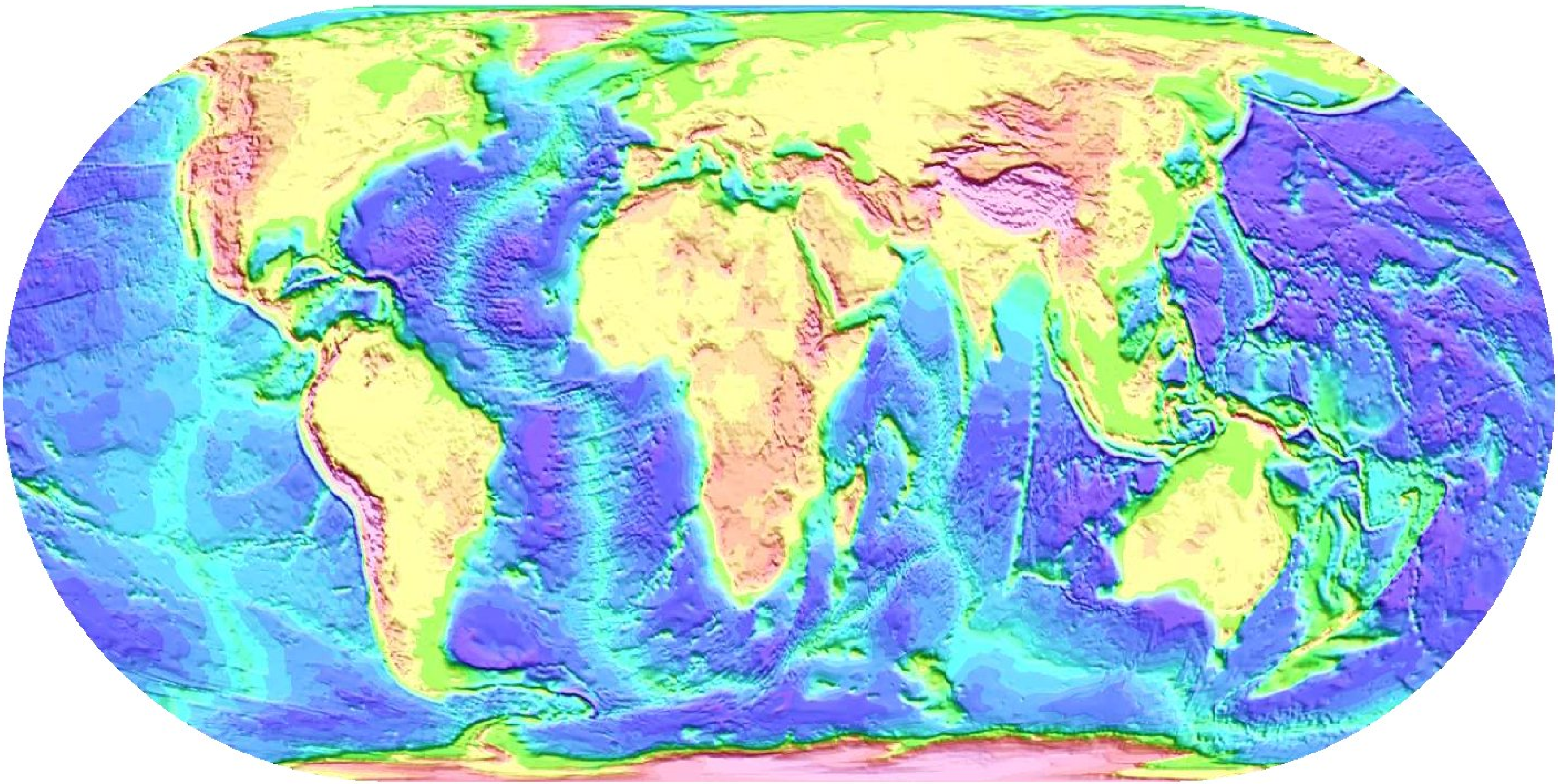

Global shallow seismic moment release

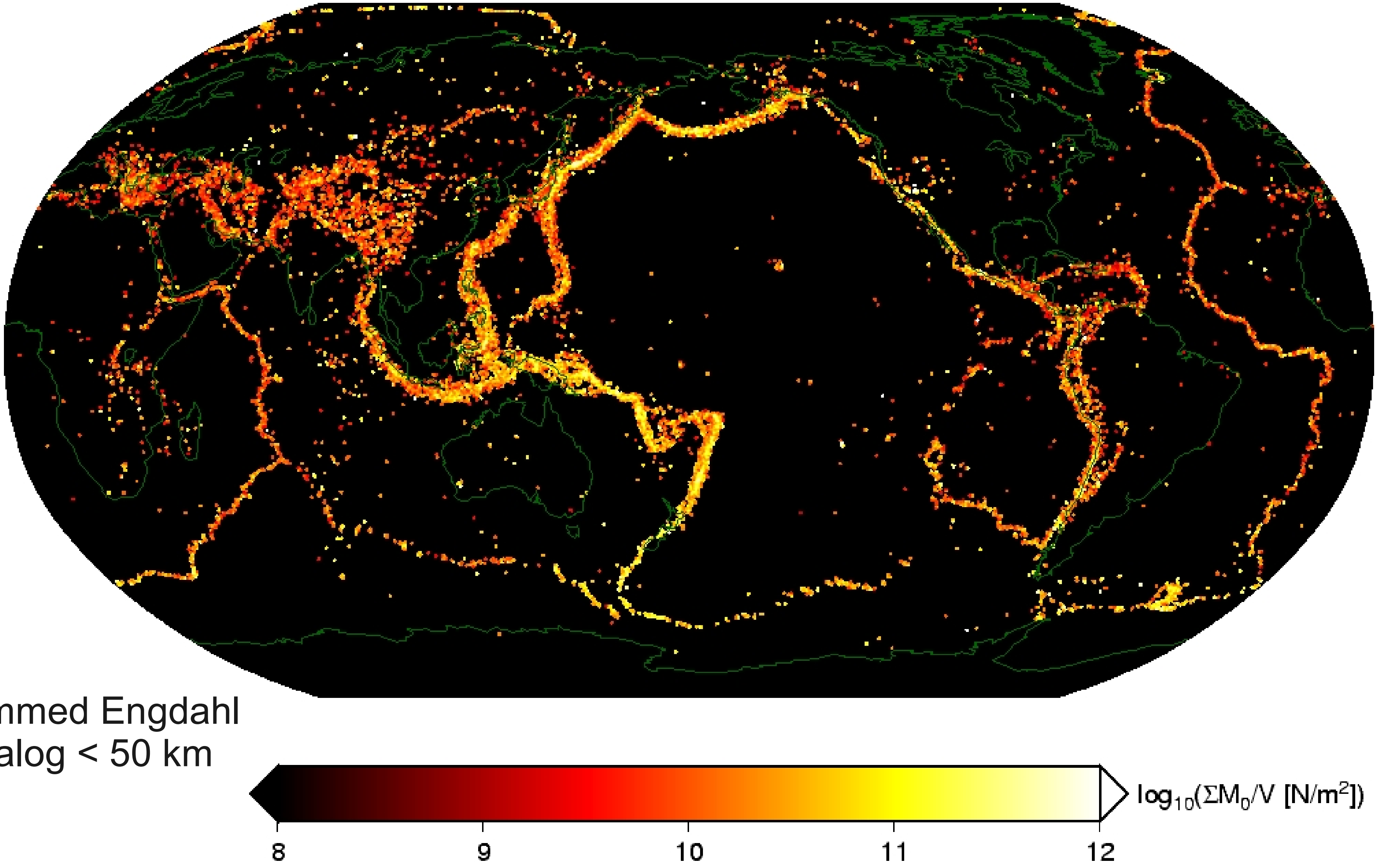

summed Engdahl catalog < 50 km

Seafloor age

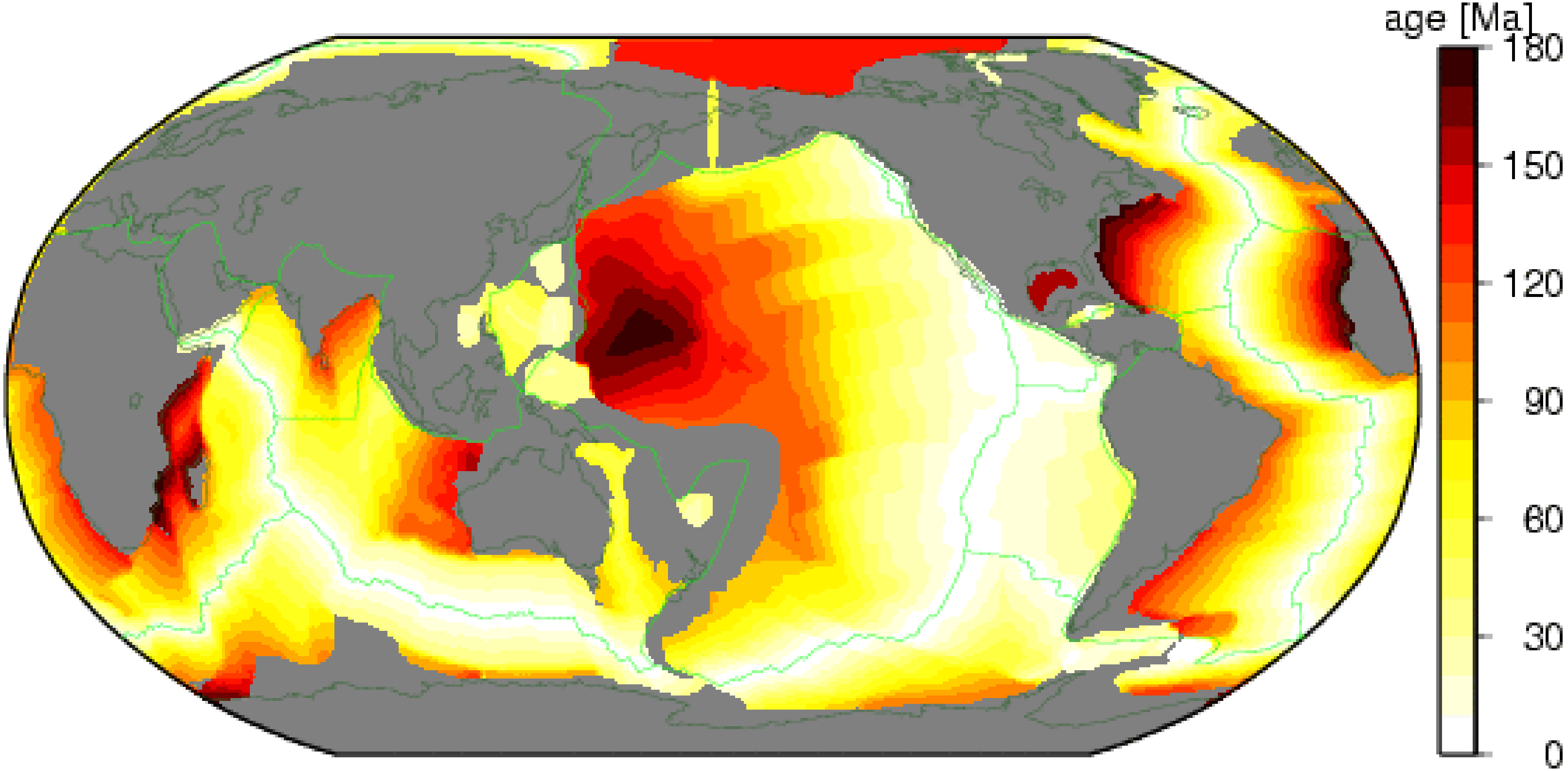

Wadati-Benioff zone seismicity

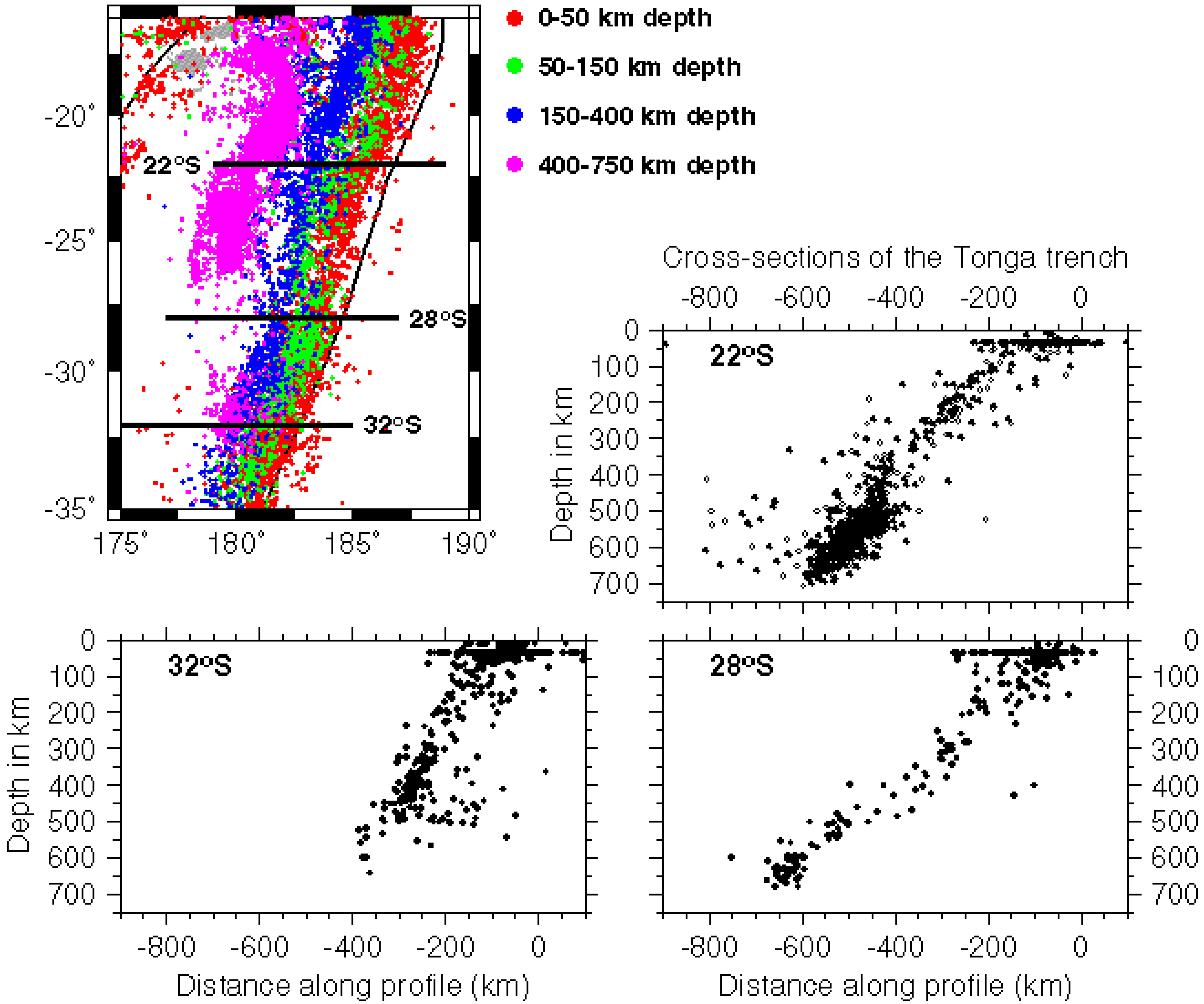

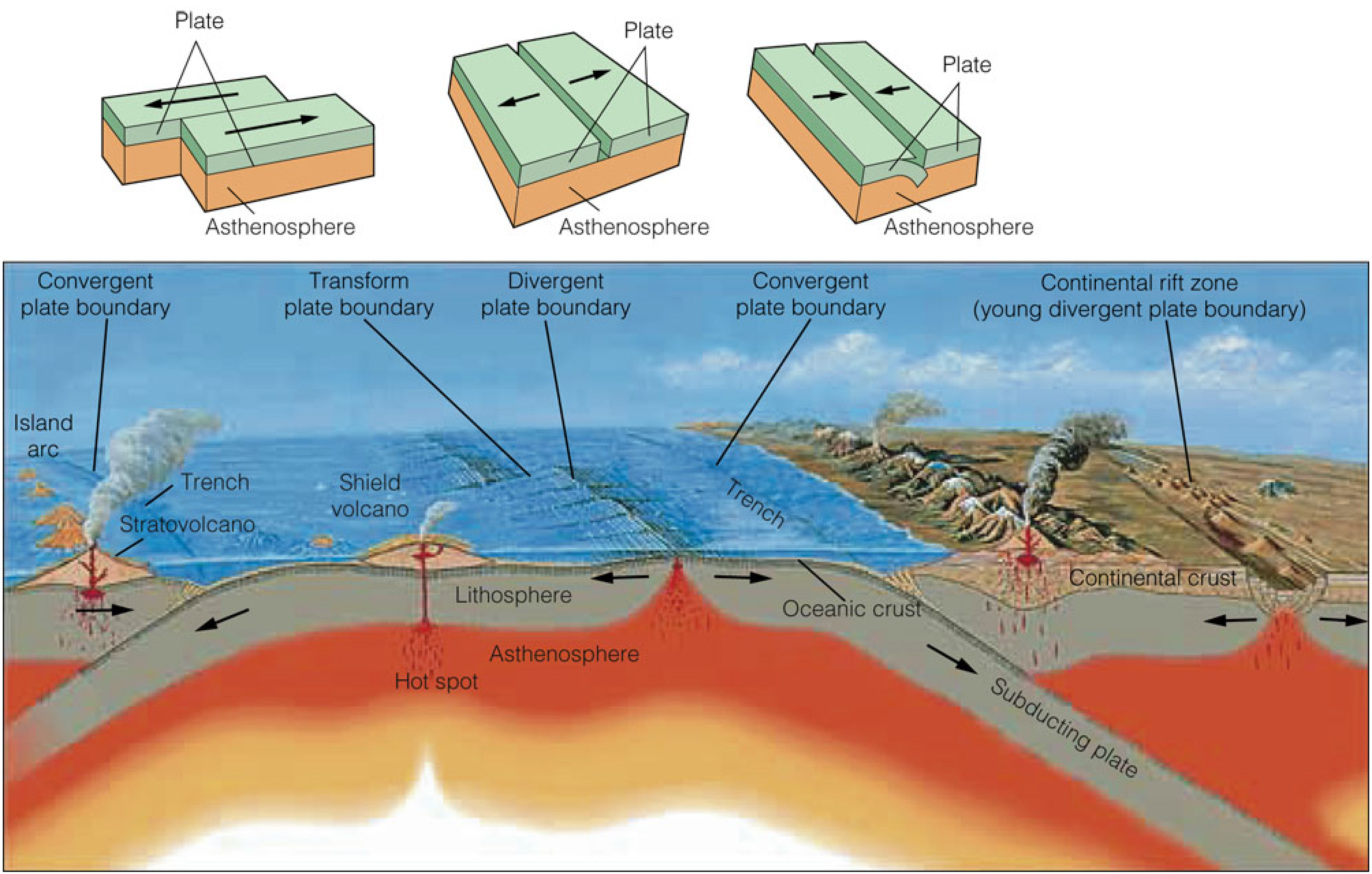

Plate
Asthenosphere
Plate
Asthenosphere
Plate
Asthenosphere
Convergent plate boundary
Transform plate boundary
Divergent plate boundary
Convergent plate boundary
Continental rift zone (young divergent plate boundary)
Island arc
Trench
Stratovolcano
Shield volcano
Trench
Lithosphere
Oceanic crust
Continental crust
Asthenosphere
Hot spot
Subducting plate

The hardest part of the puzzle

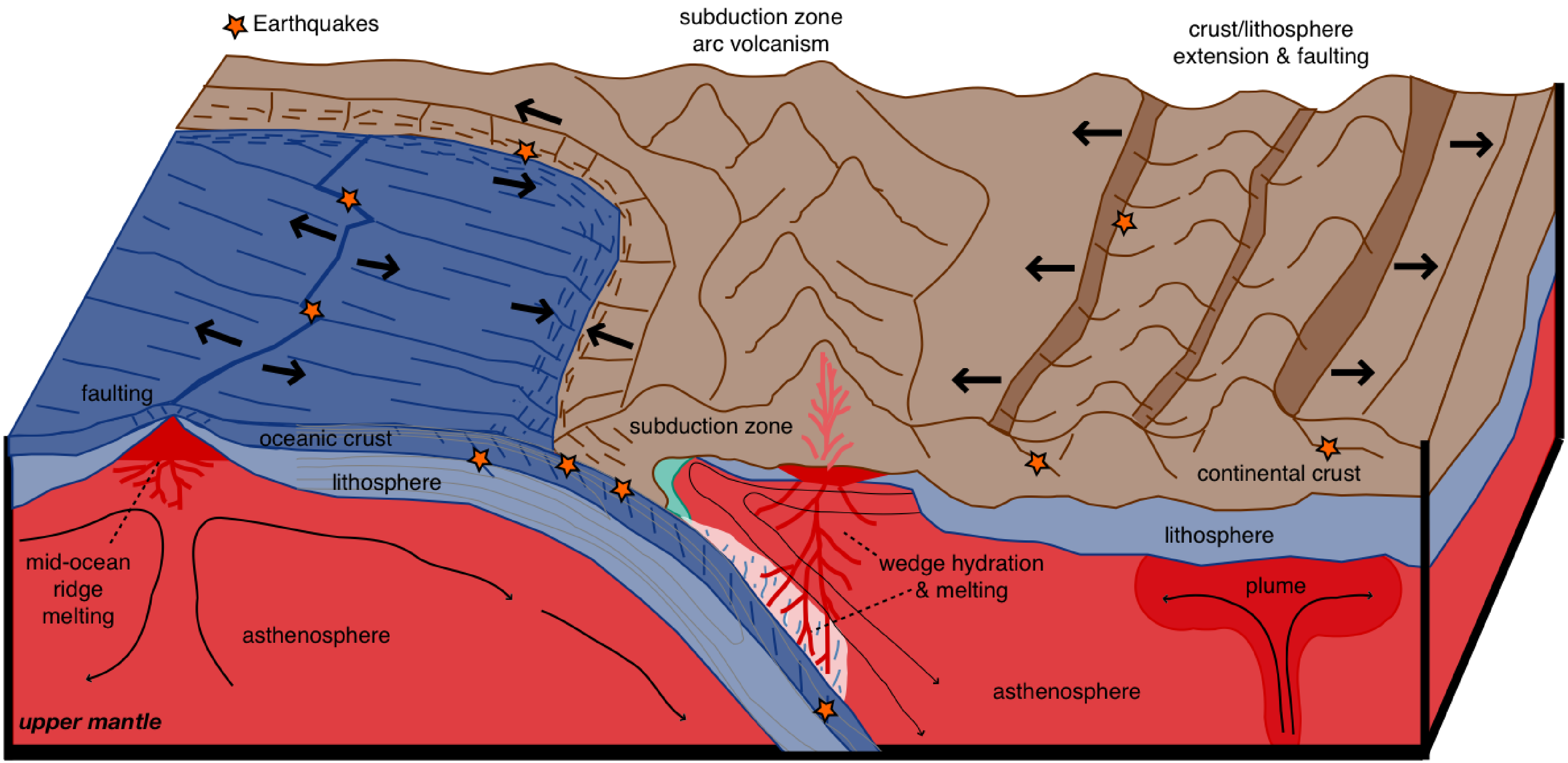

Figure courtesy of M. Billen

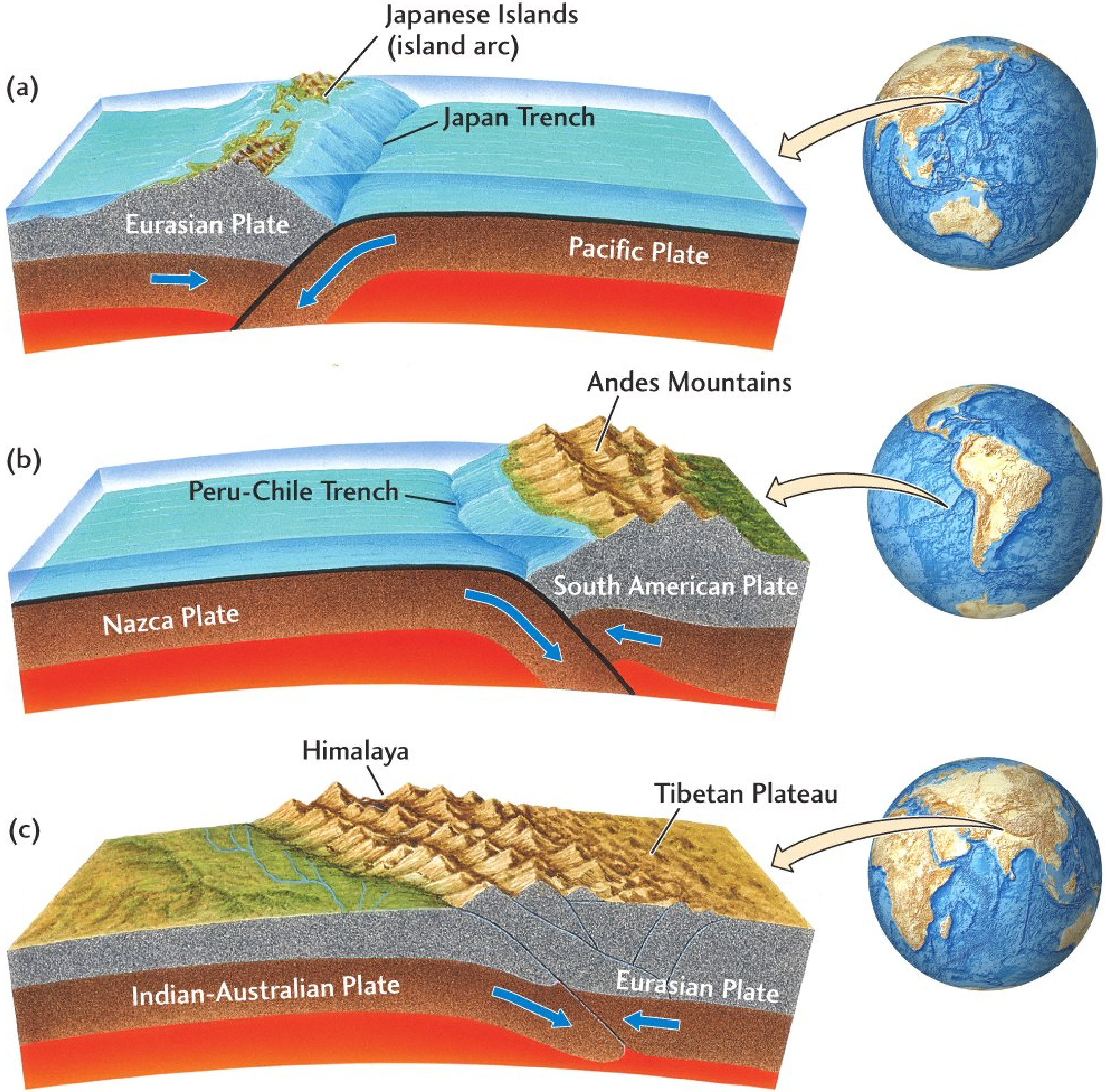

(a)
Japanese Islands
(island arc)
Japan Trench
Eurasian Plate
Pacific Plate
(b)
Andes Mountains
Peru-Chile Trench
South American Plate
Nazca Plate
(c)
Himalaya
Tibetan Plateau
Indian-Australian Plate
Eurasian Plate

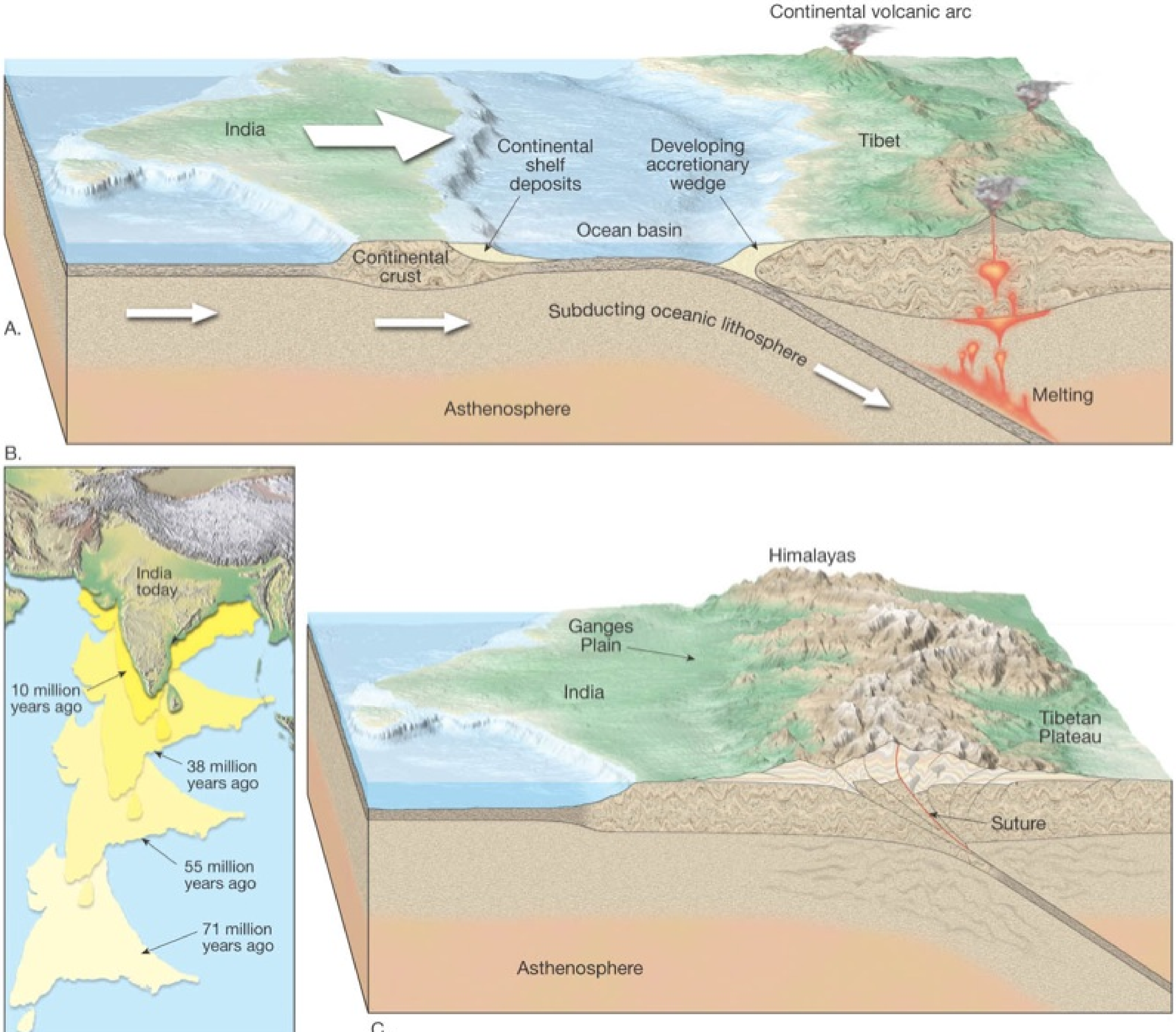
Continental volcanic arc
India
Continental shelf deposits
Developing accretionary wedge
Tibet
Ocean basin
Continental crust
Subducting oceanic lithosphere
Melting
Asthenosphere
A.
B.
India today
10 million years ago
38 million years ago
55 million years ago
71 million years ago
Himalayas
Ganges Plain
India
Tibetan Plateau
Suture
Asthenosphere
C.

Subduction zones

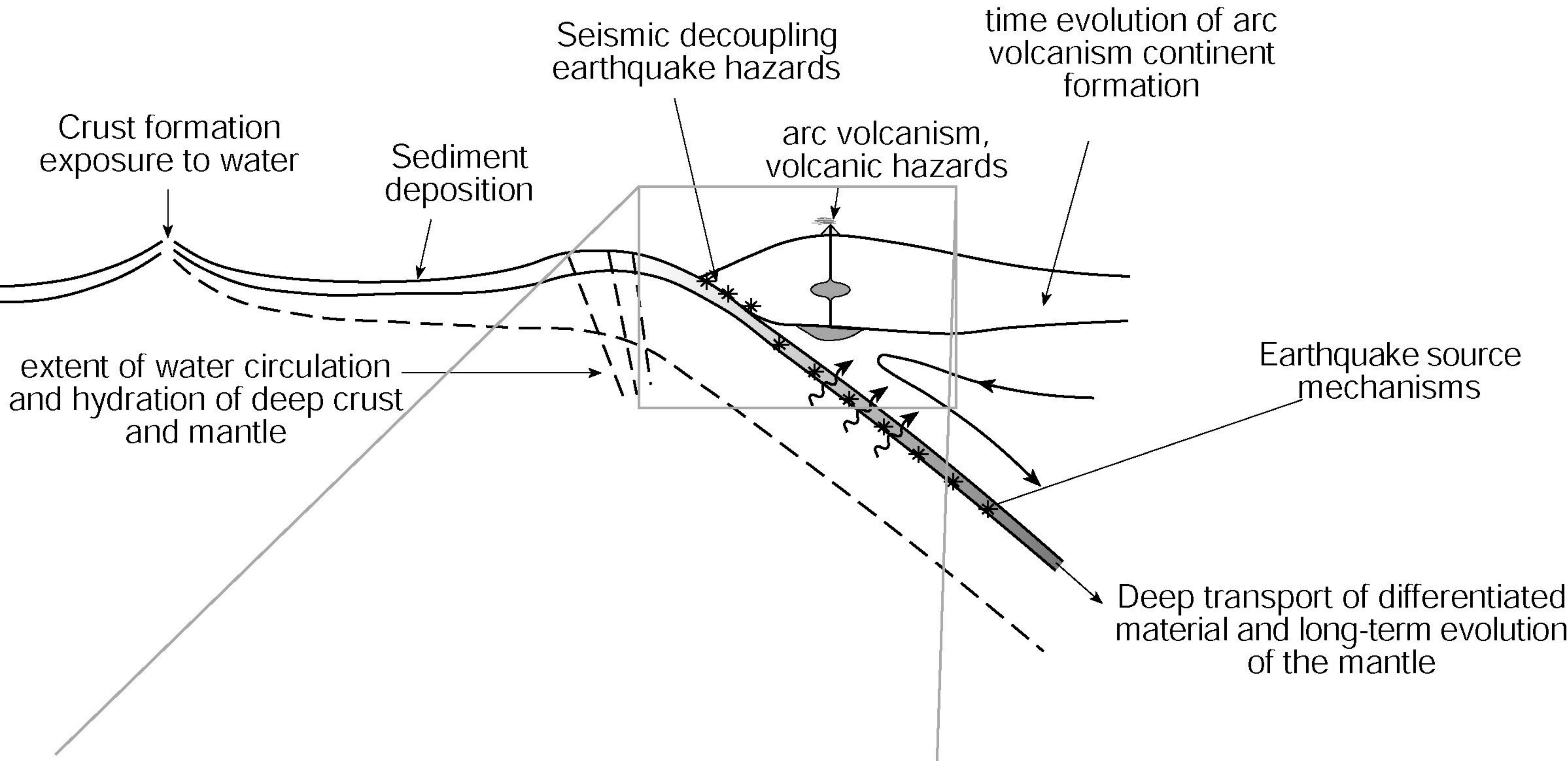

Subduction zone terms

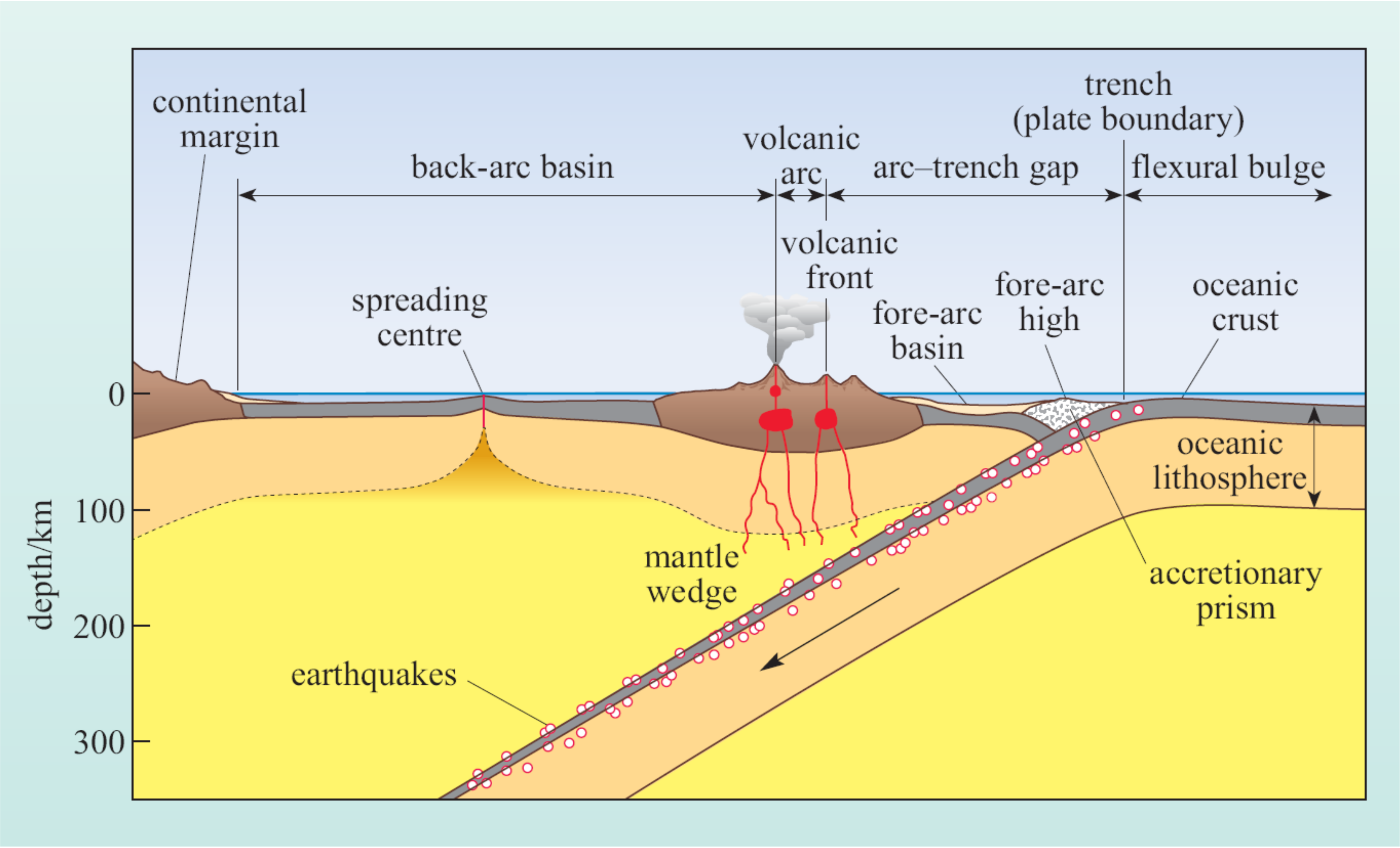

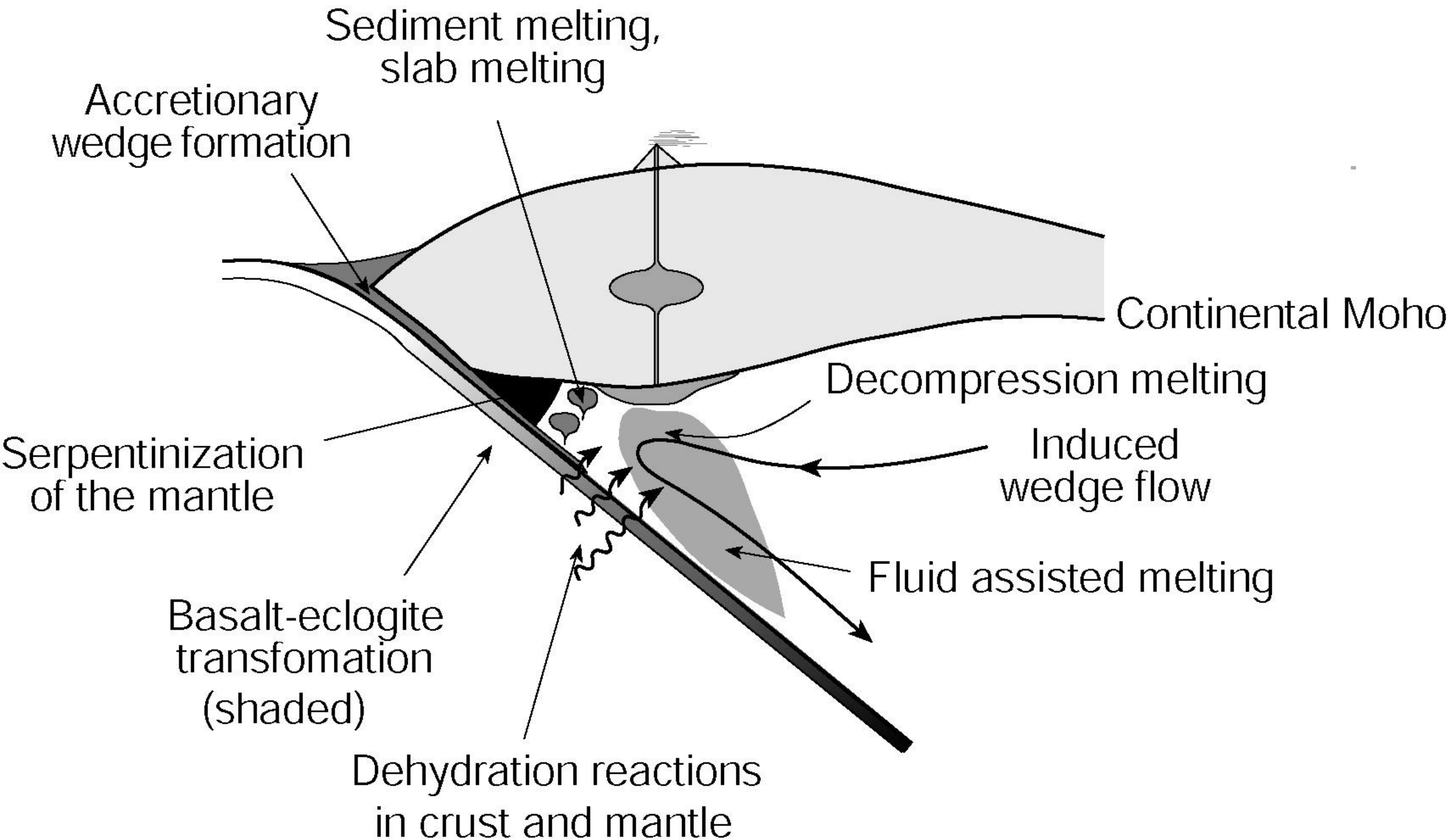
Sediment melting,
slab melting
Accretionary
wedge formation
Continental Moho
Decompression melting
Induced
wedge flow
Serpentinization
of the mantle
Fluid assisted melting
Basalt-eclogite
transfomation
(shaded)
Dehydration reactions
in crust and mantle

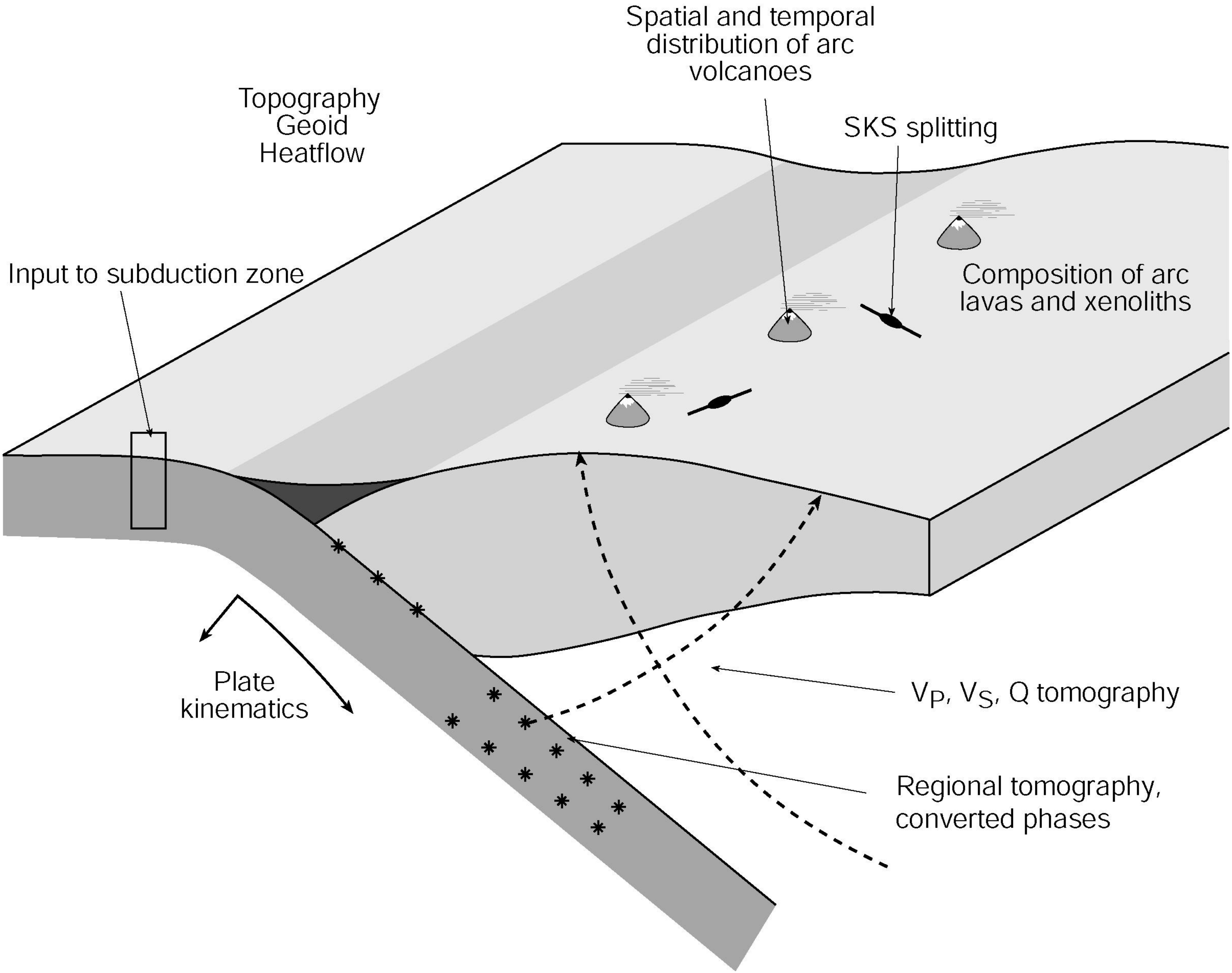
Spatial and temporal distribution of arc volcanoes
Topography
Geoid
Heatflow
SKS splitting
Input to subduction zone
Composition of arc lavas and xenoliths
Plate kinematics
V_P, V_S, Q tomography
Regional tomography, converted phases

What drives the plates?

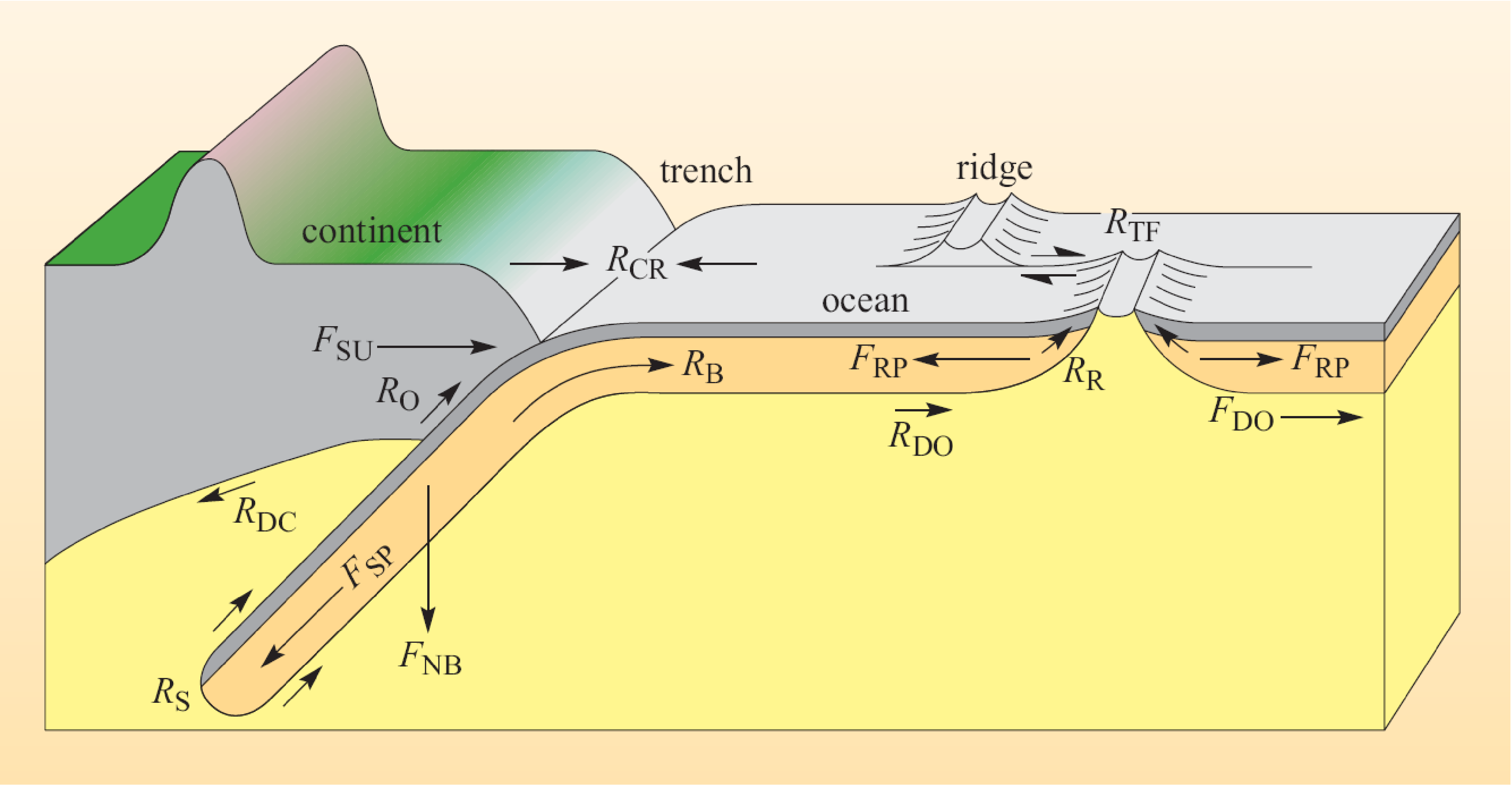

Plate driving forces

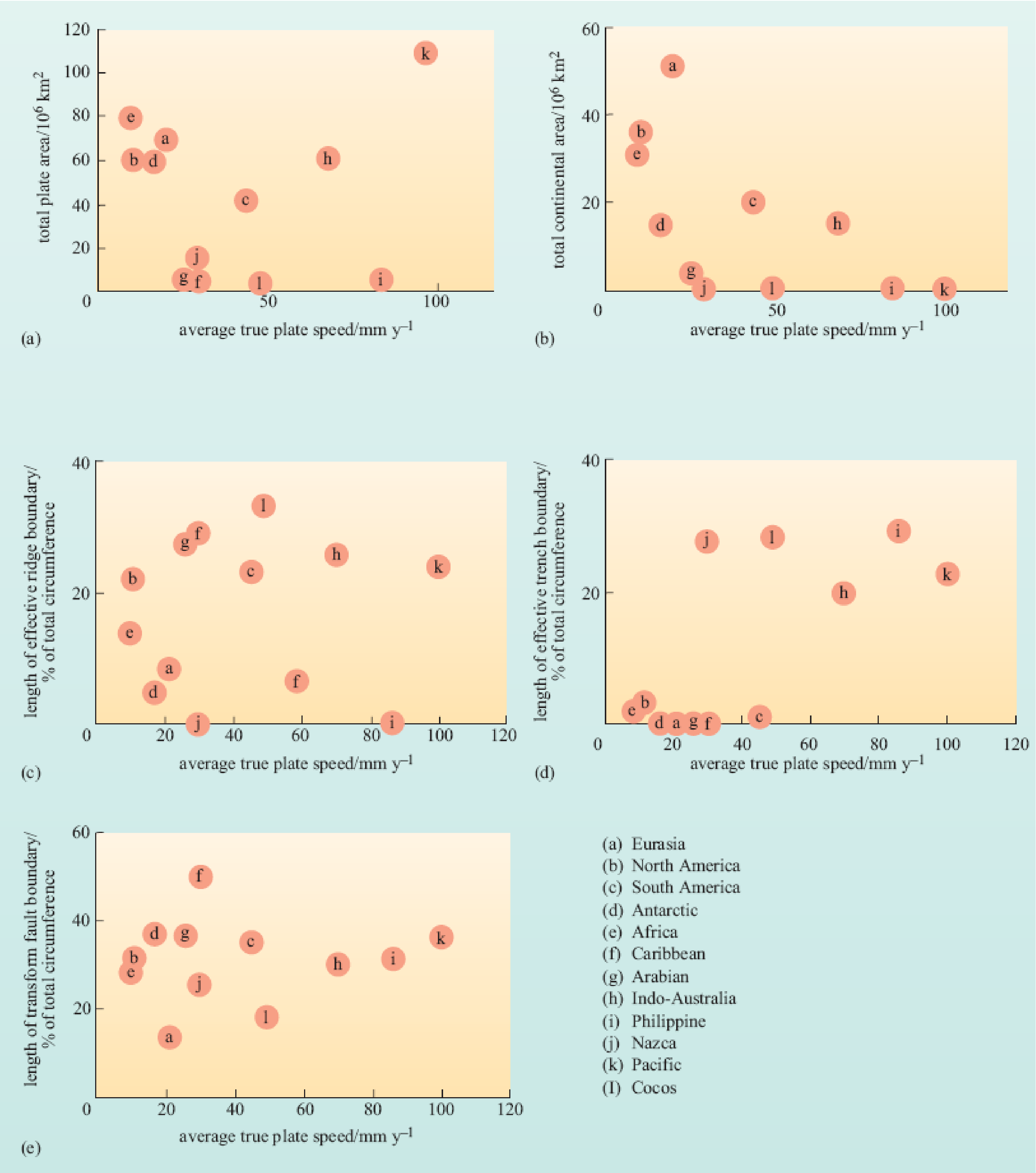

Forsyth & Uyeda (1975)

Plate driving forces

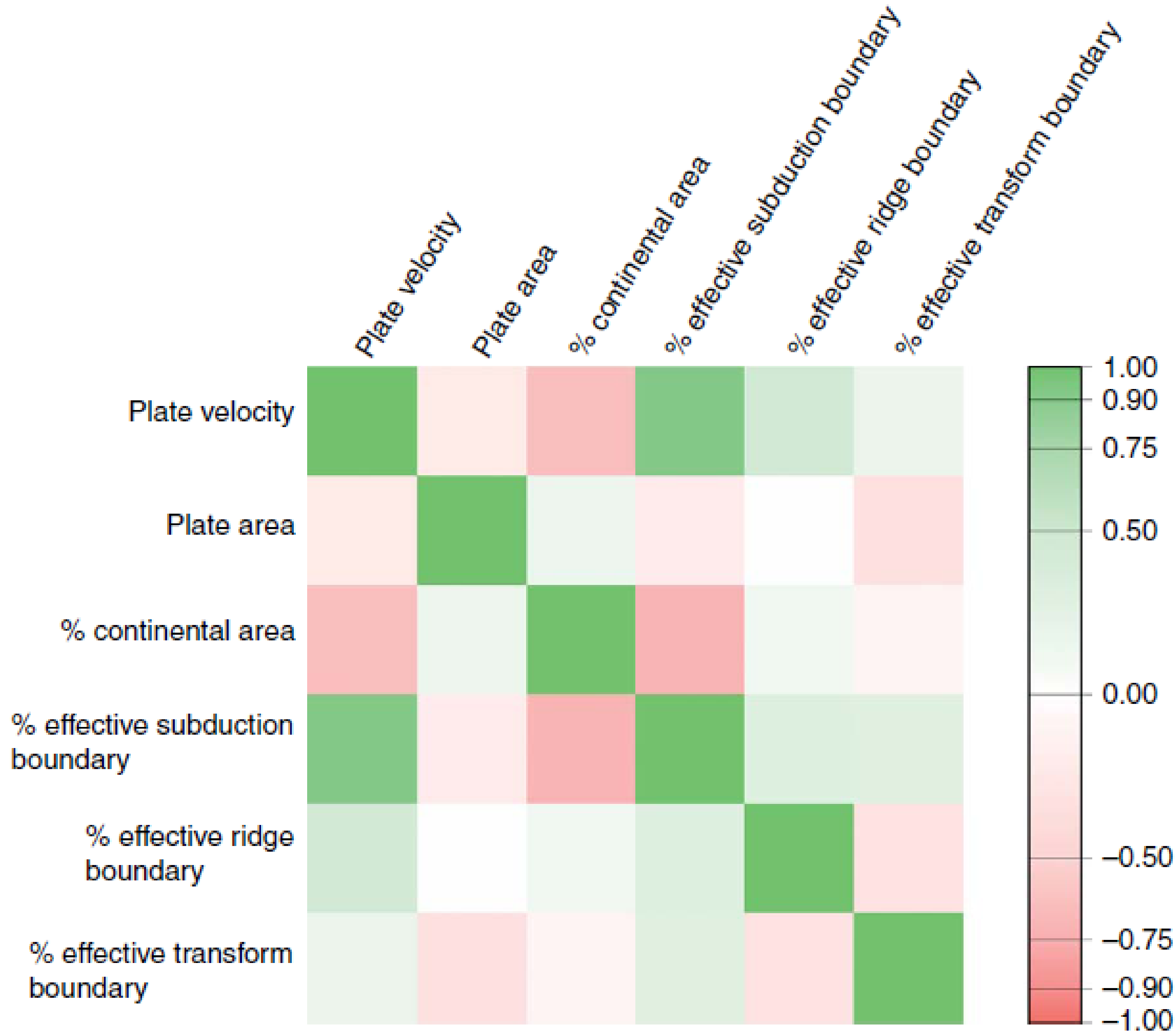

Forsyth & Uyeda (1975), plotted by King (2008)

Relevance of subduction

- Plate tectonics and Earth evolution (life) might be intrinsically linked
- Subducted slabs are responsible for ~70% of the plate driving forces
- Subduction zones host the largest earthquakes
- Subduction zone volcanism and sediment transport major players in volatile and carbon cycle

Half space cooling

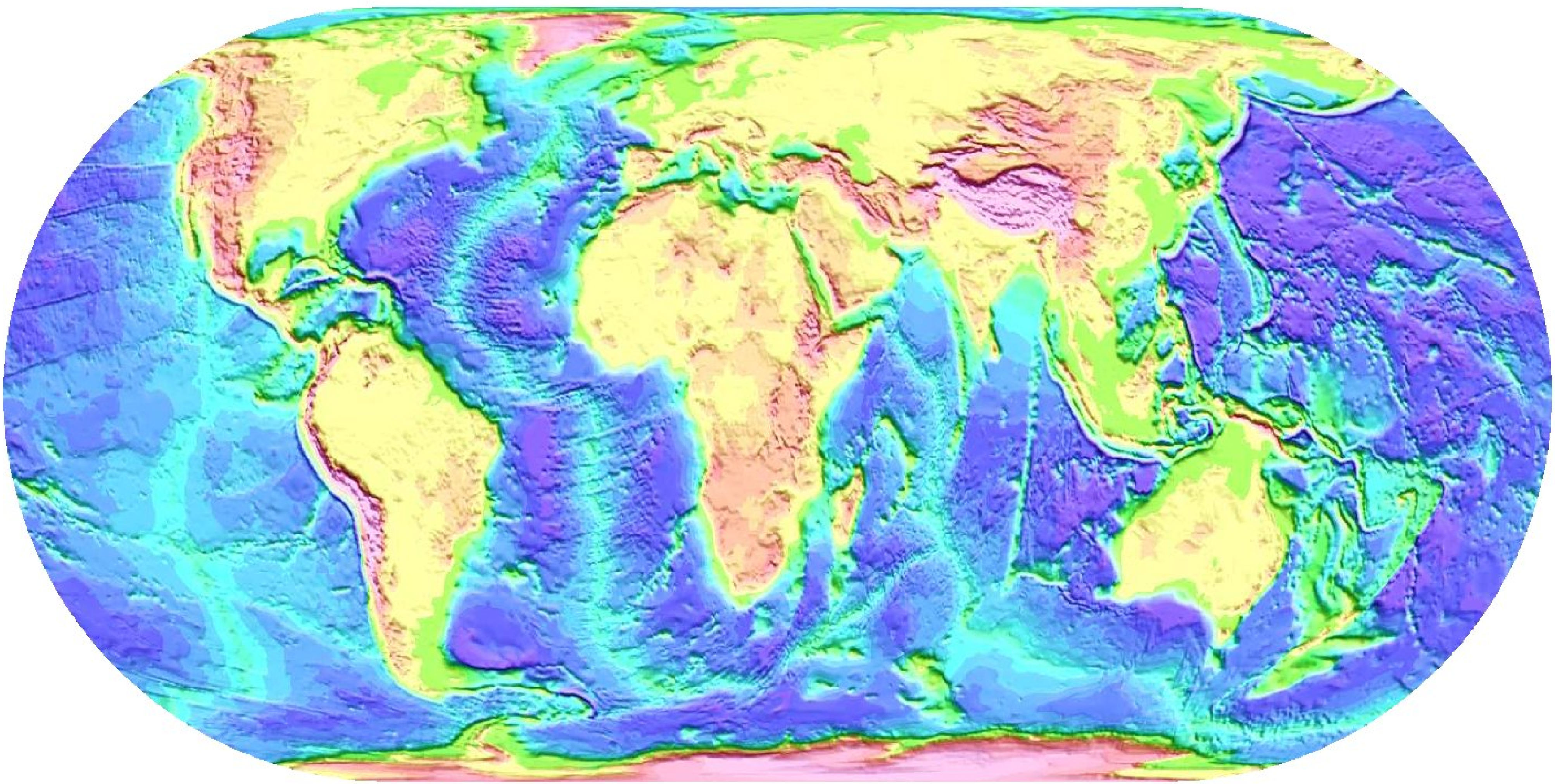

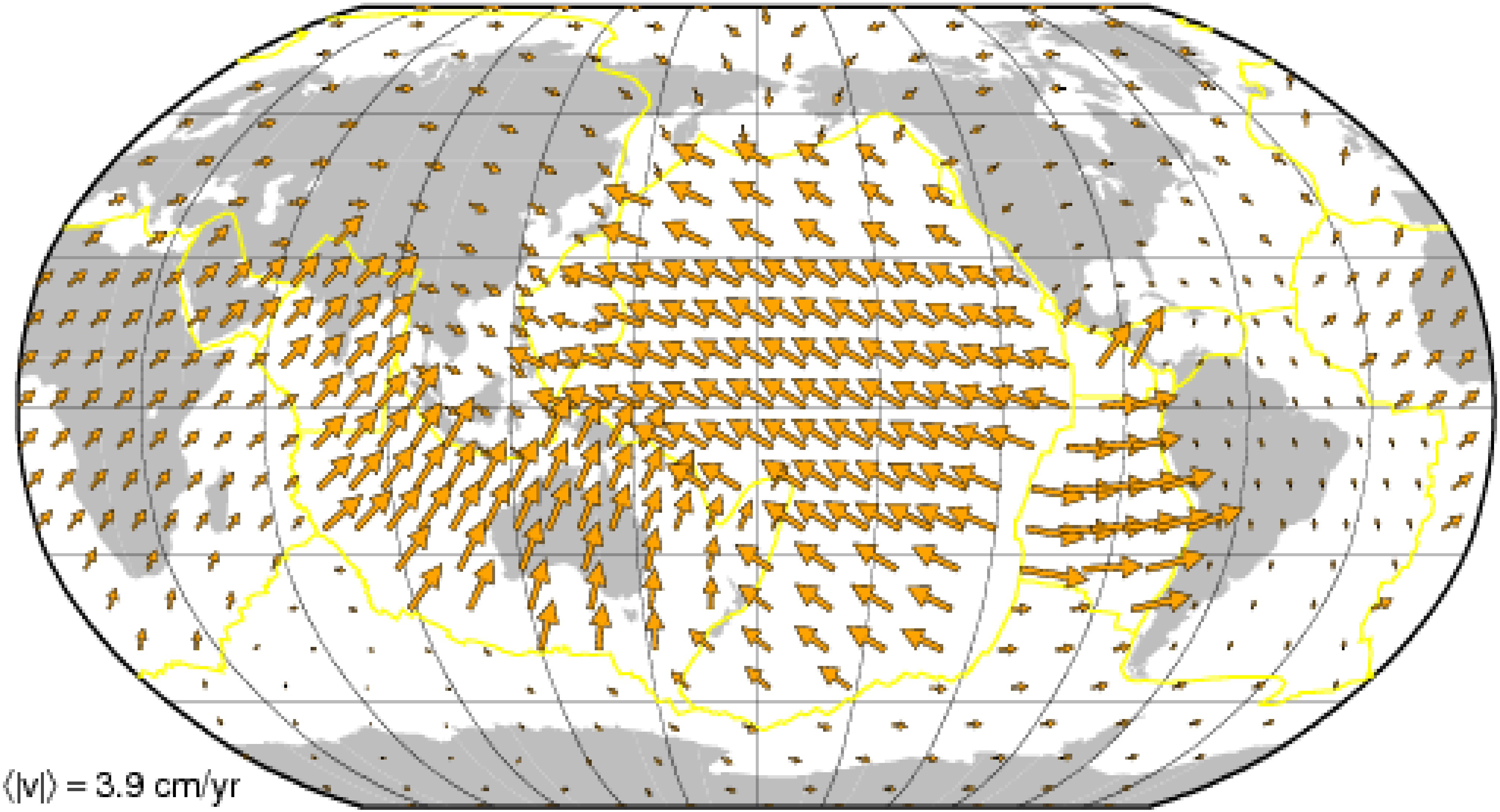

NNR Nuvel

Thermal structure of oceanic lithosphere

Cooling halfspace

$$\frac{\partial T}{\partial t} = \kappa \frac{\partial^2 T}{\partial z^2}$$

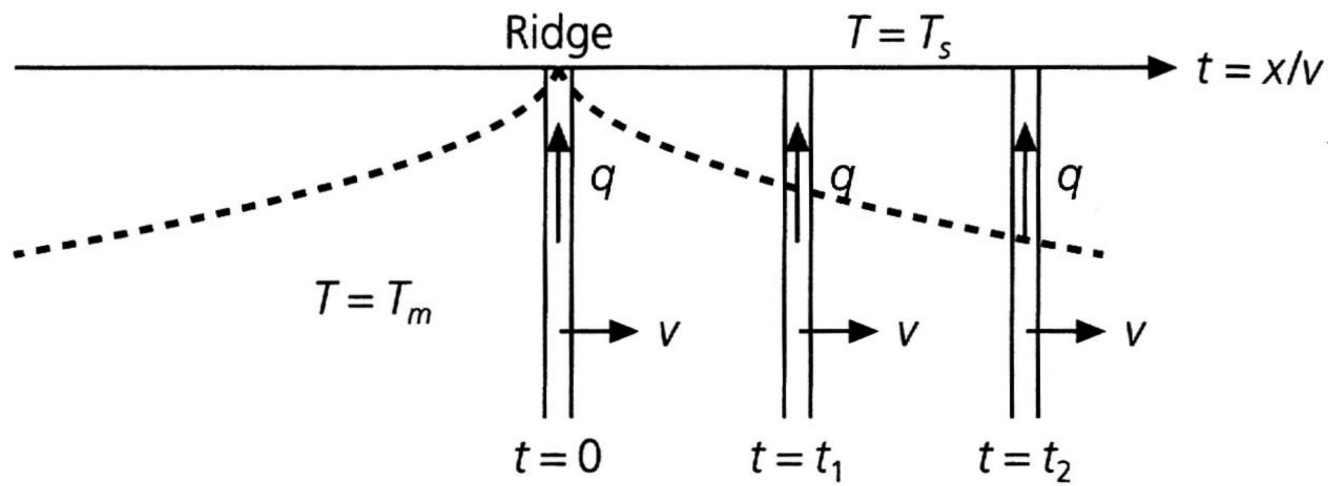

$T = T_m$ at $x = 0$
$T = 0$ at $z = 0$
$T = T_m$ at $z \to \infty$

$$T(x,z) = T_m \, erf\left(\frac{z}{2\sqrt{\kappa t(x)}}\right) = T_m \, erf\left(\frac{z}{2\sqrt{\kappa x/v}}\right)$$

$$T(x,z) = T_m \, erf\left(\frac{z}{2\sqrt{\kappa x / v}}\right)$$

Depth of an isotherm $z_{iso} = C\sqrt{\kappa t}$

Surface heat flow $q_s = -k\left(\frac{\partial T}{\partial z}\right)_{z=0} = \frac{k T_m}{\sqrt{\pi \kappa t}} = \frac{k T_m}{\sqrt{\pi \kappa x / v}}$

Bathymetry $w(x) = \frac{2\rho_m \alpha_V T_m}{(\rho_m - \rho_w)}\sqrt{\frac{\kappa x}{\pi v}}$

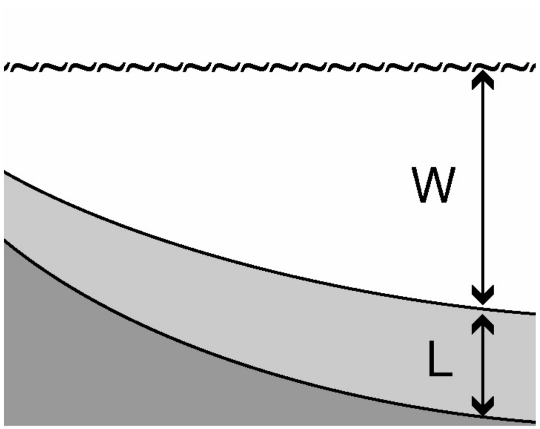

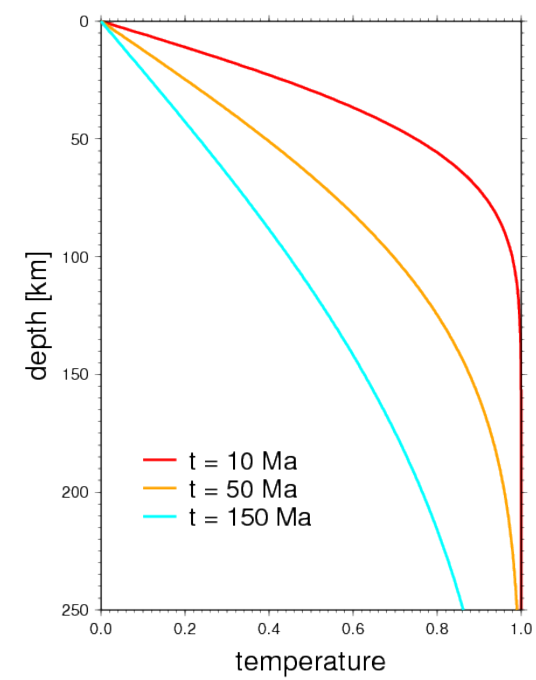

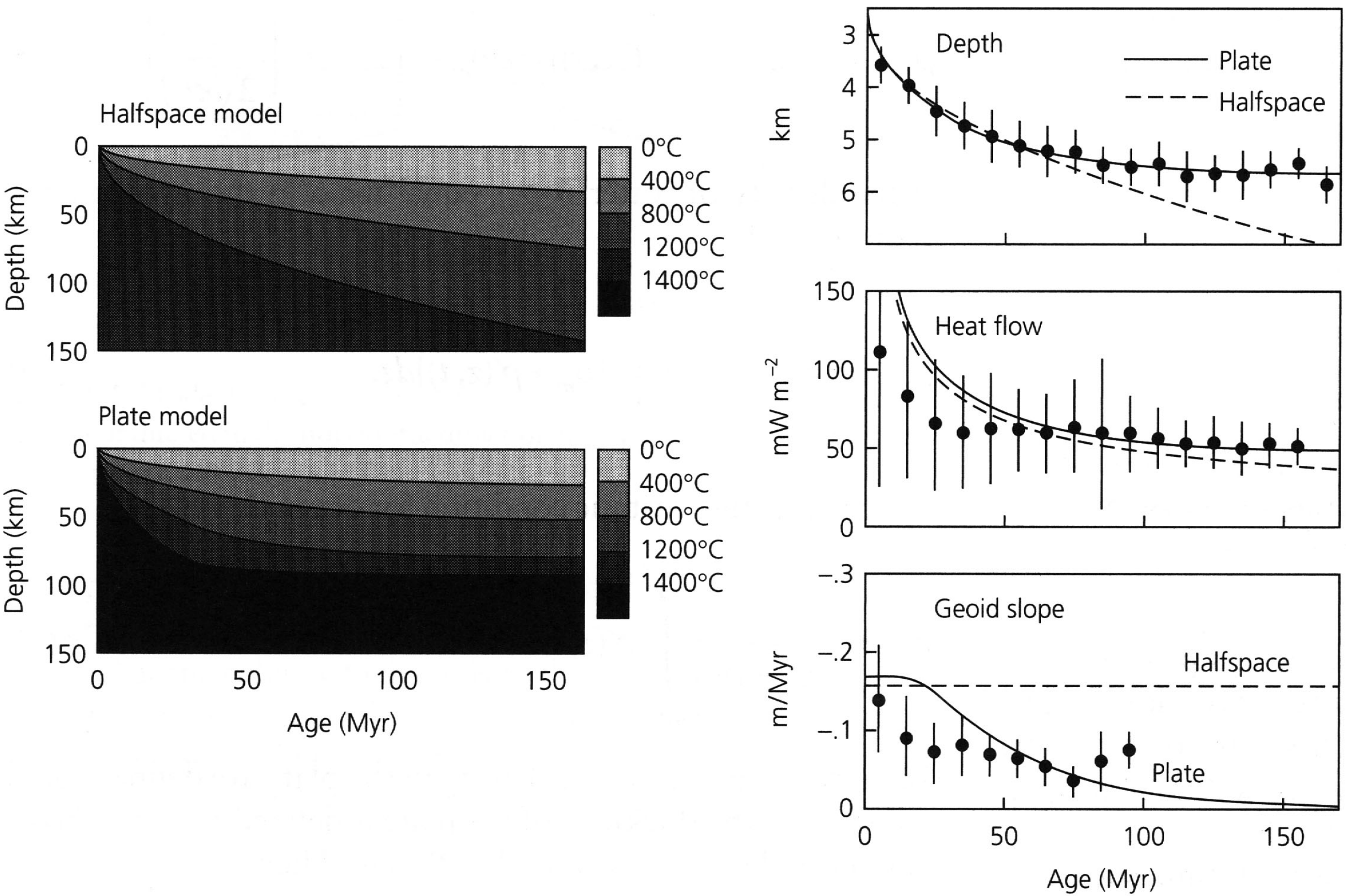

Fig.
evol
Left
litho
in a
~70
a 95
plate
temp
Righ
pred
litho
(but
of a
thos
(Ric
Lett
Ame

Richardson et al. (1995)

Heat flow data

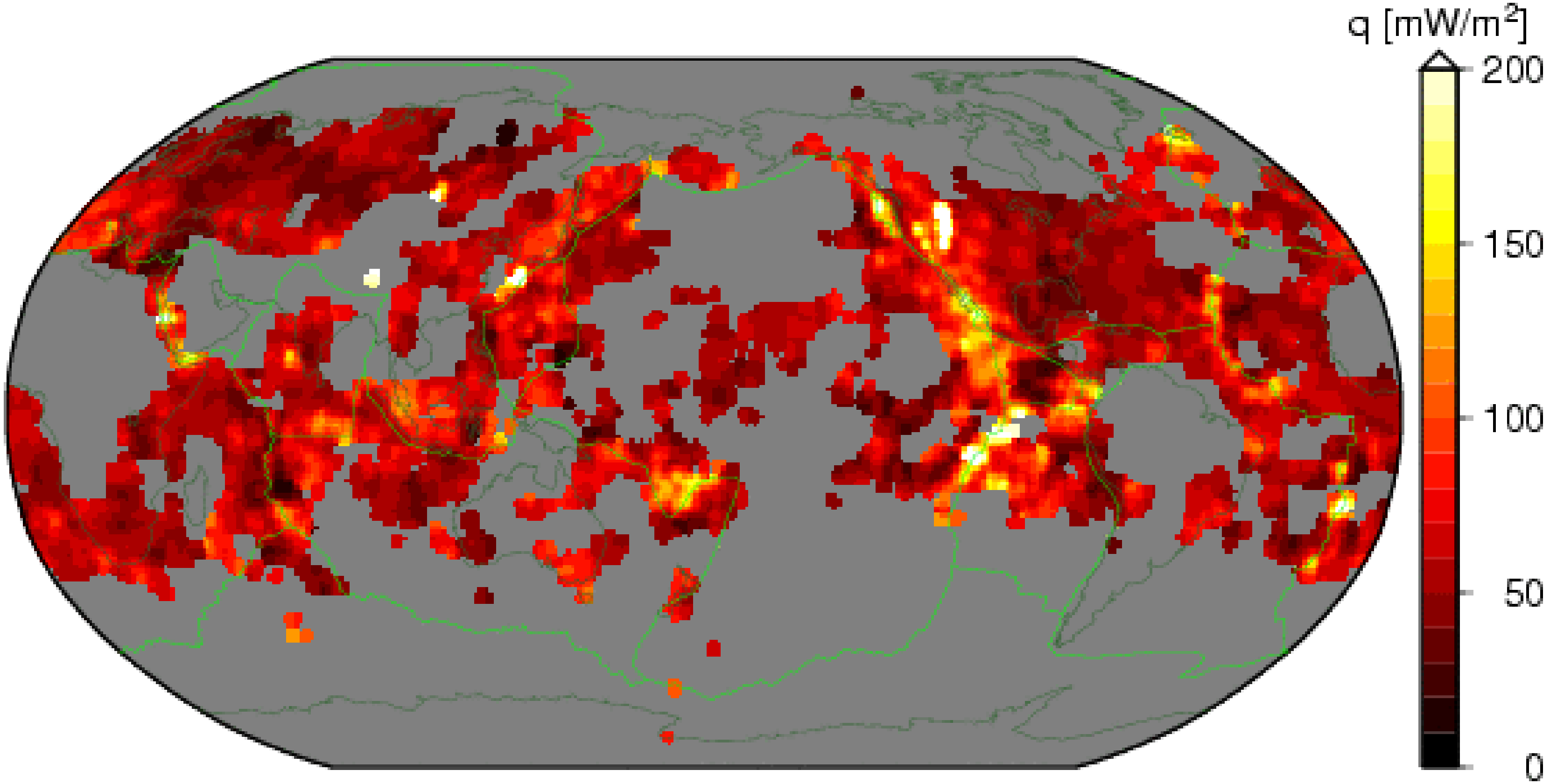

Seafloor age

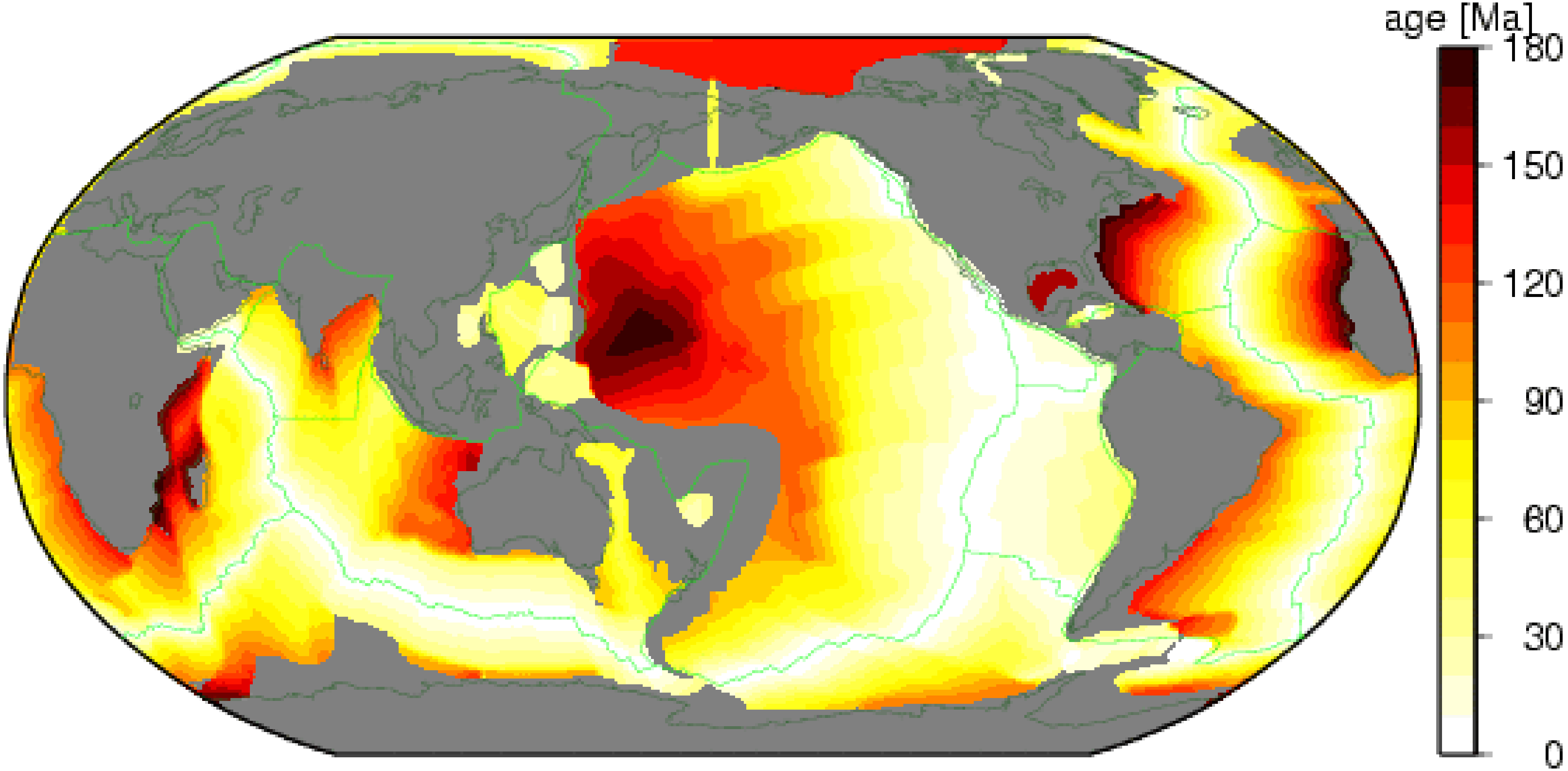

Global heat flow

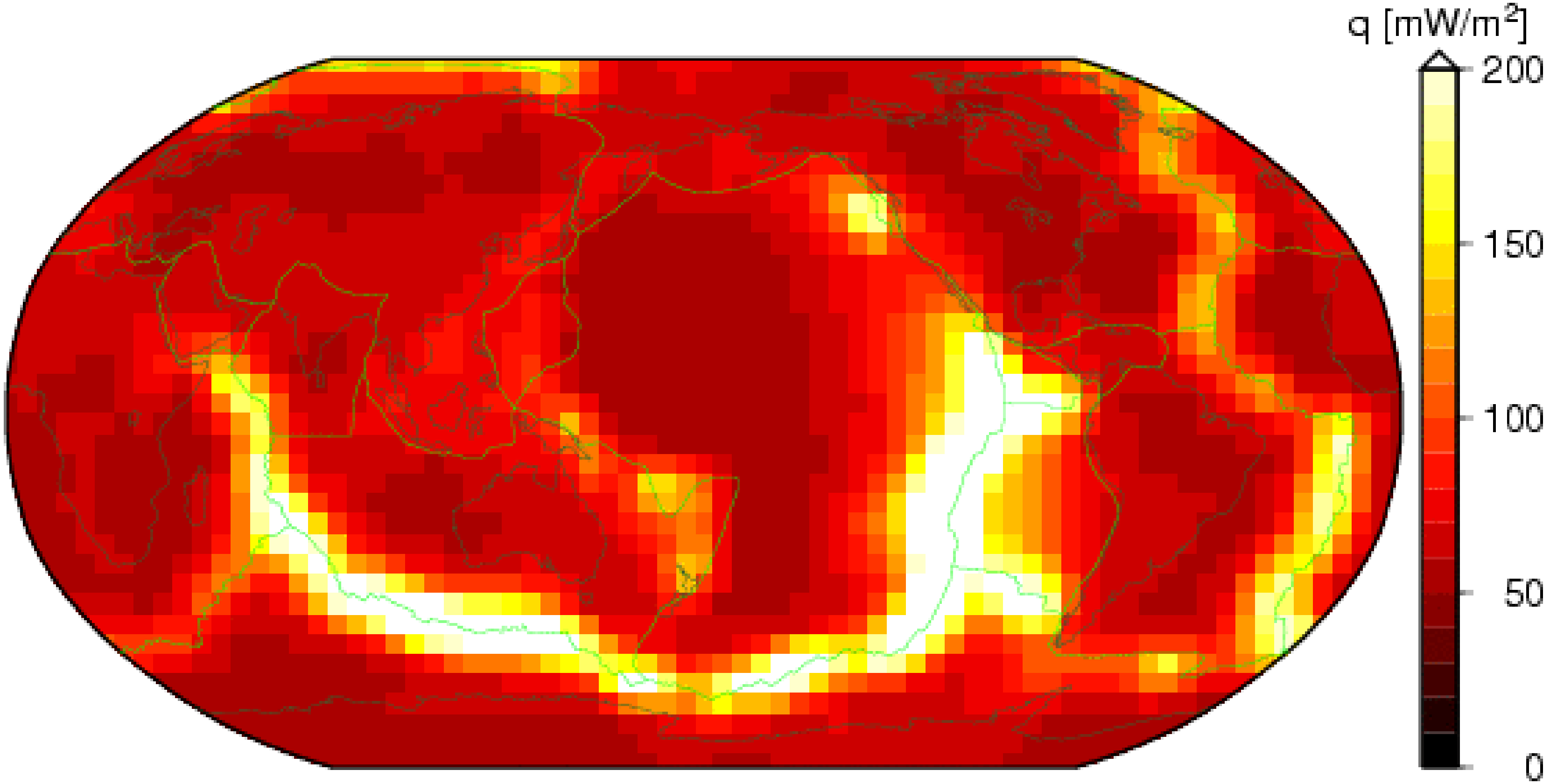

Force balance based on half-space cooling slab pull

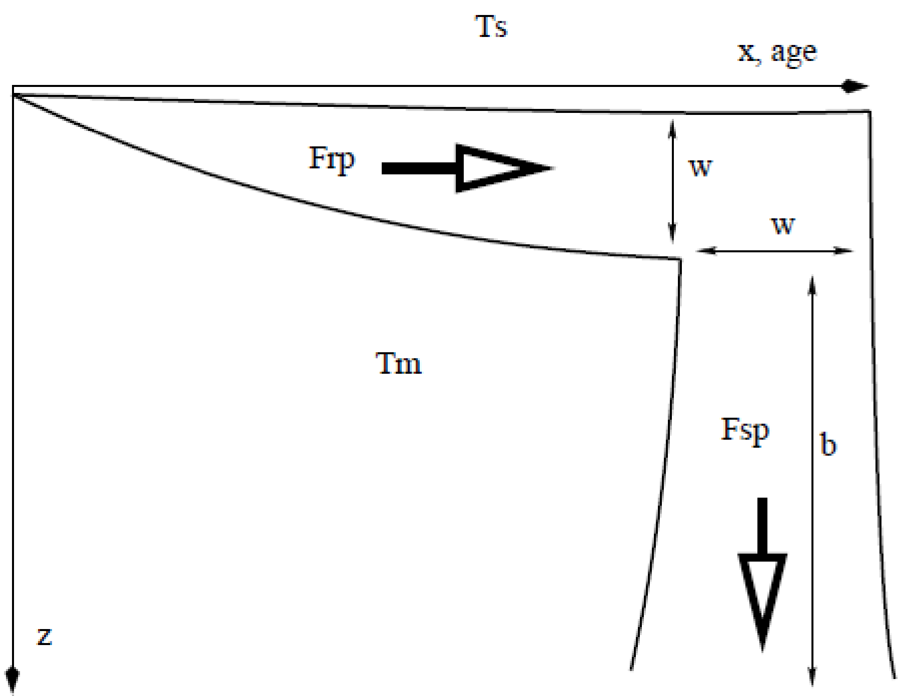

$$F_b = -2\rho_0 g \alpha b (T_m - T_s) \sqrt{\frac{\kappa t_s}{\pi}}$$

Lithospheric thickening

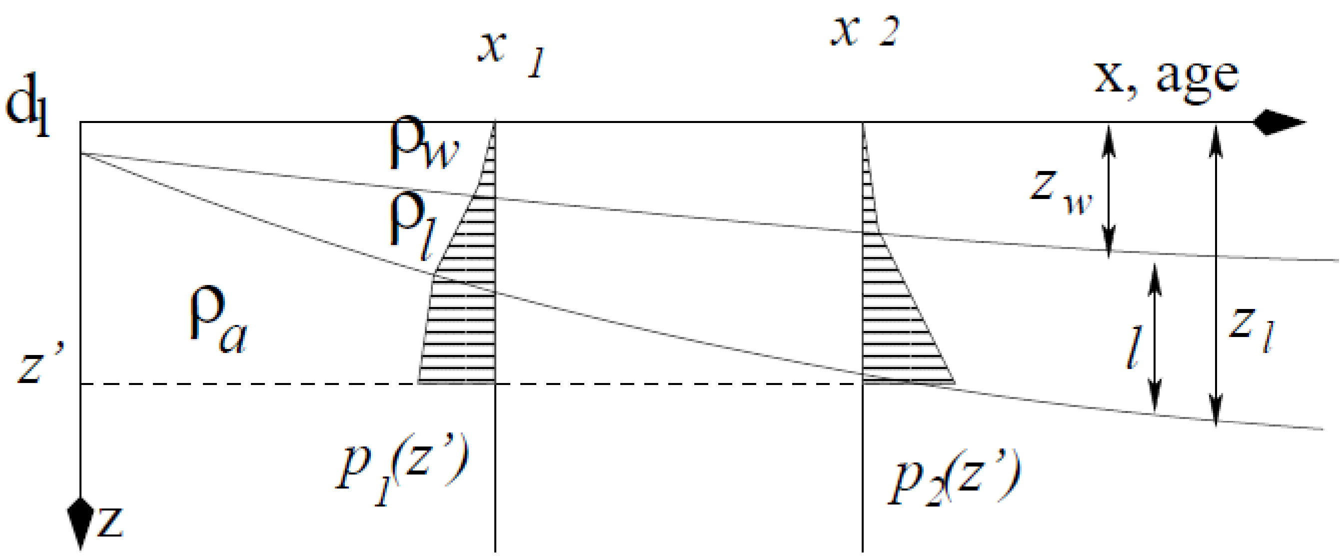

$$l = a(z_w - d_l) = a\Delta z_w \qquad a = \frac{\rho_w - \rho_a}{\rho_a - \rho_l} \qquad z_w(x) = c\sqrt{\frac{x}{u_0}}$$

$$F = \frac{ac^2}{2u_0} g \Delta\rho \Delta x$$

Force estimates from half-space cooling

- Ridge push (lithospheric thickening) ~ 10^{12} N/m
- Slab pull ~ 10^{13} N/m

Geophysical constraints on slab dynamics

Crustal velocities in plate model

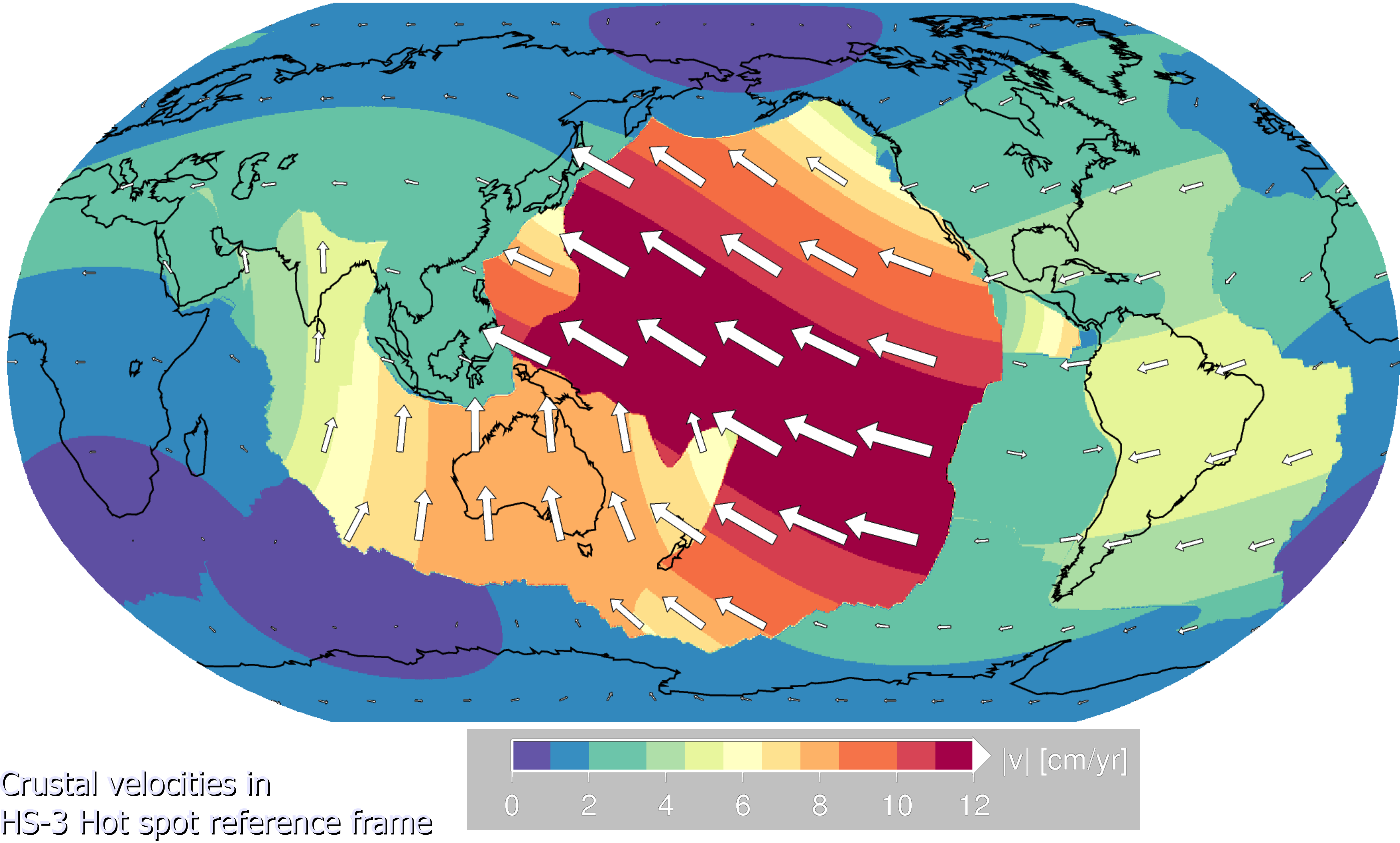

Crustal velocities in
HS-3 Hot spot reference frame

Kinematic characteristics of present-day plate tectonics

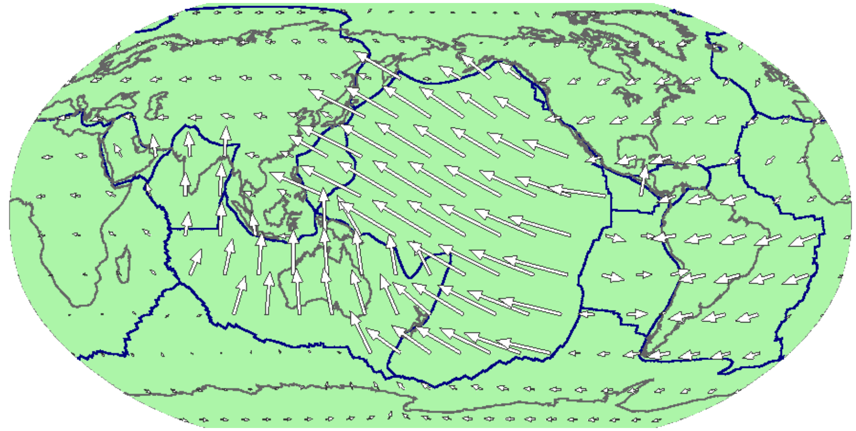

Poloidal component

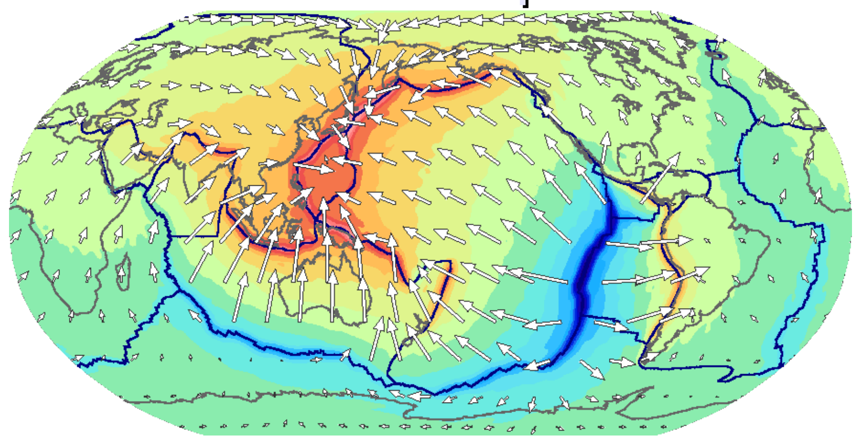

Sources and sinks

Toroidal component

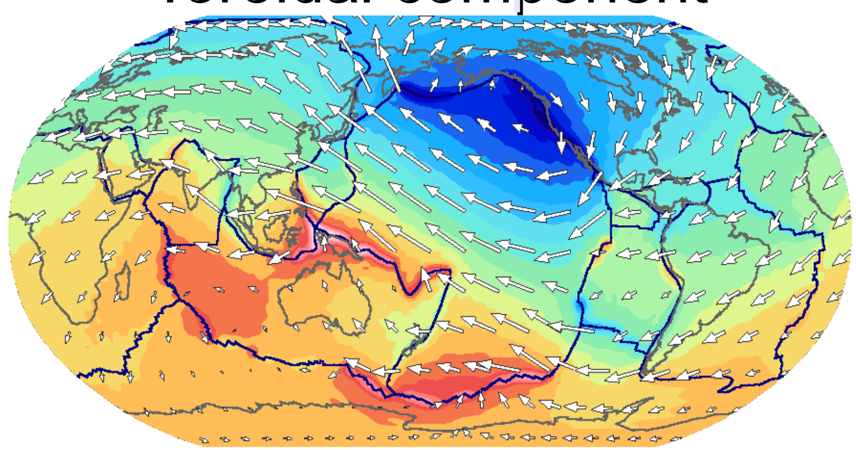

Strike slip motion,
Transform faults

Spin for l = 1
(net rotation, NR)

Time variability in plate motions (and heat transport)

Plate reconstruction A: Mueller et al. (2008)

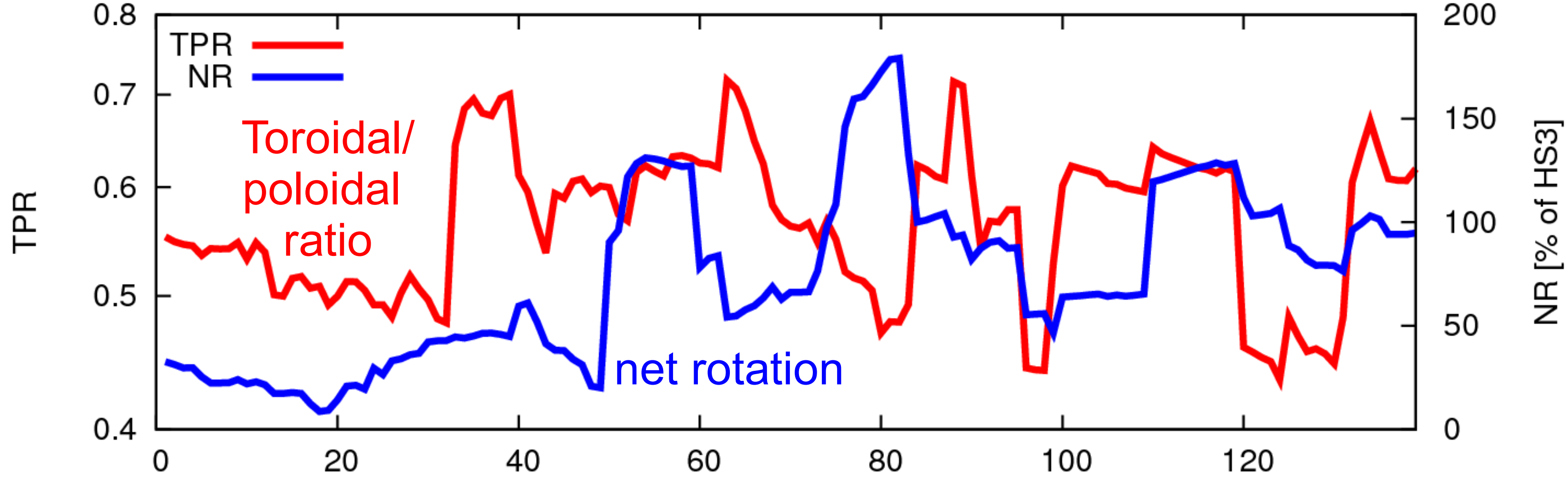

Plate reconstruction B: Lithgow-Bertelloni et al. (1993)

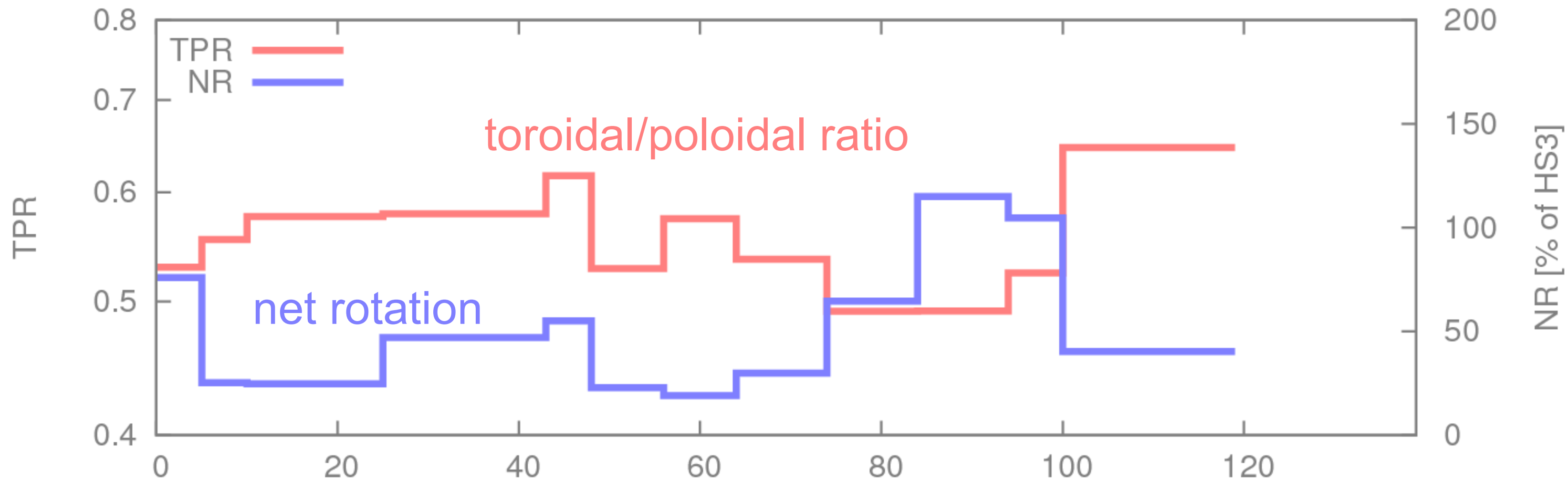

Seismicity constraints

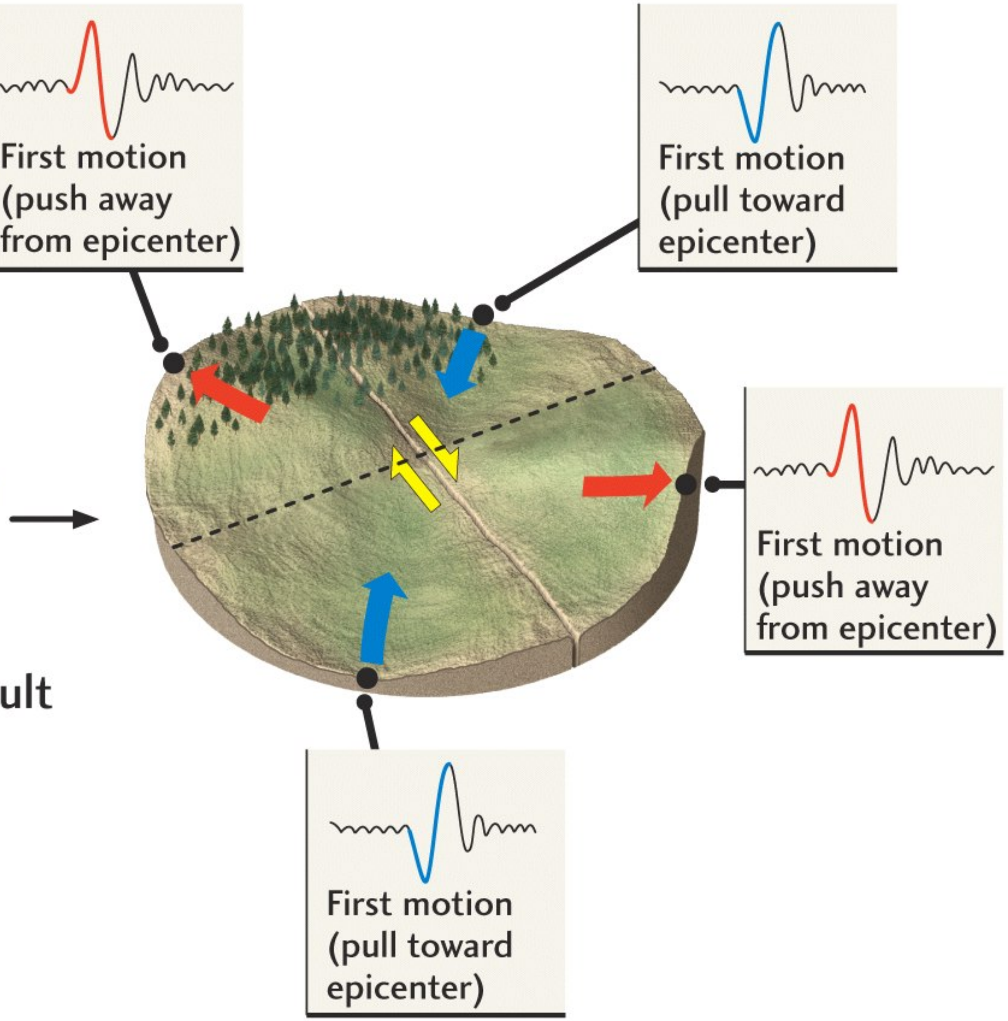

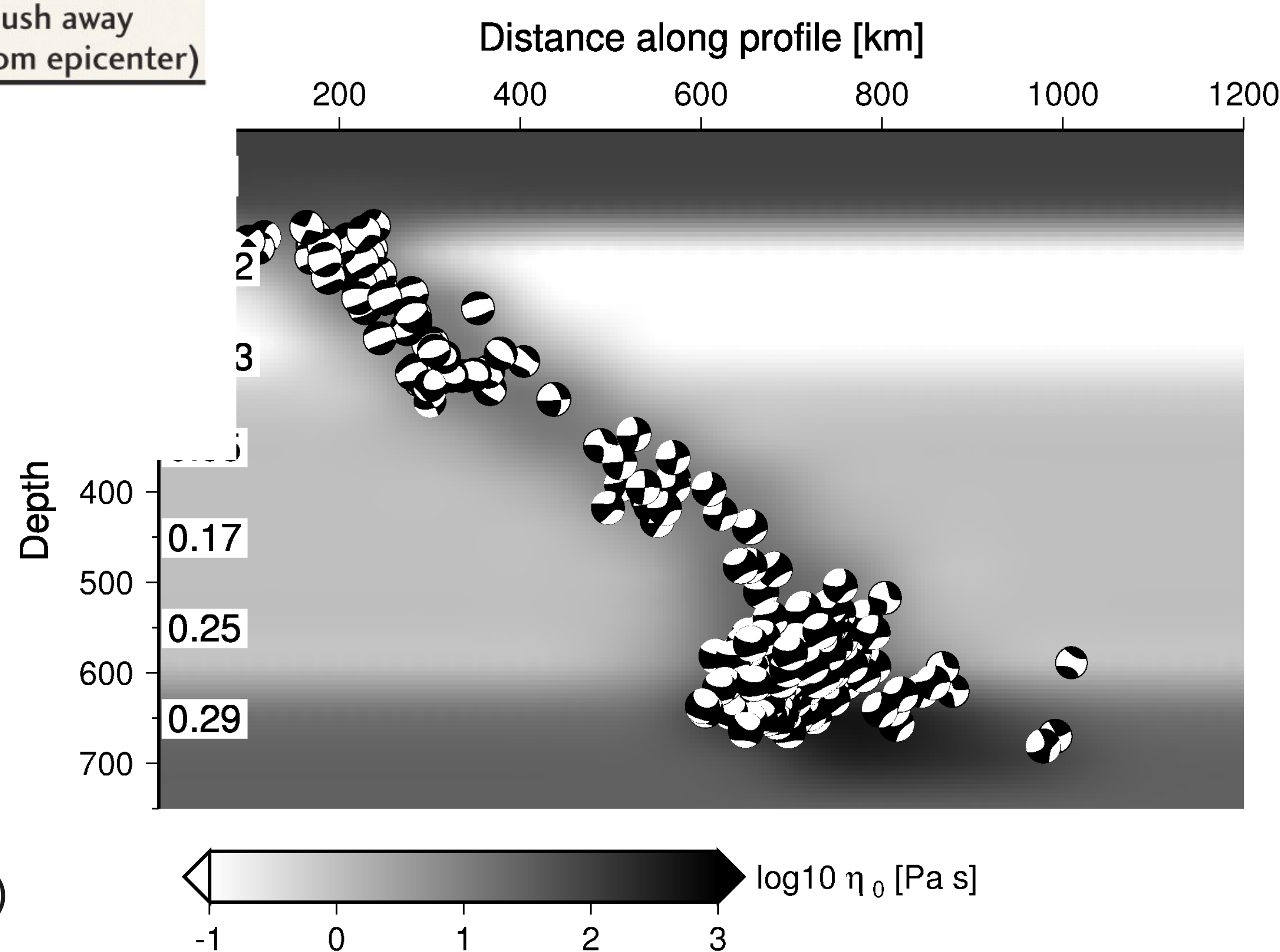

Alpert et al. (2010)

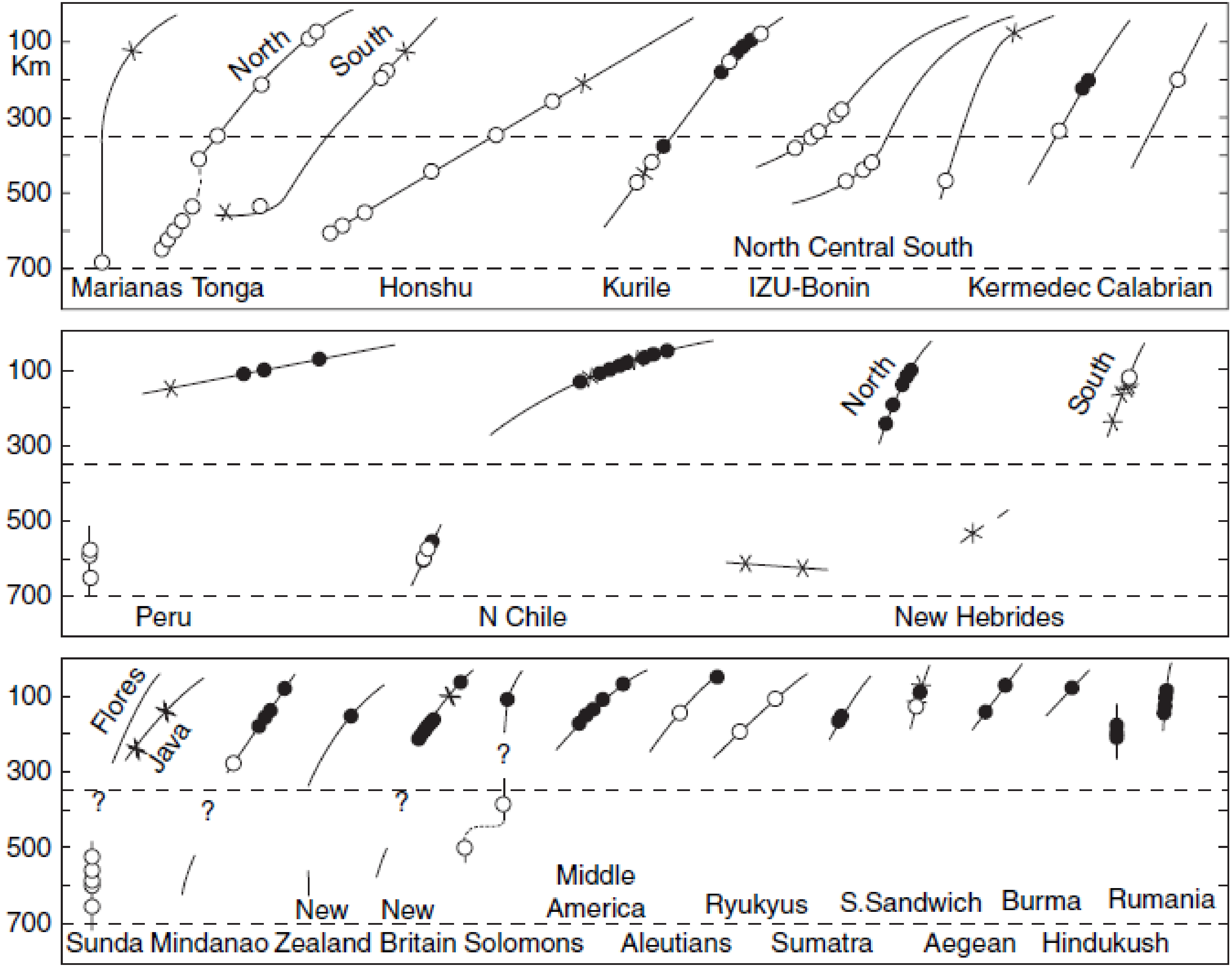

Isacks and Molnar (1971)

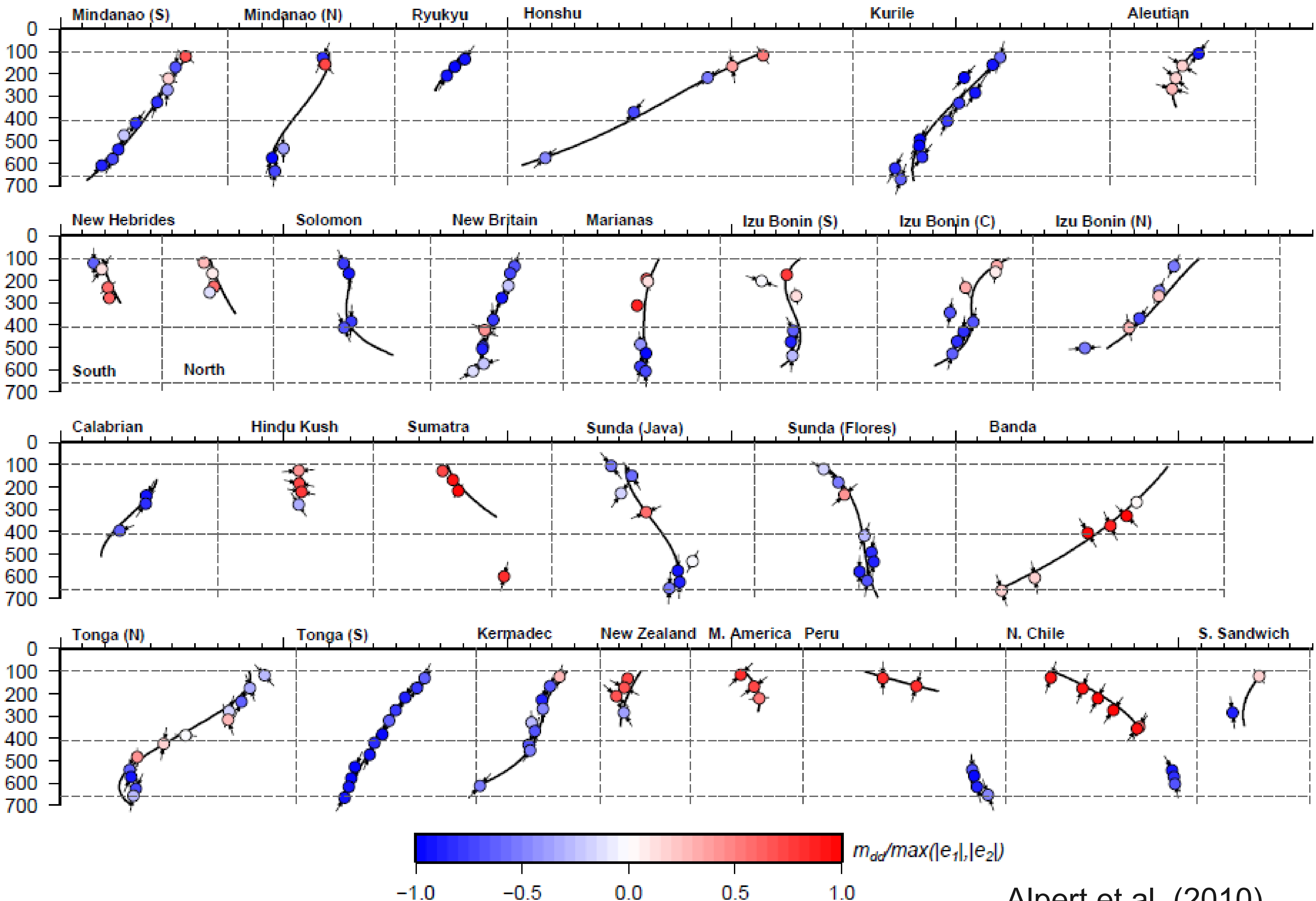

Alpert et al. (2010)

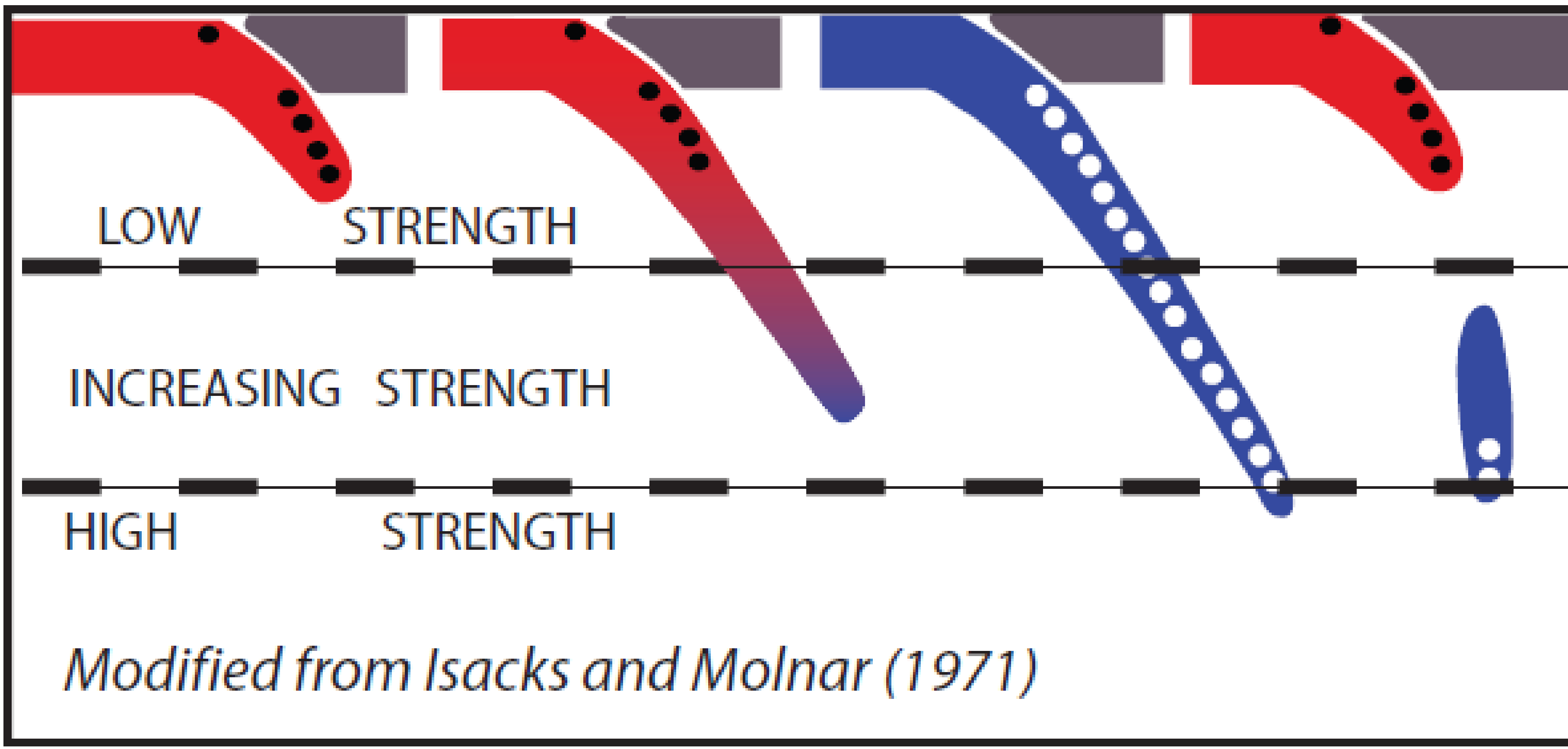
LOW STRENGTH
INCREASING STRENGTH
HIGH STRENGTH
Modified from Isacks and Molnar (1971)

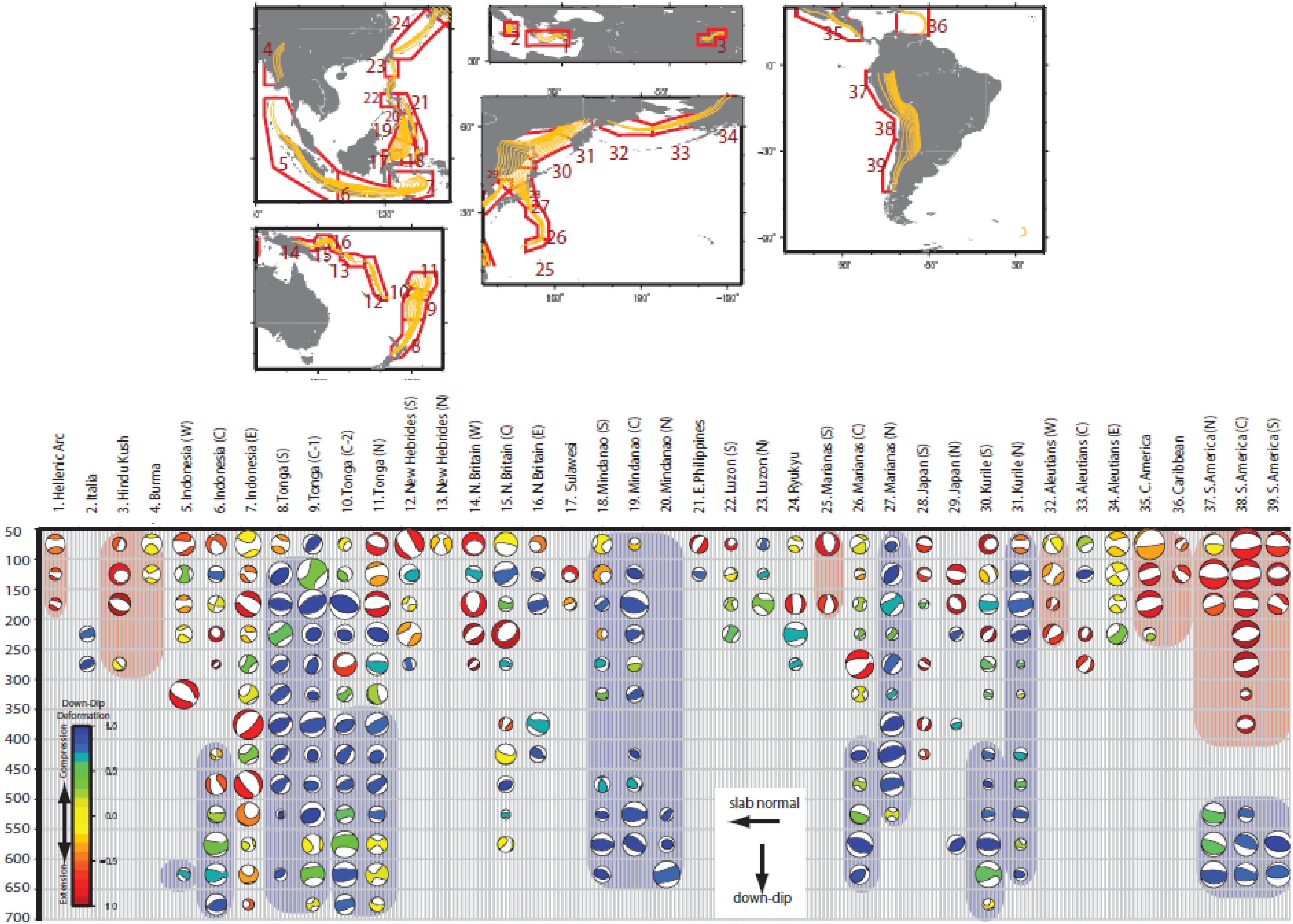

Alpert et al. (in prep)

Structural seismology
Seismic waves

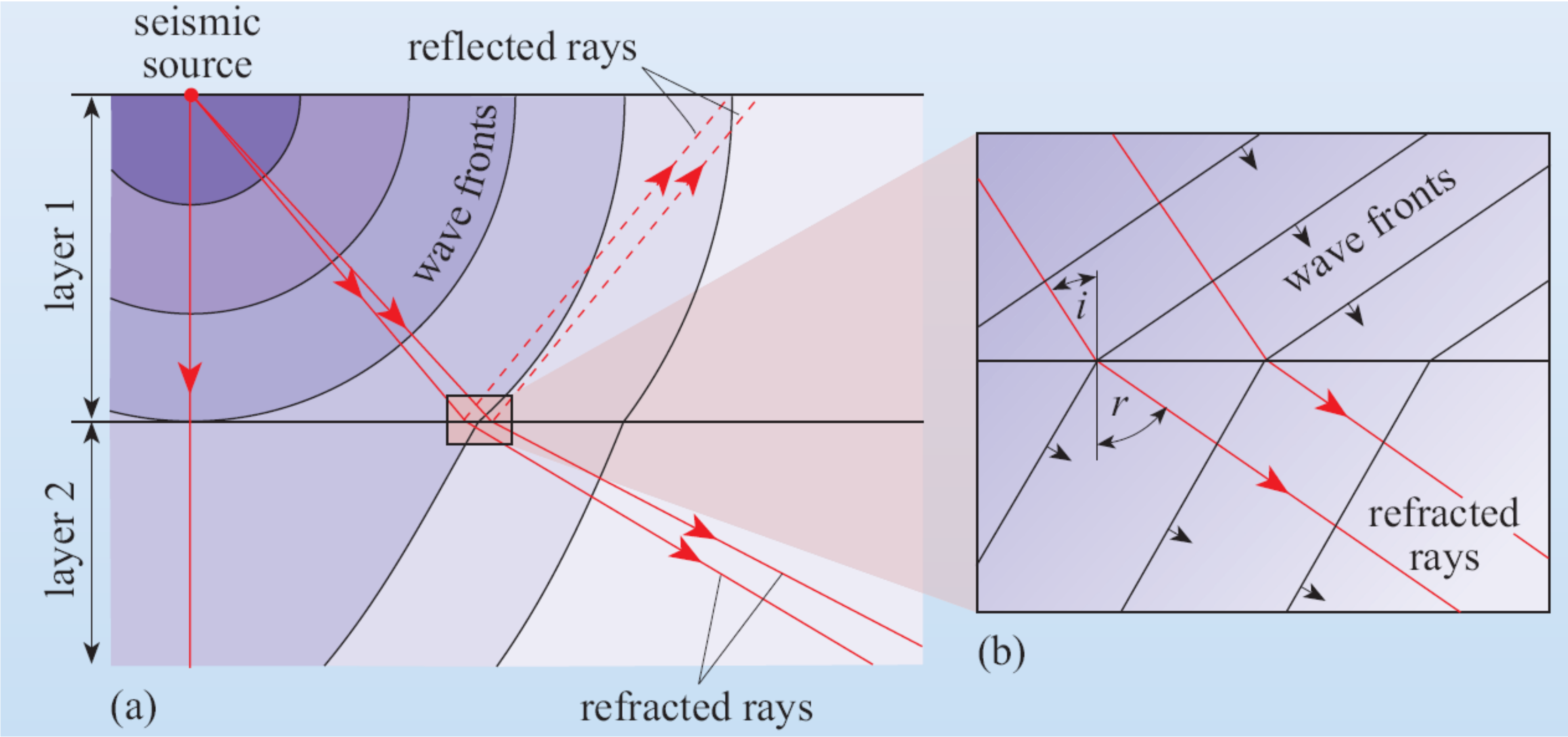

Seismic phases

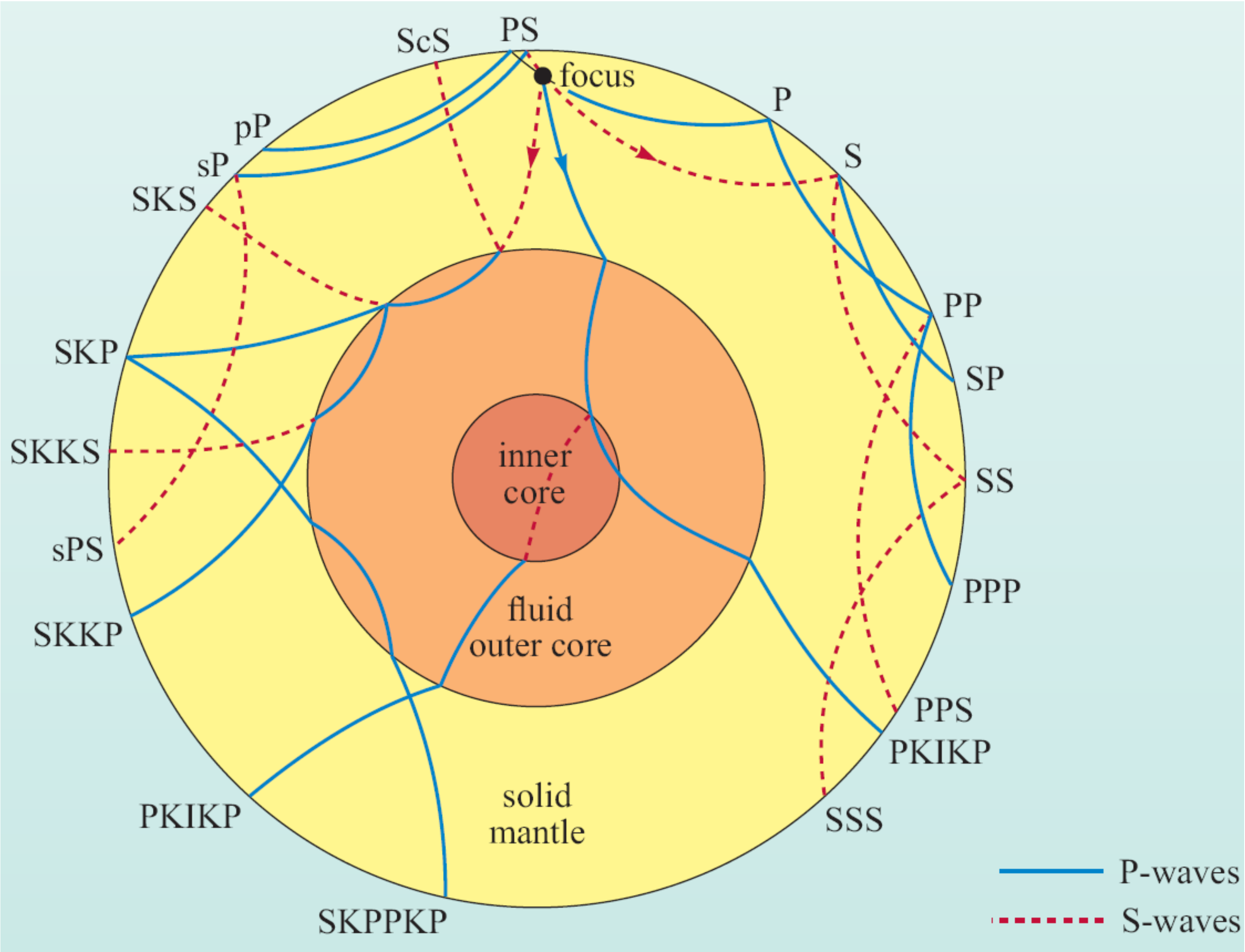

PREM - Preliminary Earth Reference model (1981)

based on travel times, surface wave dispersion curves, normal mode frequencies, constraints on mass and moment of inertia + some constraints on V_P-ρ relation.

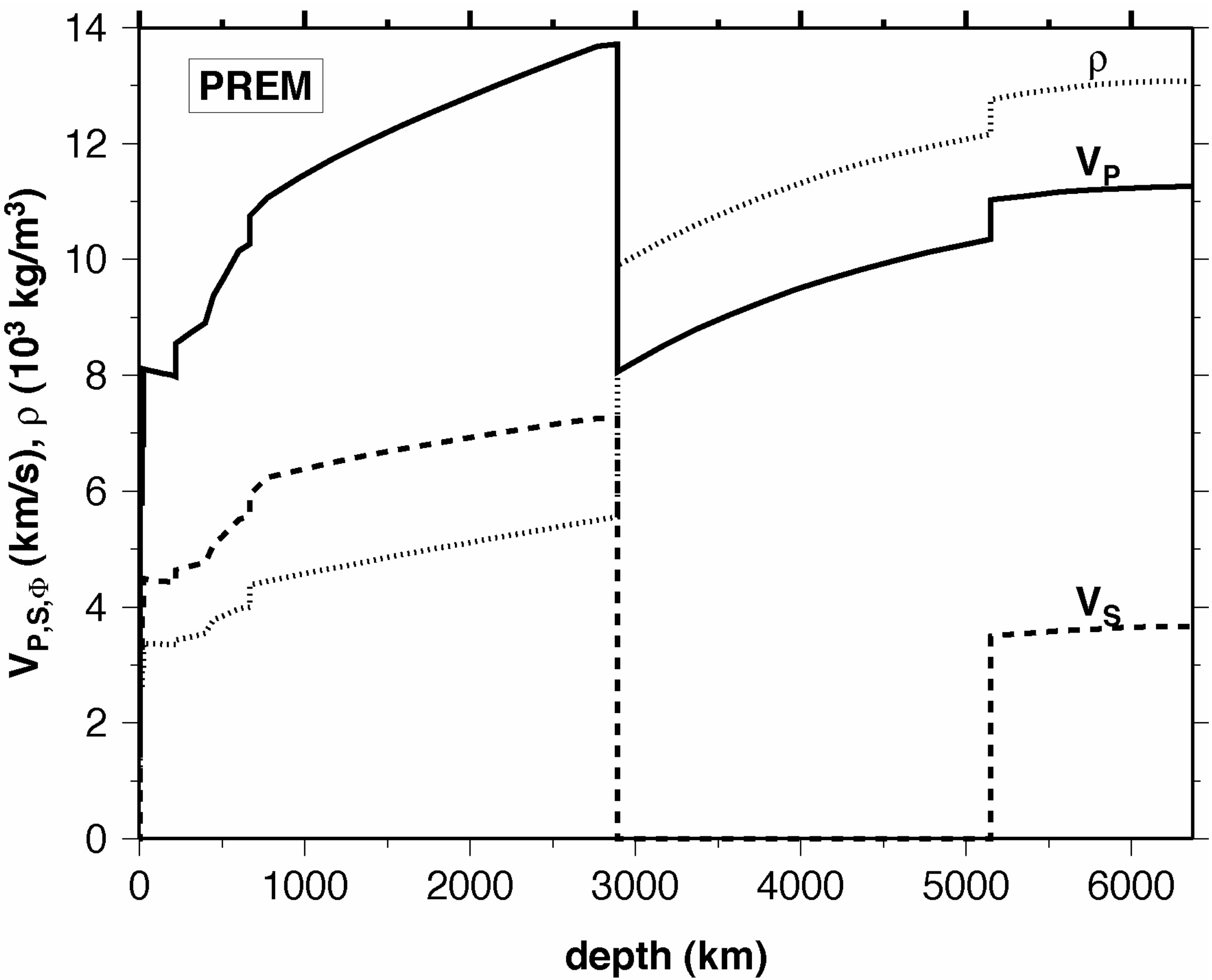

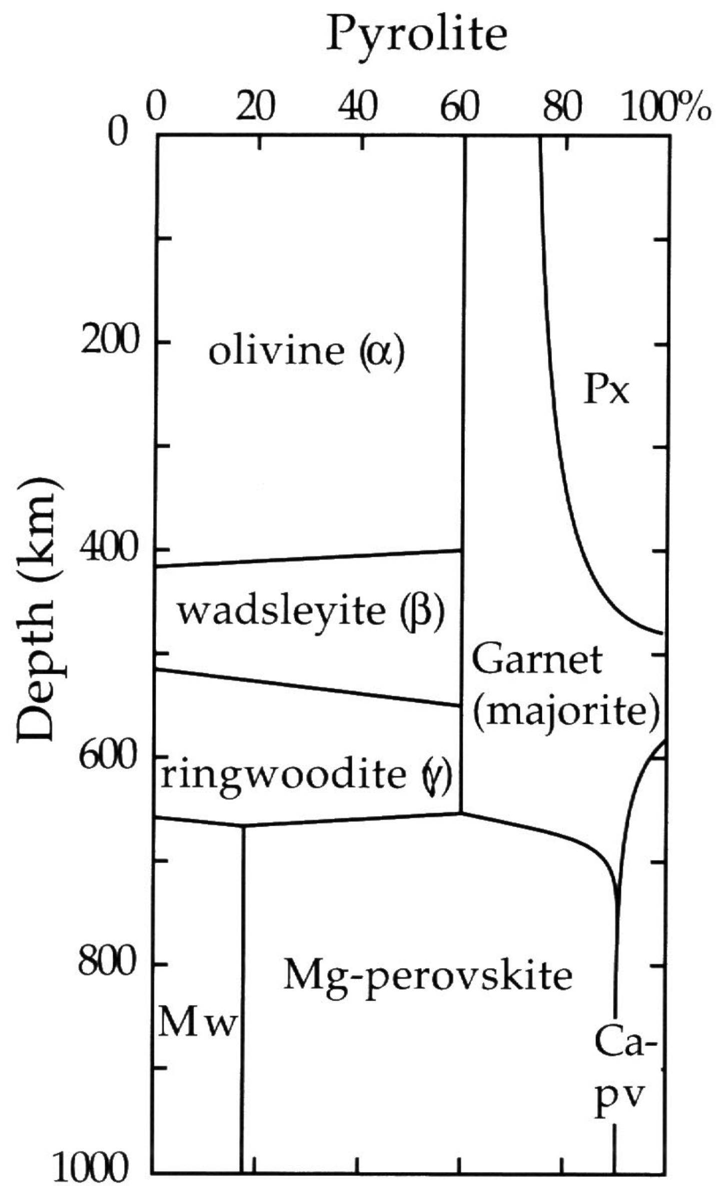

Figure 5.8. Sequence of pressure-induced transformations and reactions as a function of depth in a mantle of pyrolite composition. Px: pyroxene, Mw: magnesiowüstite, pv: perovskite. After Irifune [44].

from Davies (1999)

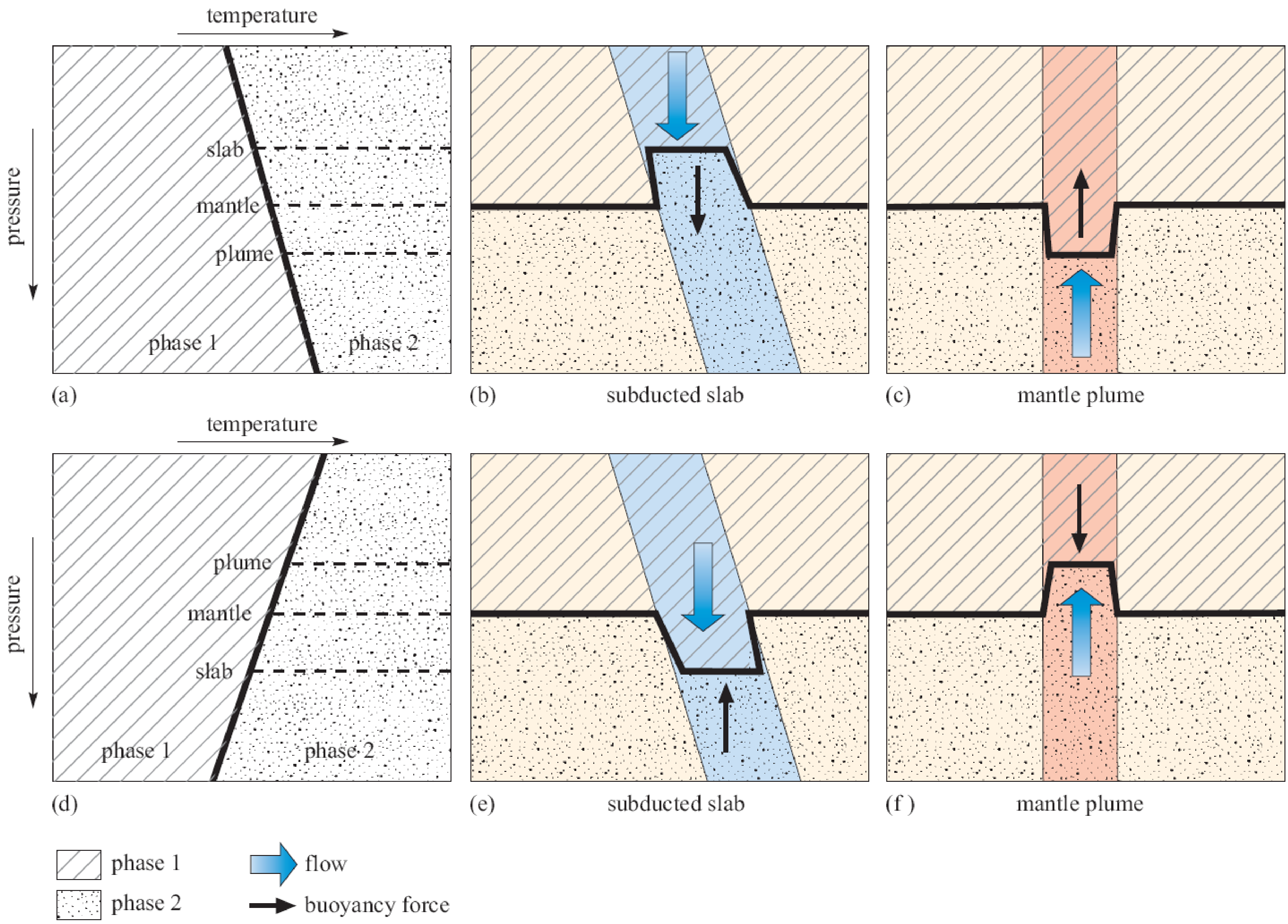
temperature
pressure
slab
mantle
plume
phase 1
phase 2
(a)
(b) subducted slab
(c) mantle plume
temperature
pressure
plume
mantle
slab
phase 1
phase 2
(d)
(e) subducted slab
(f) mantle plume
phase 1
phase 2
flow
buoyancy force

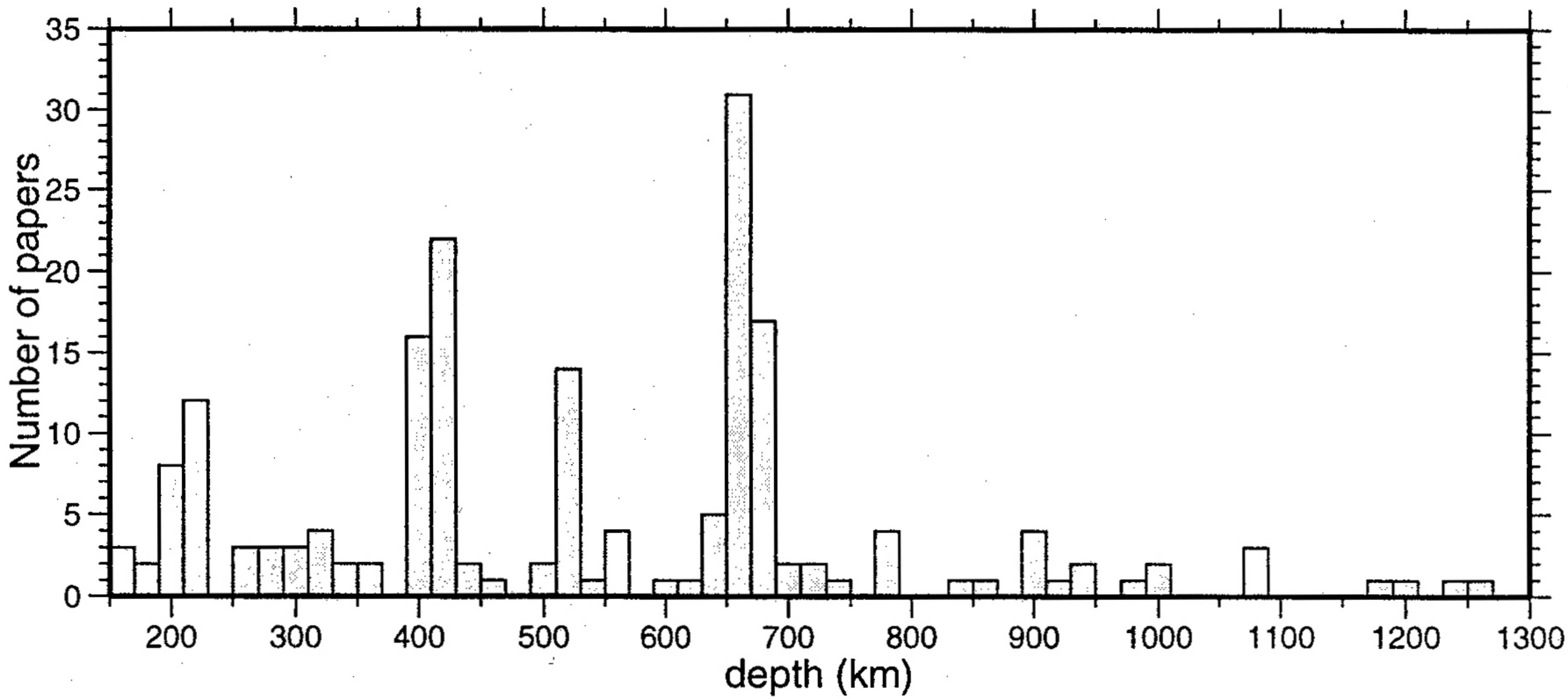
Number of papers
35
30
25
20
15
10
5
0
200
300
400
500
600
700
800
900
1000
1100
1200
1300
depth (km)

Deuss (2002)

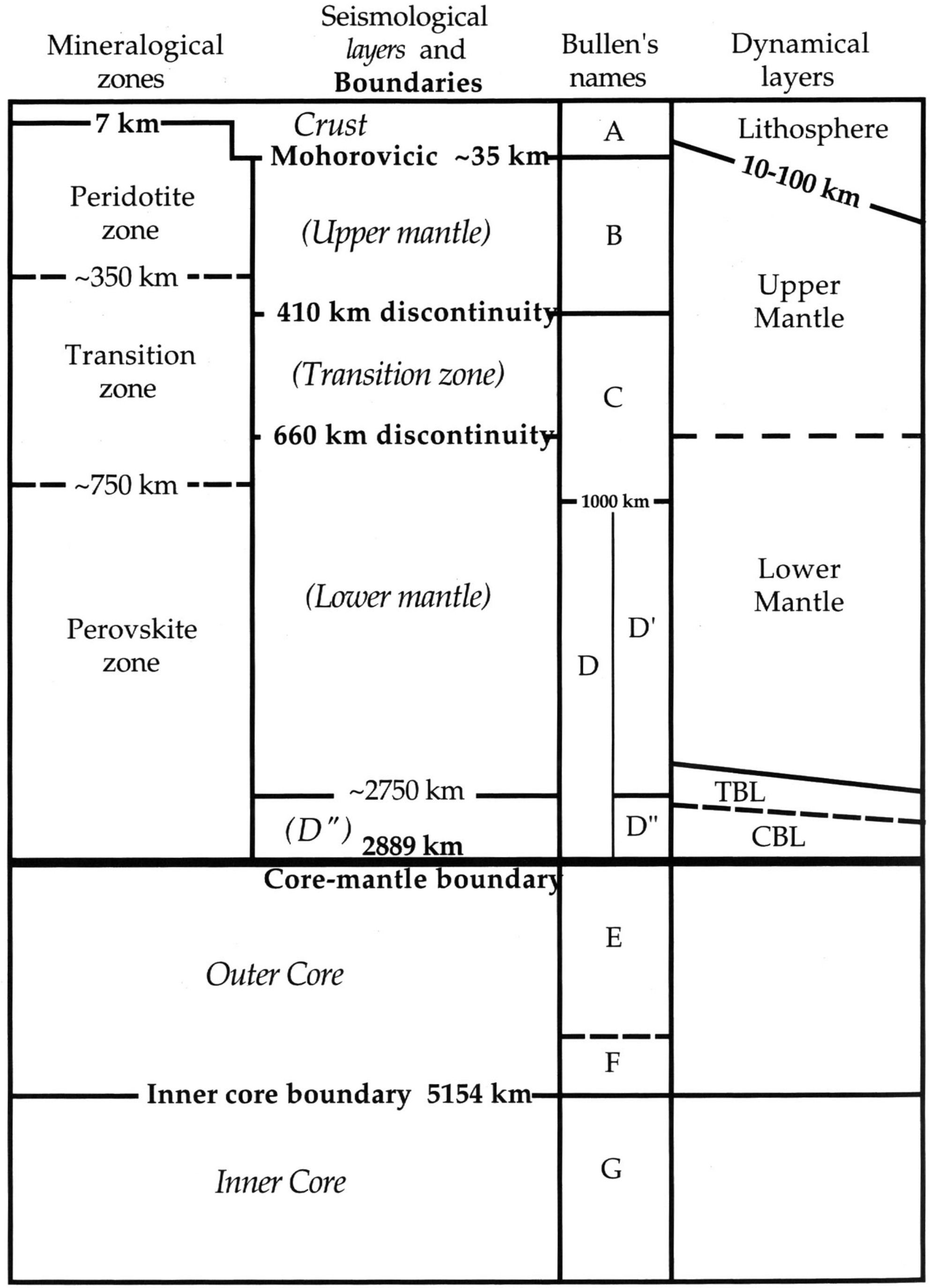

Figure 5.2. A partial terminology of mantle layers that distinguishes the different concerns and usages of mineral physics, seismology and dynami
TBL: thermal boundary layer; CBL: chemical boundary layer.

from Davies (1999)

SS precursors

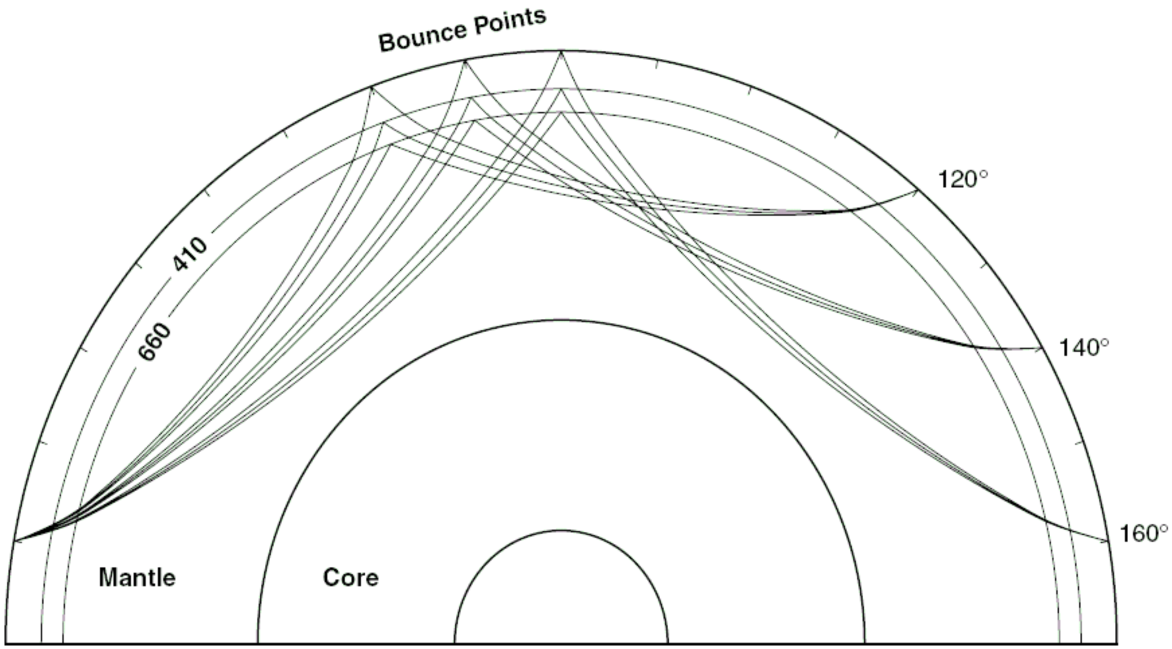

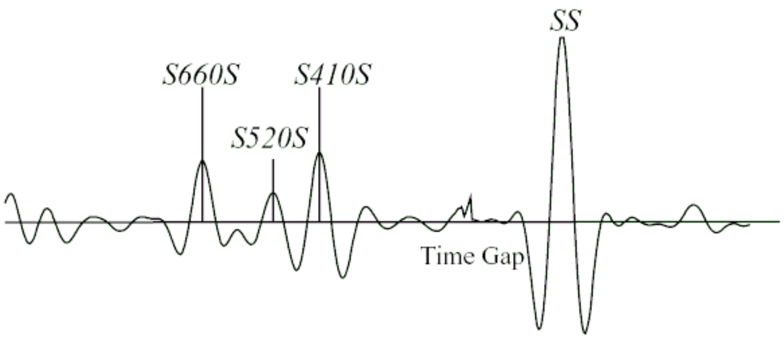

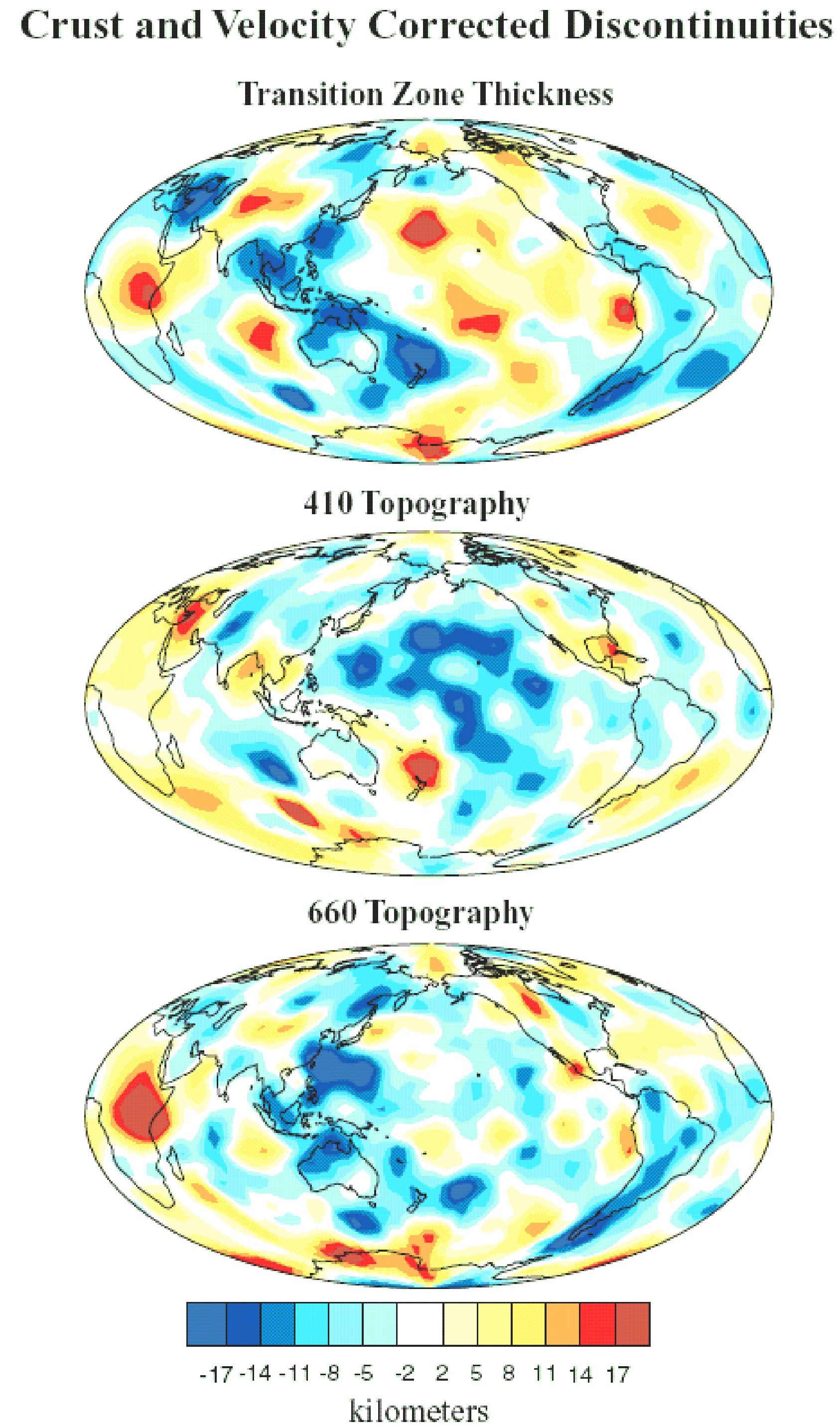

Houser et al. (2008)

A modified set of forces

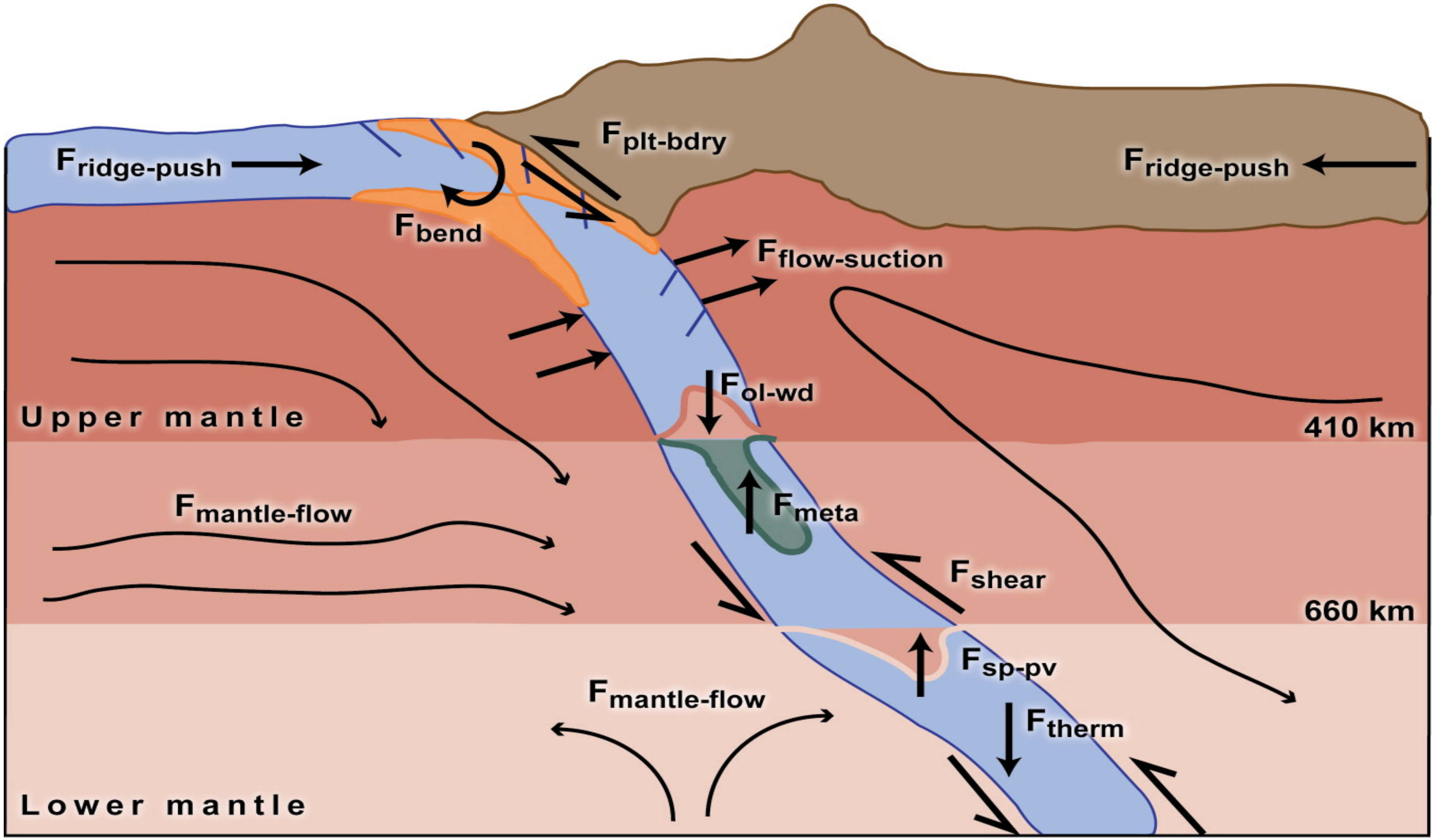

Billen MI. 2008.
Annu. Rev. Earth Planet. Sci. 36:325–56.

Figue courtesy of M. Billen

Seismic tomography

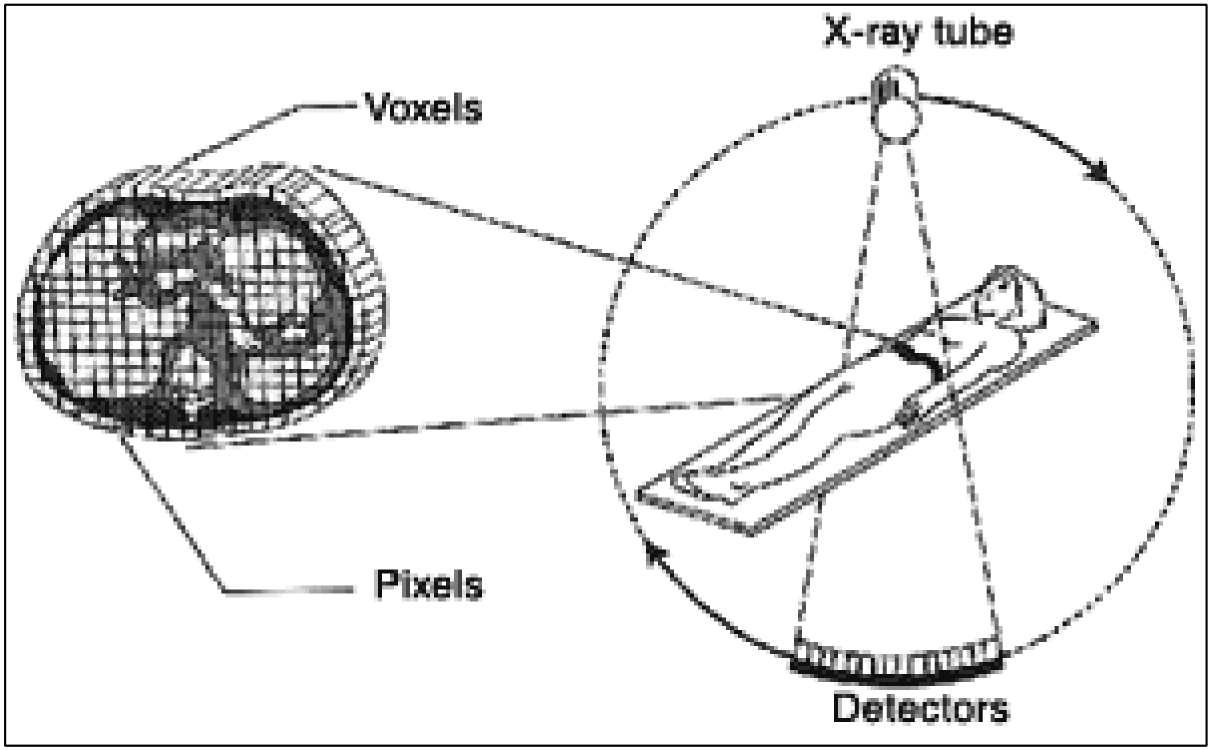

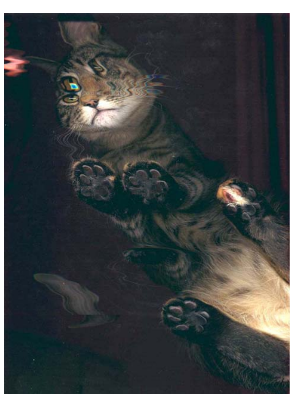

- CAT-scan like technique
- Earthquakes : sources Seismometers : receivers
- Measure travel times to invert for 3-D velocity structure

Theory of linear, ray tomography

Travel time *t* of a ray given by integral over slowness *p* = 1/*v* along path *s*

$$t = \int_{\text{path}} p\,[r(s), \theta(s), \phi(s)]\,ds$$

Travel time anomaly δt from reference model given by slowness perturbations δp, same path

$$\delta t = \int_{\text{path}} \delta p\,[r(s), \theta(s), \phi(s)]\,ds$$

Choose *n* basis functions for parameterization

$$\delta p(r, \theta, \phi) = \sum_{i=1}^{n} \delta p_i f_i(r, \theta, \phi)$$

Evaluate path integral for every δt observation for *m* number of observations

$$\delta t = \sum_{i=1}^{n} \delta p_i \int_{\text{path}} f_i\,[r(s), \theta(s), \phi(s)]\,ds$$

$$\delta t_j = \sum_{i=1}^{n} \delta p_i \int_{\text{path}_j} f_i\,[r(s), \theta(s), \phi(s)]\,ds \quad (j = 1, ..., m)$$

Write in matrix form, A is *m* x *n*, solve

$$A_{ji} = \int_{\text{path}_j} f_i\,[r(s), \theta(s), \phi(s)]\,ds \qquad \mathsf{A} \cdot \mathsf{x} = \mathsf{d}$$

For *m* > *n*, system is overdetermined (and δt has errors), solve in least squares sense, $(A^T A)^{-1}$ is the “general inverse”

$$||\mathsf{A} \cdot \mathsf{x} - \mathsf{d}|| = \min \iff \mathsf{x} = \mathsf{x}_{LS} \qquad \mathsf{A}^T \cdot \mathsf{A} \cdot \mathsf{x} = \mathsf{A}^T \cdot \mathsf{d} \qquad \mathsf{x}_{LS} = \left(\mathsf{A}^T \cdot \mathsf{A}\right)^{-1} \cdot \mathsf{A}^T \cdot \mathsf{d}$$

Tomographic problems typically ill-conditioned, introduce regularization (“damping”):

$$\mathsf{B} \cdot \mathsf{x} = \mathsf{c} \qquad \begin{bmatrix} \mathsf{A} \\ \lambda \mathsf{B} \end{bmatrix} \cdot \mathsf{x} = \begin{bmatrix} \mathsf{d} \\ \lambda \mathsf{c} \end{bmatrix} \qquad \mathsf{x}_{LS} = \left[\mathsf{A}^T \cdot \mathsf{A} + \lambda^2 \mathsf{B}^T \cdot \mathsf{B}\right]^{-1} \cdot \left[\mathsf{A}^T \cdot \mathsf{d} + \lambda^2 \mathsf{B}^T \cdot \mathsf{c}\right]$$

Tomography example

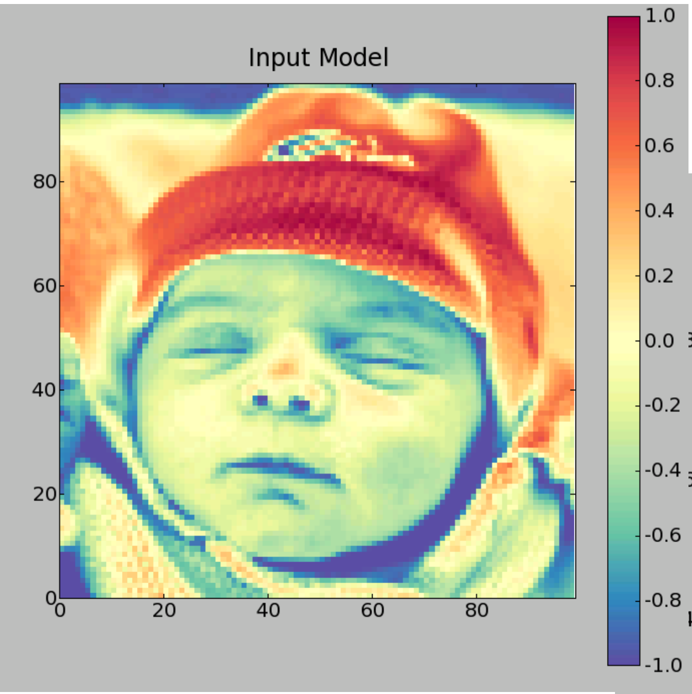

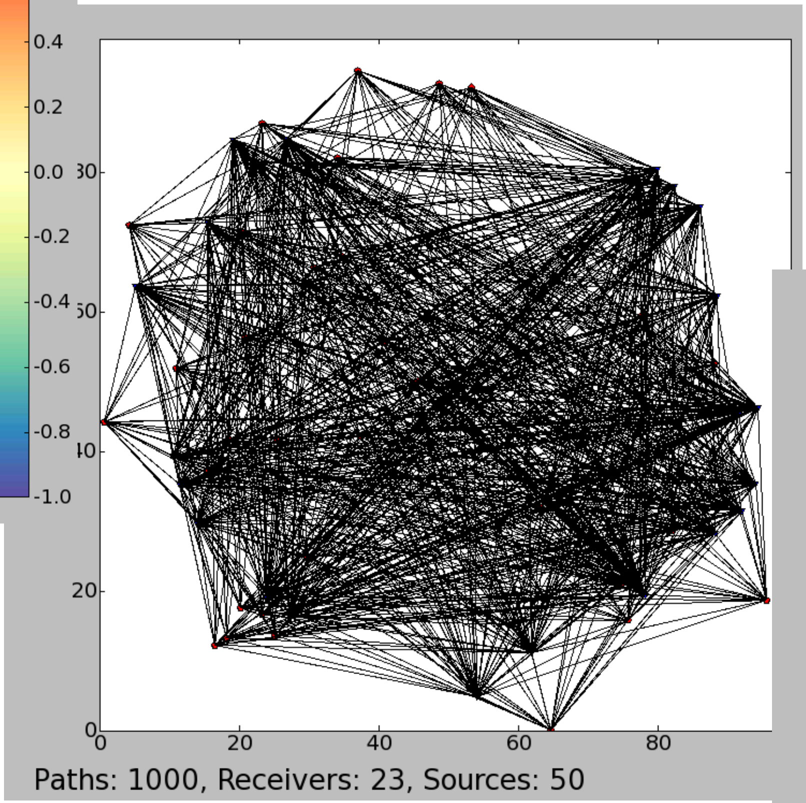

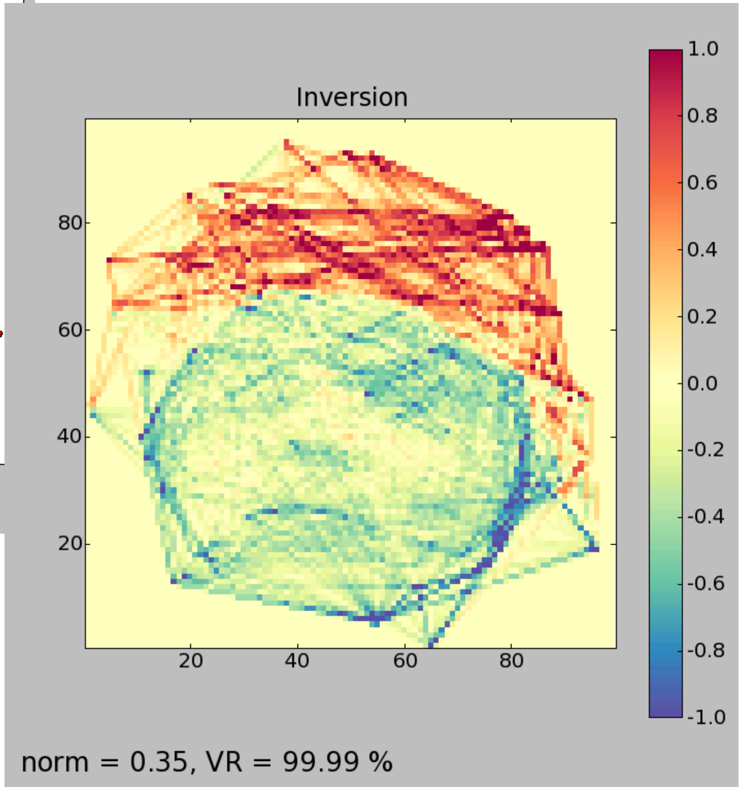

Milner et al. (2009)

P wave tomography

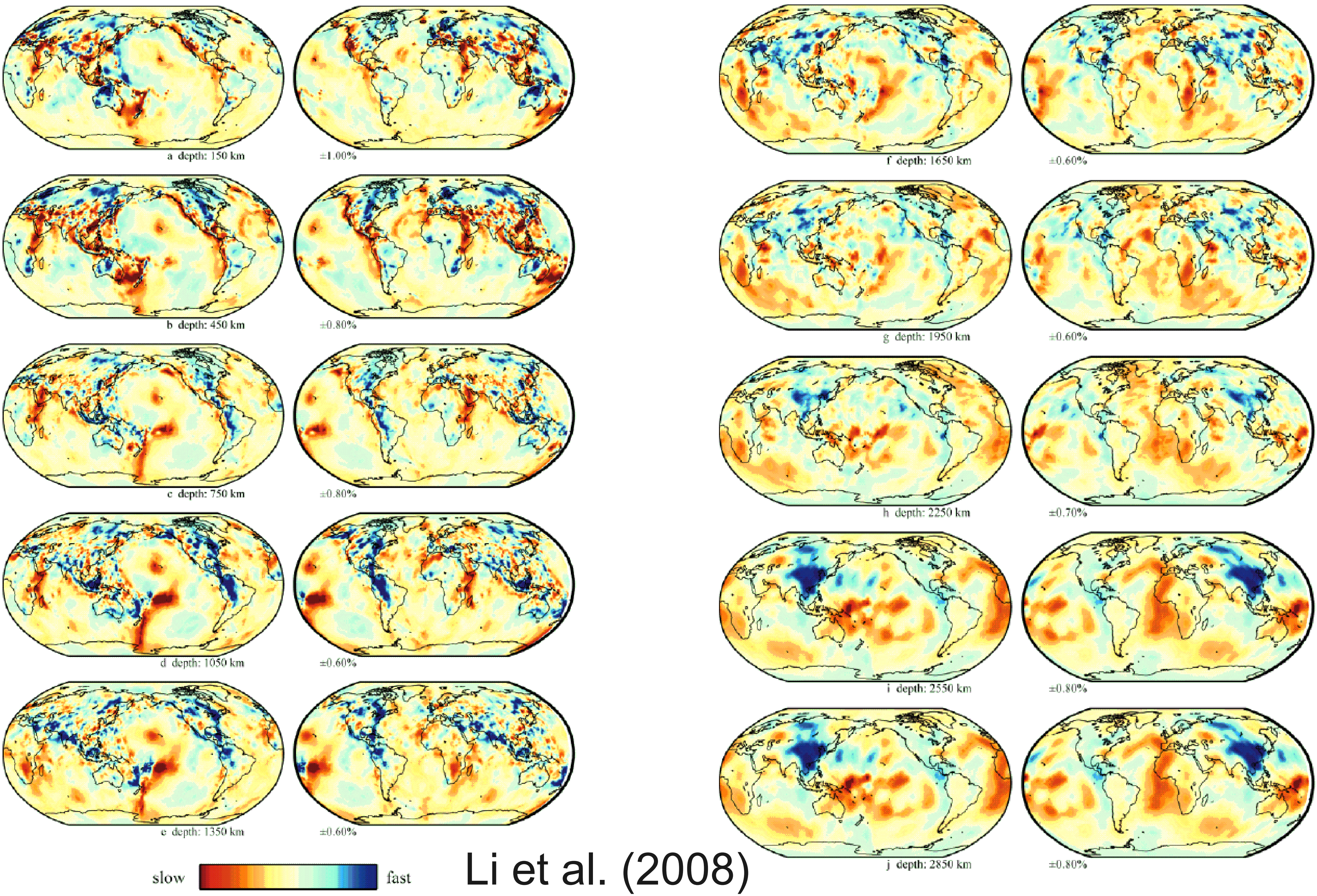

Li et al. (2008)

S wave tomography

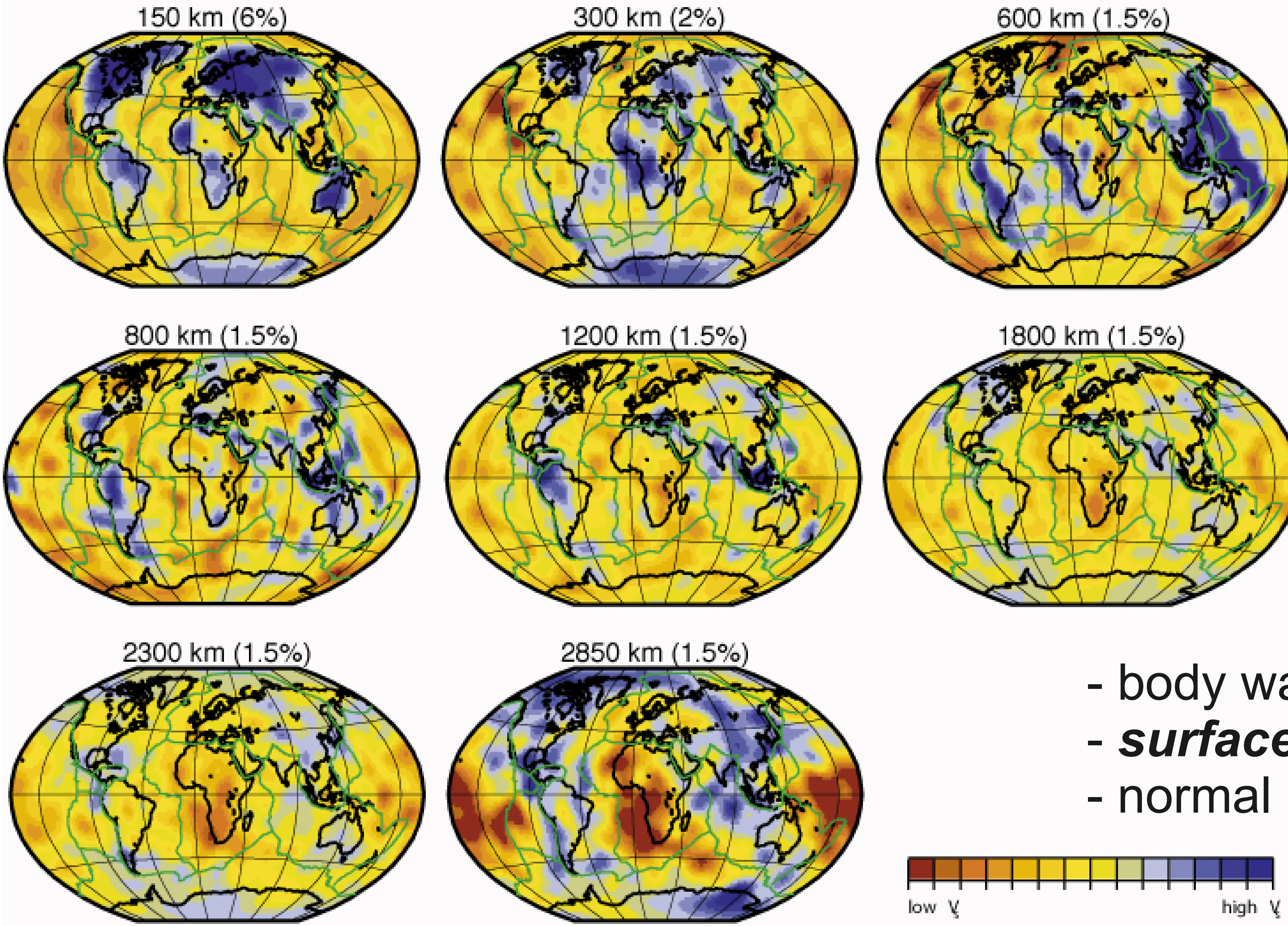

Figure 8: Depth slices through S20RTS. High (relatively to PREM) shear velocity regions are indicated by blue and red colours, respectively, with an intensity that is proportional to the amplitude of the shear velocity perturbations. The range of shear velocity variation (in %) is given above each map. Green lines represent plate boundaries.

- body waves
- ***surface waves***
- normal modes

Ritsema et al. (2000)

Slabs in the lower mantle

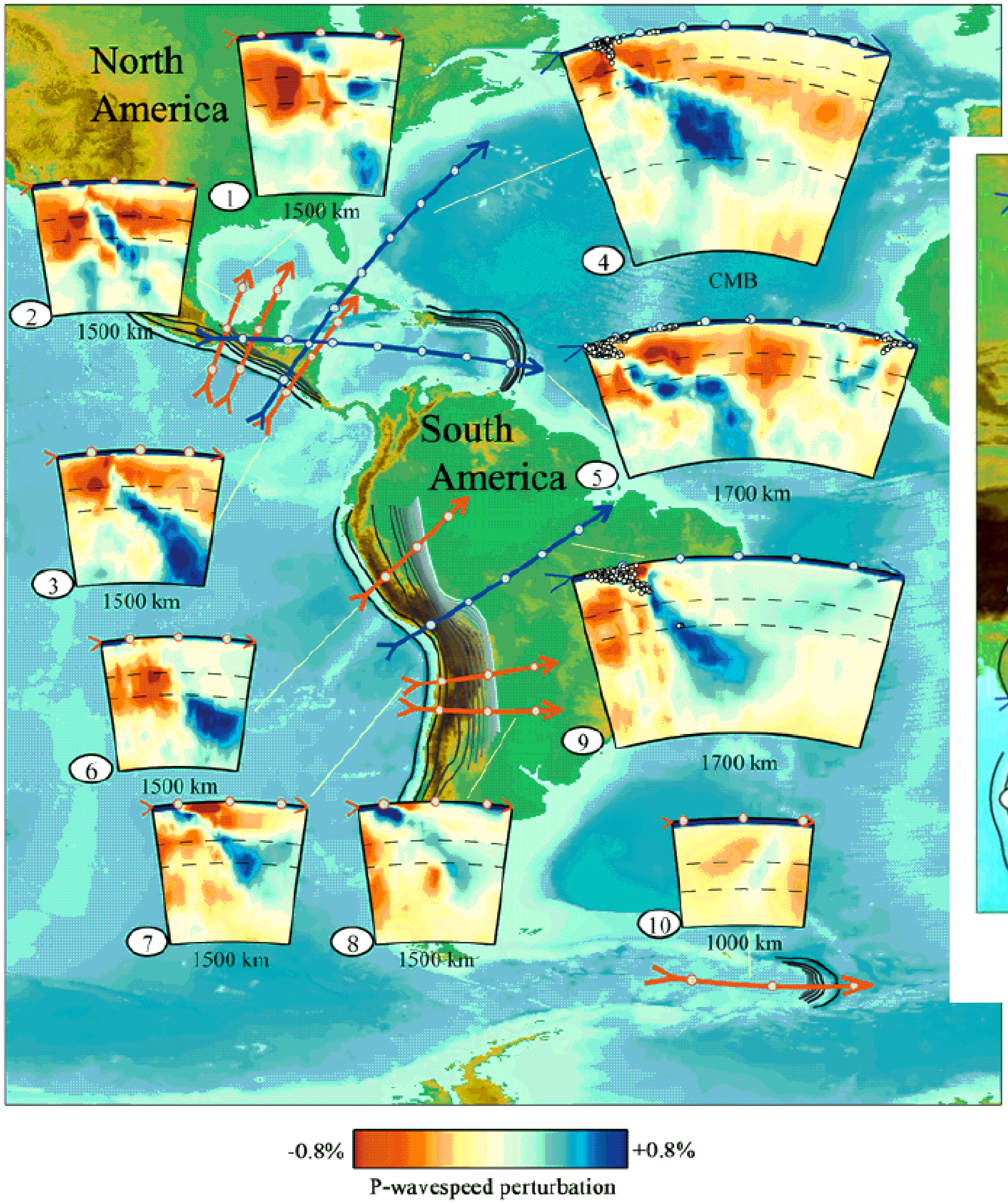

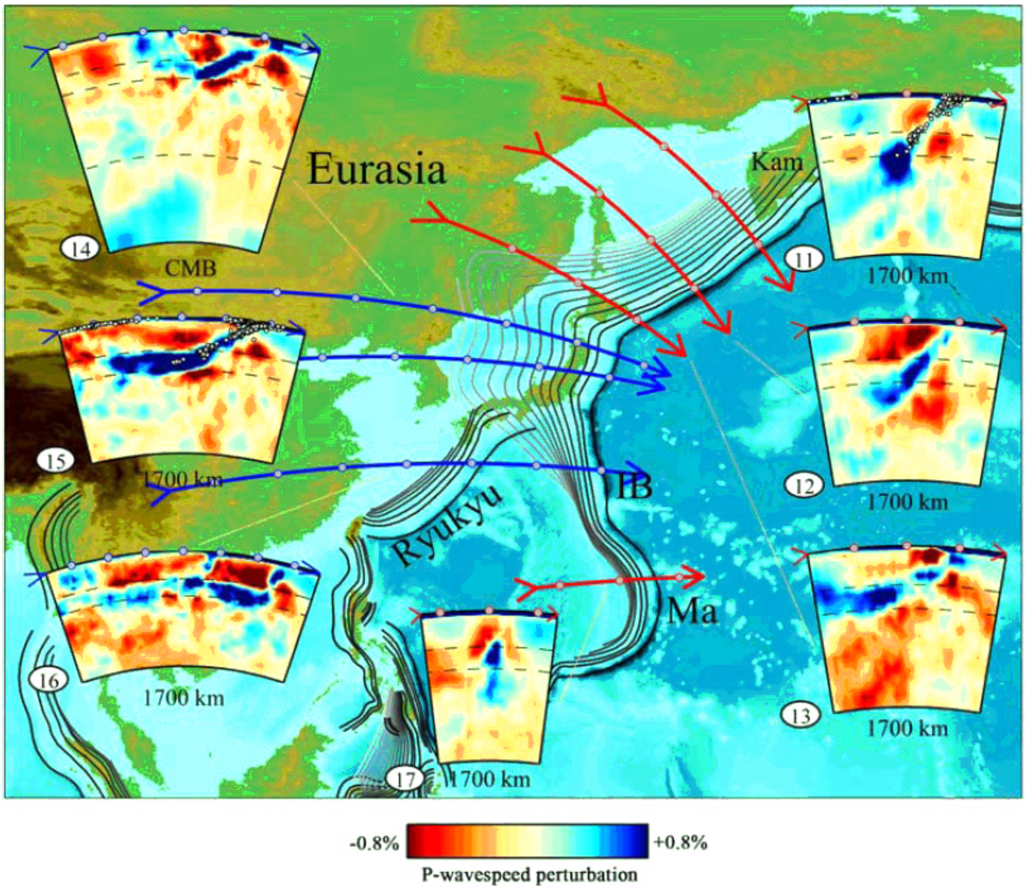

Li et al. (2008)

Damping and L curves

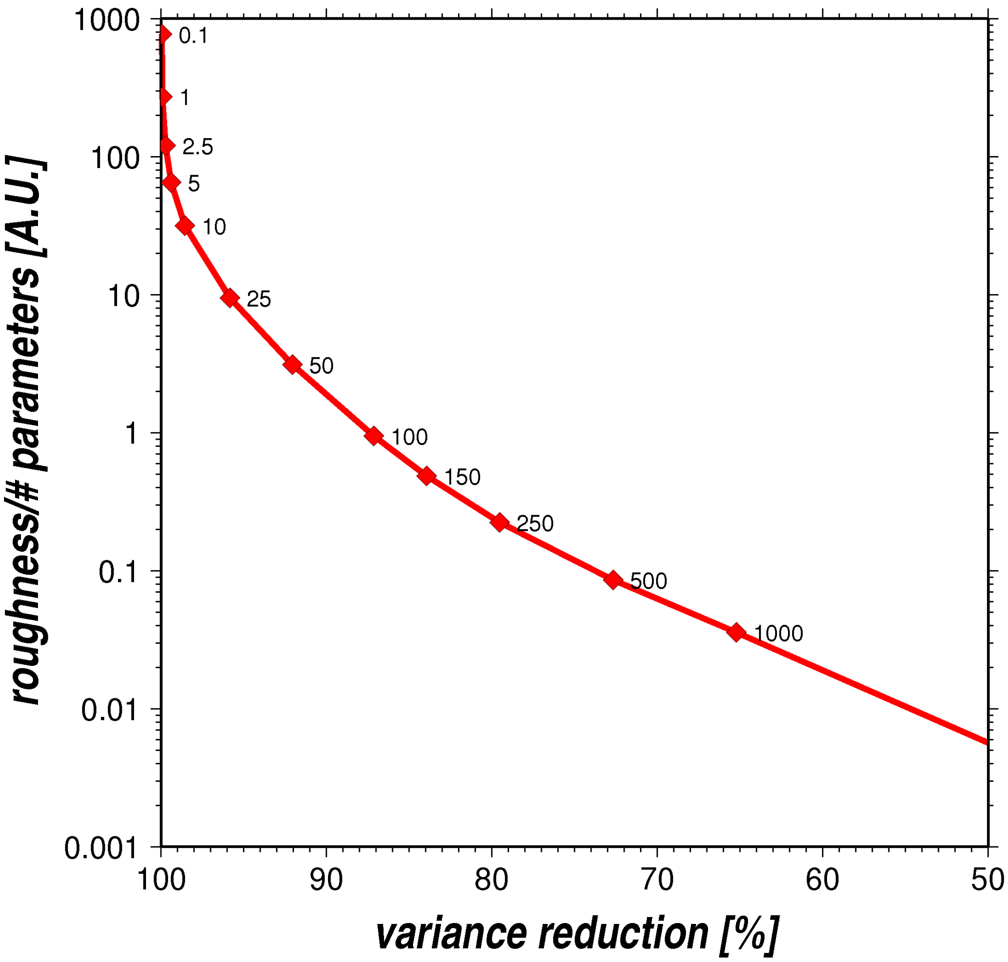

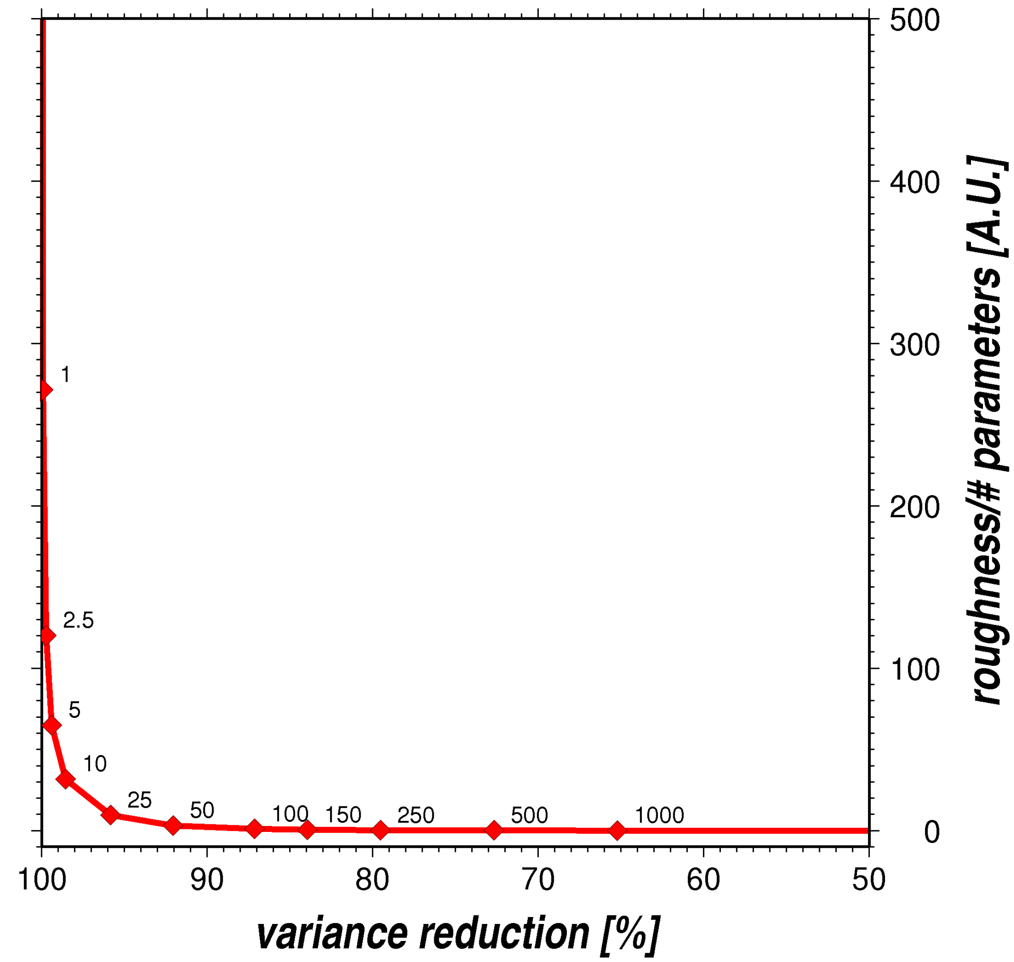

Damping and L curves

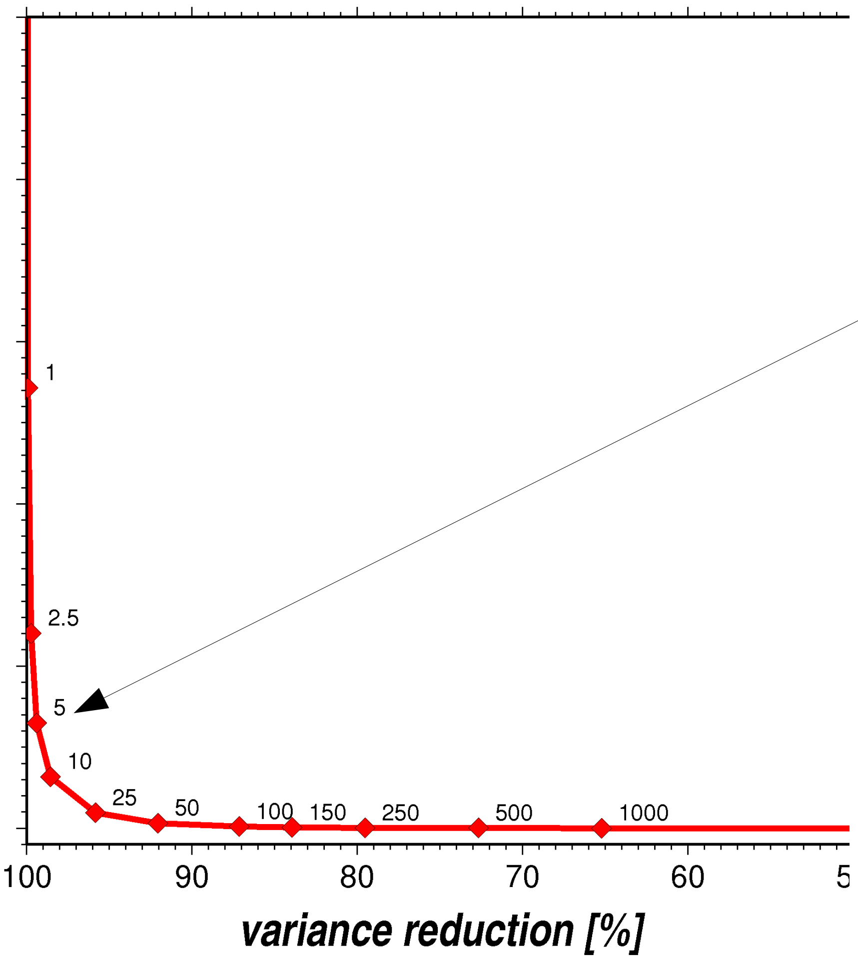

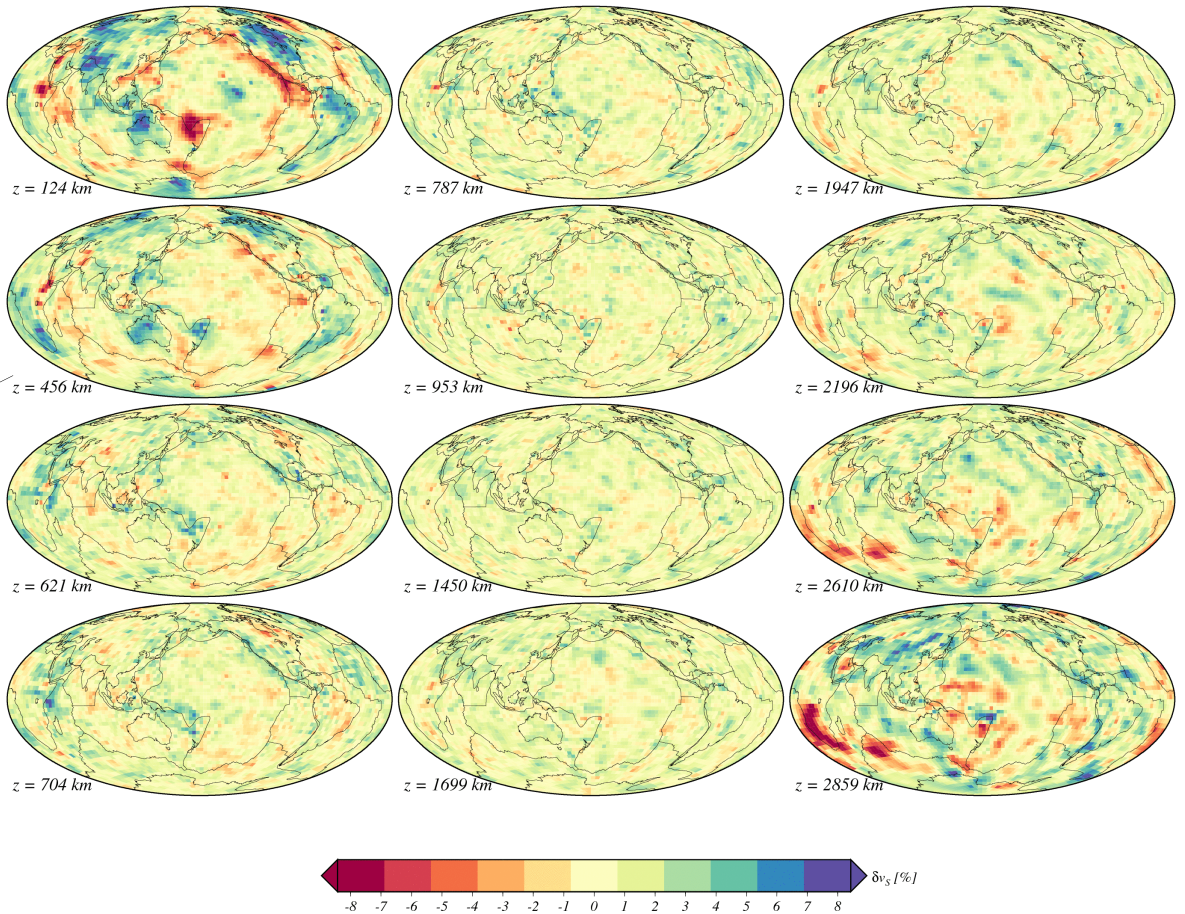

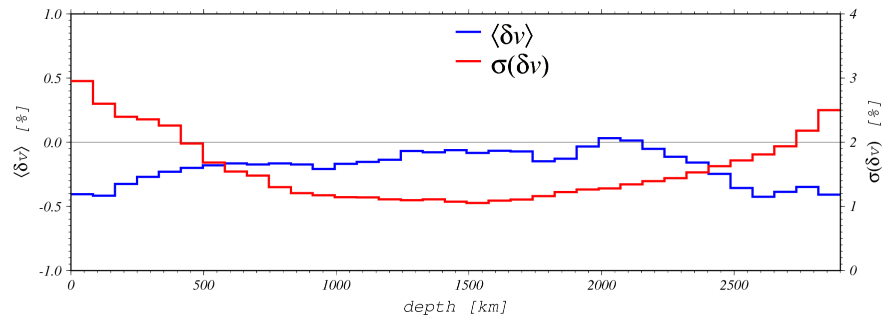

Damping and L curves

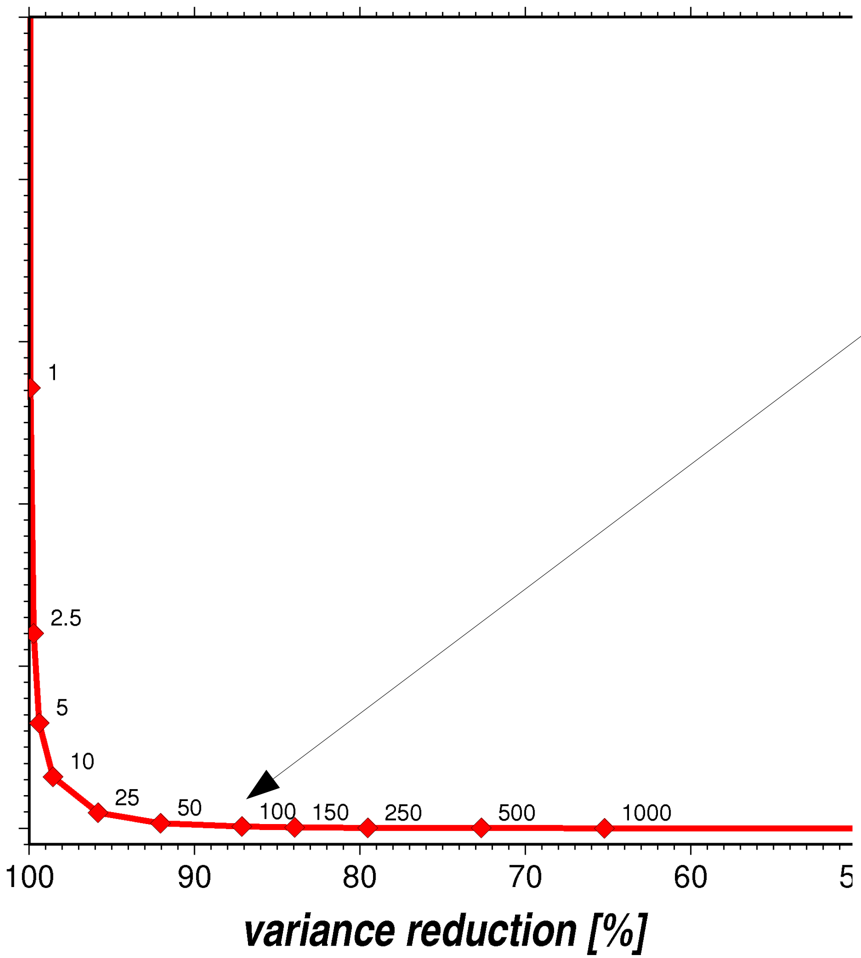

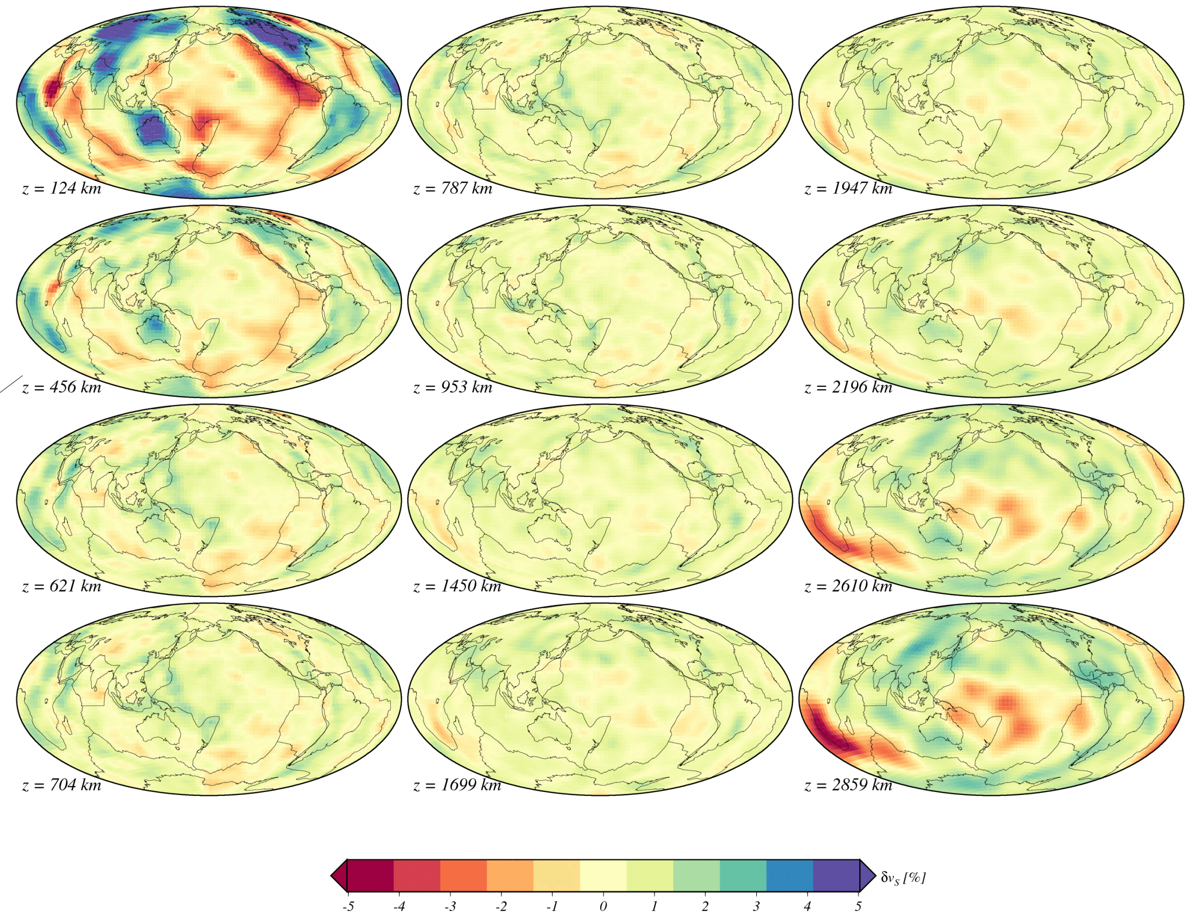

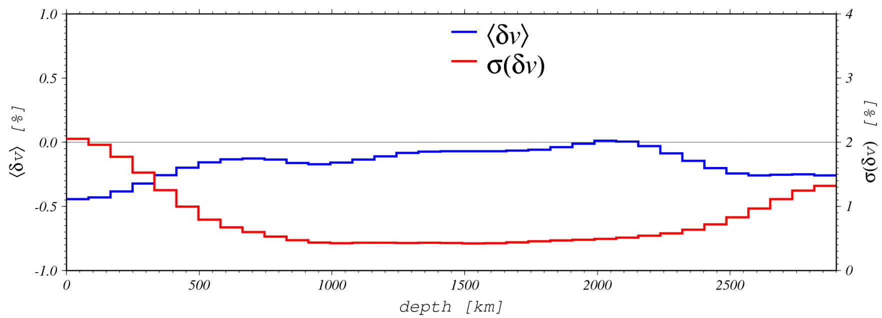

Damping and L curves

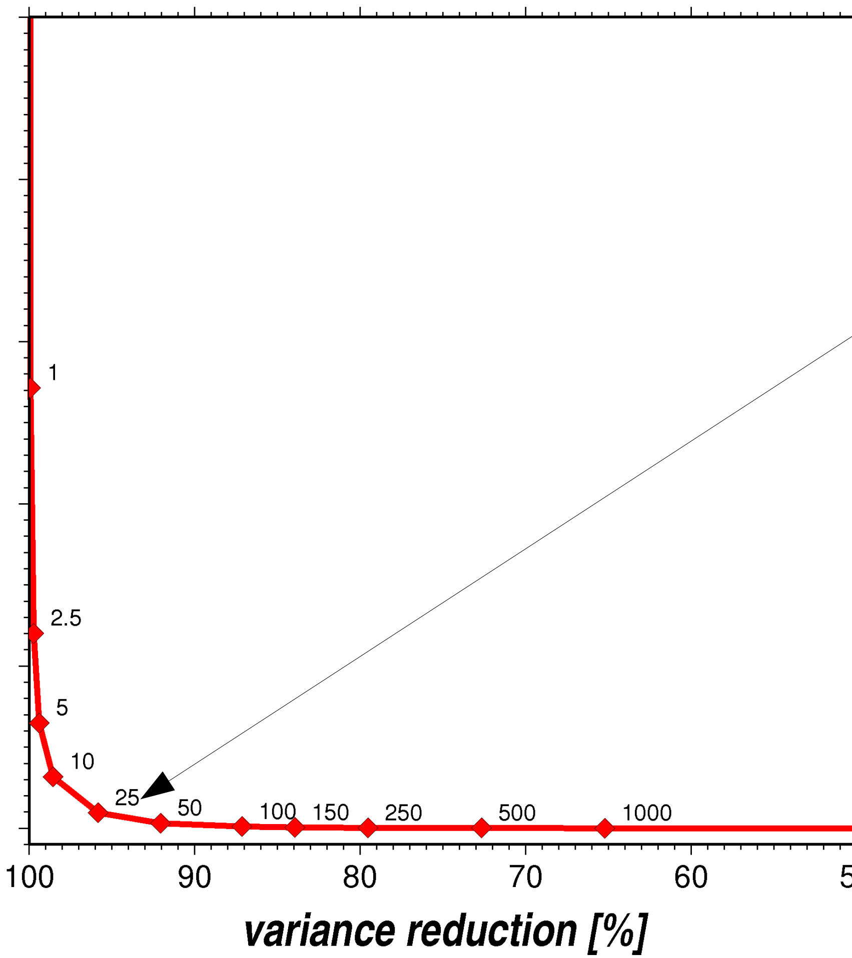

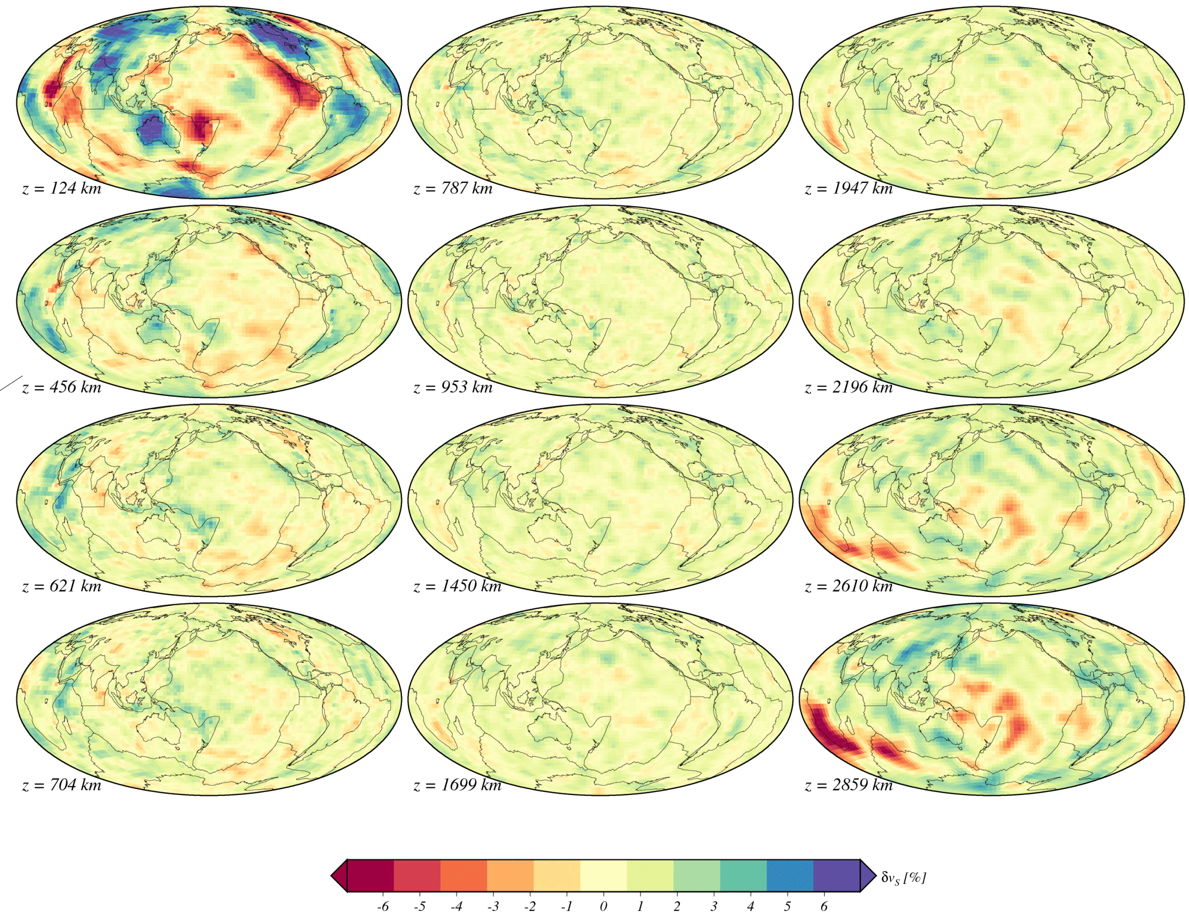

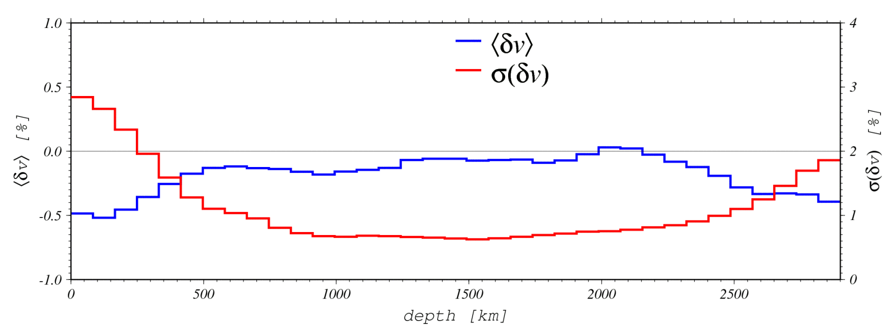

P wave tomography checkerboards

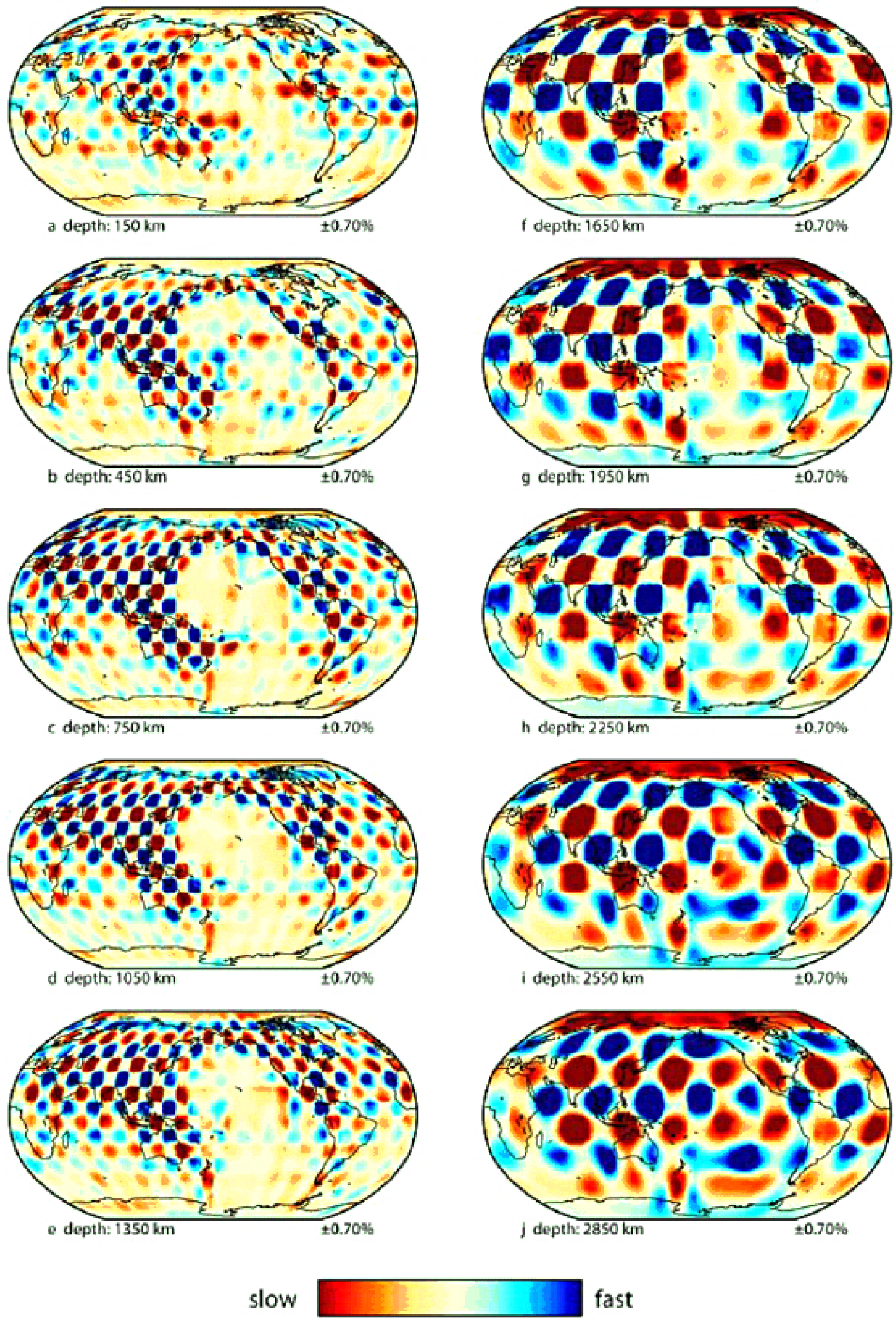

Figure 5. Recovery fields of global resolution tests, using harmonic input patterns with constant amplitude ±1.5% in wave speed throughout the mantle. (a–e) Half-wavelength of ~5° (spatial wavelength of ~550 km at the surface). (f–j) Half-wavelength of ~10° (~600 km at the CMB).

Li et al. (2008)

Cross-section tests

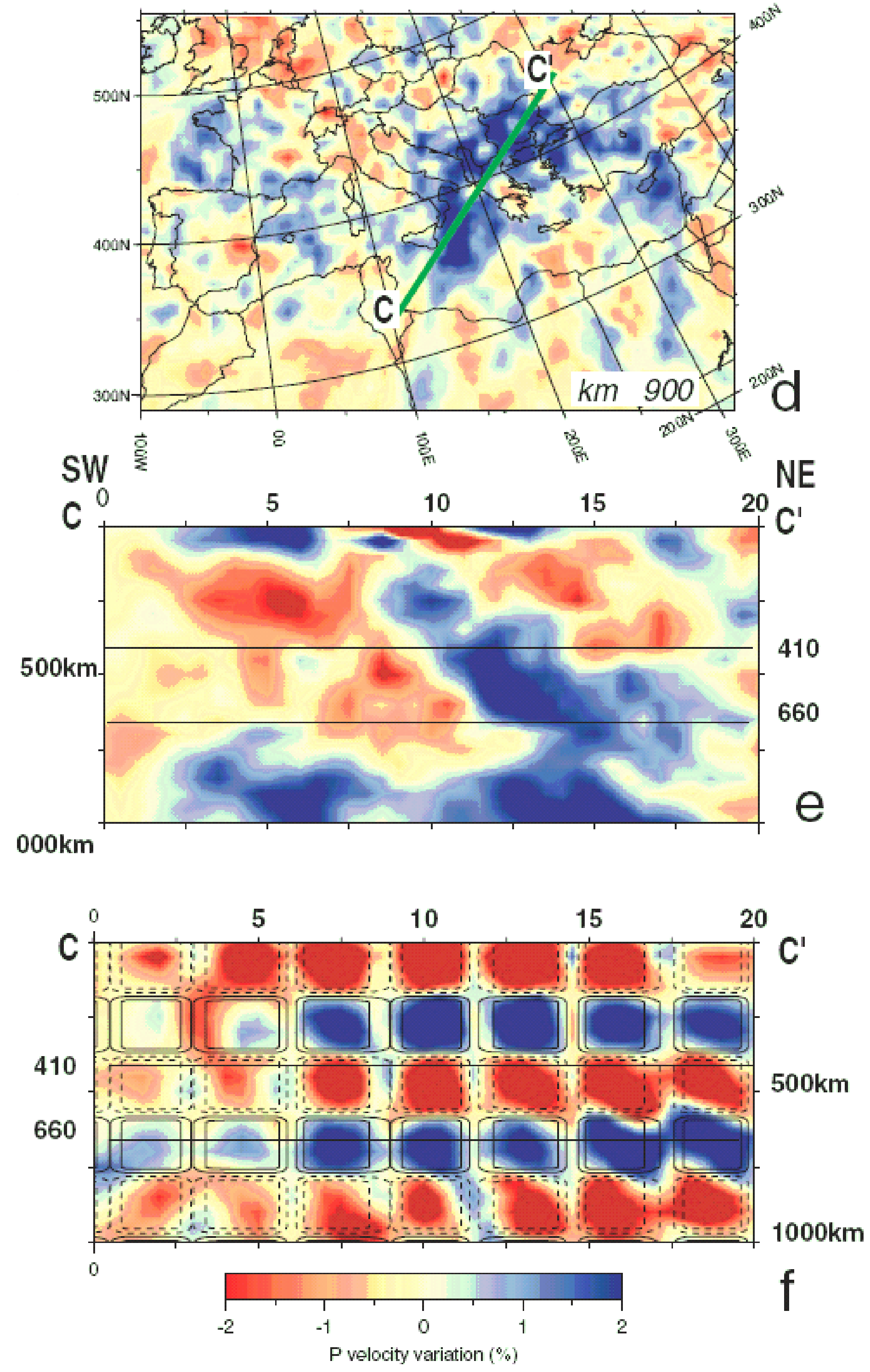

Faccenna et al. (2003)

Quantitative analysis: RMS power

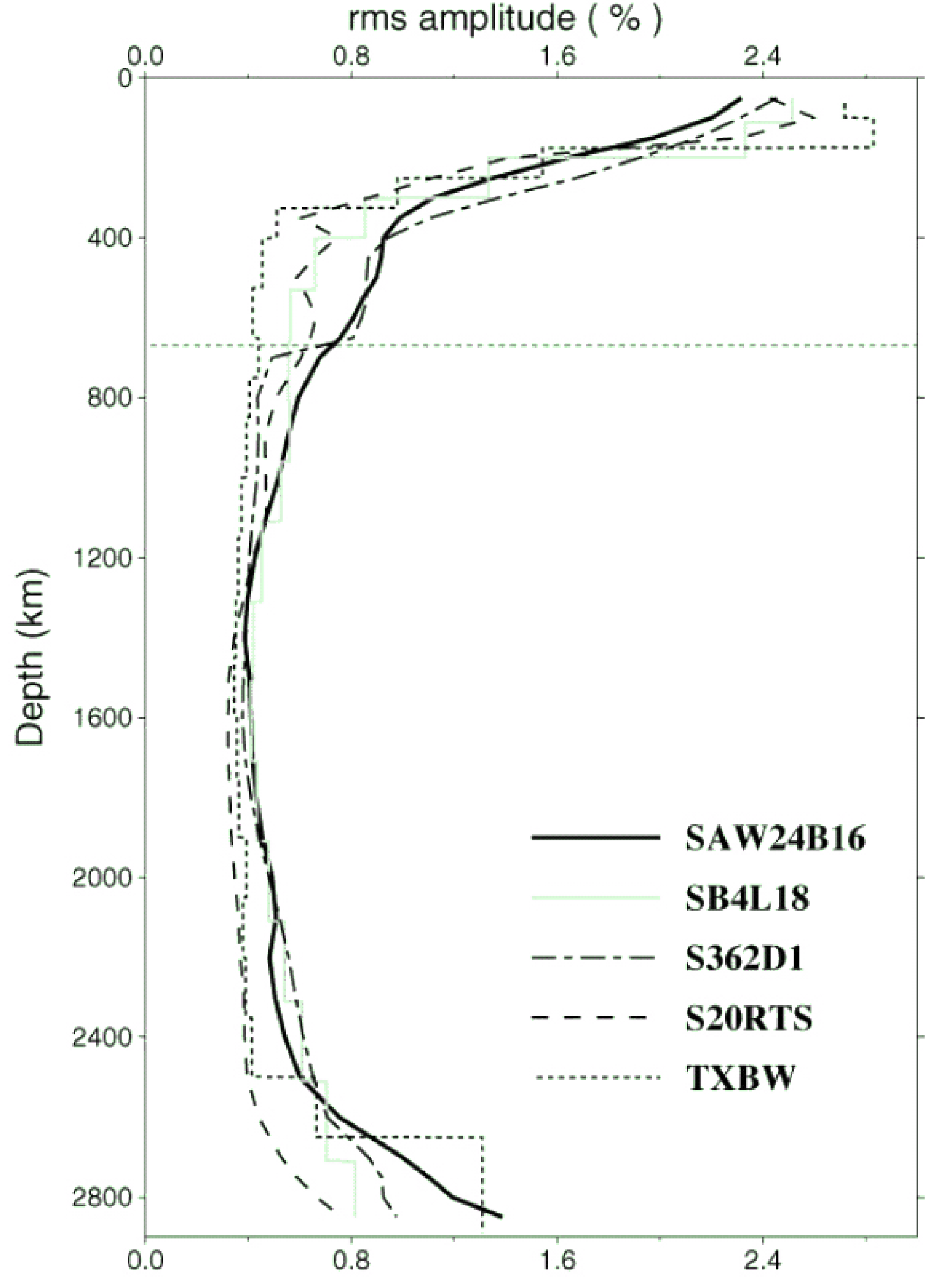

Spherical harmonics

Definition

$$\delta v(\theta,\ \phi) \approx \sum_{l=0}^{\ell_{\max}} \left[a_{\ell 0} X_{\ell 0}(\theta) + \sqrt{2} \sum_{m=1}^{\ell} X_{\ell m}(\theta) \times (a_{\ell m} \cos m\phi + b_{\ell m} \sin m\phi) \right]$$

Power per degree and unit area

$$\sigma_\ell^2 = \frac{1}{2\ell + 1} \sum_{m=0}^{\ell} (a_{\ell m}^2 + b_{\ell m}^2)$$

Correlation

$$r^\ell = \frac{\sum_{m=0}^{\ell} (a_{\ell m} c_{\ell m} + b_{\ell m} d_{\ell m})}{\sqrt{\sum_{m=0}^{\ell} (a_{\ell m}^2 + b_{\ell m}^2)} \sqrt{\sum_{m=0}^{\ell} (c_{\ell m}^2 + d_{\ell m}^2)}}$$

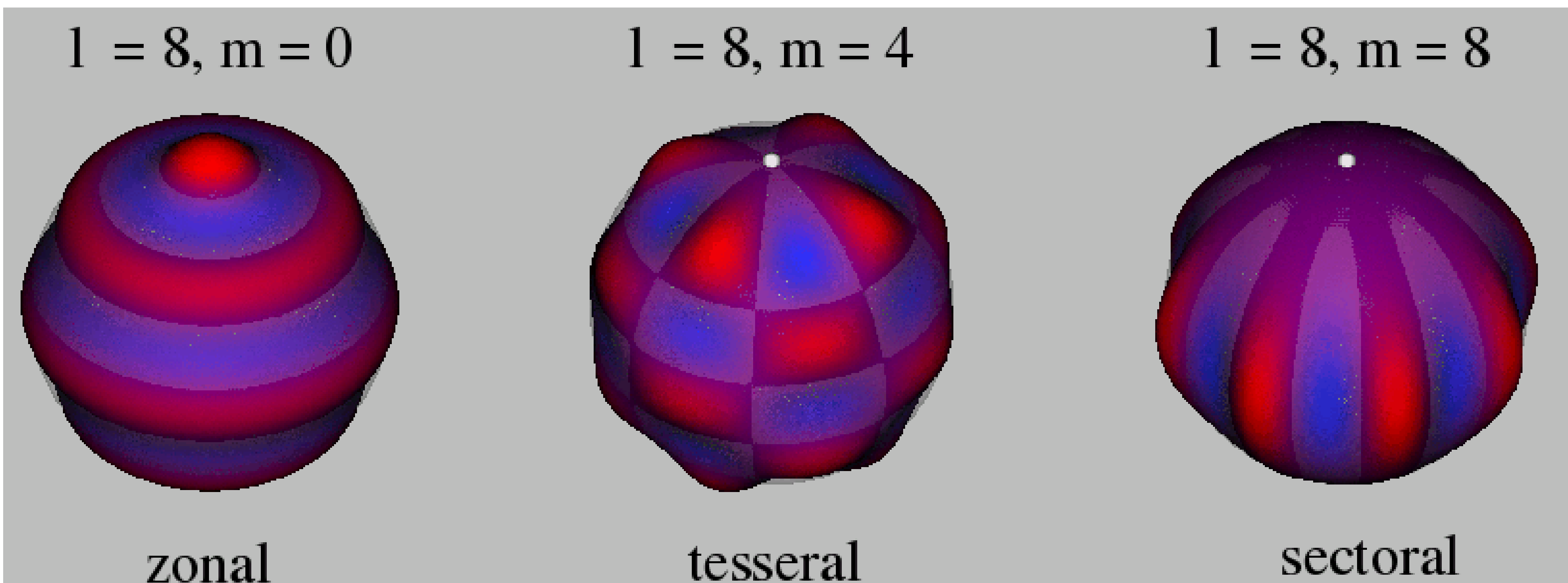

Spherical harmonics: tesseral wavelengths

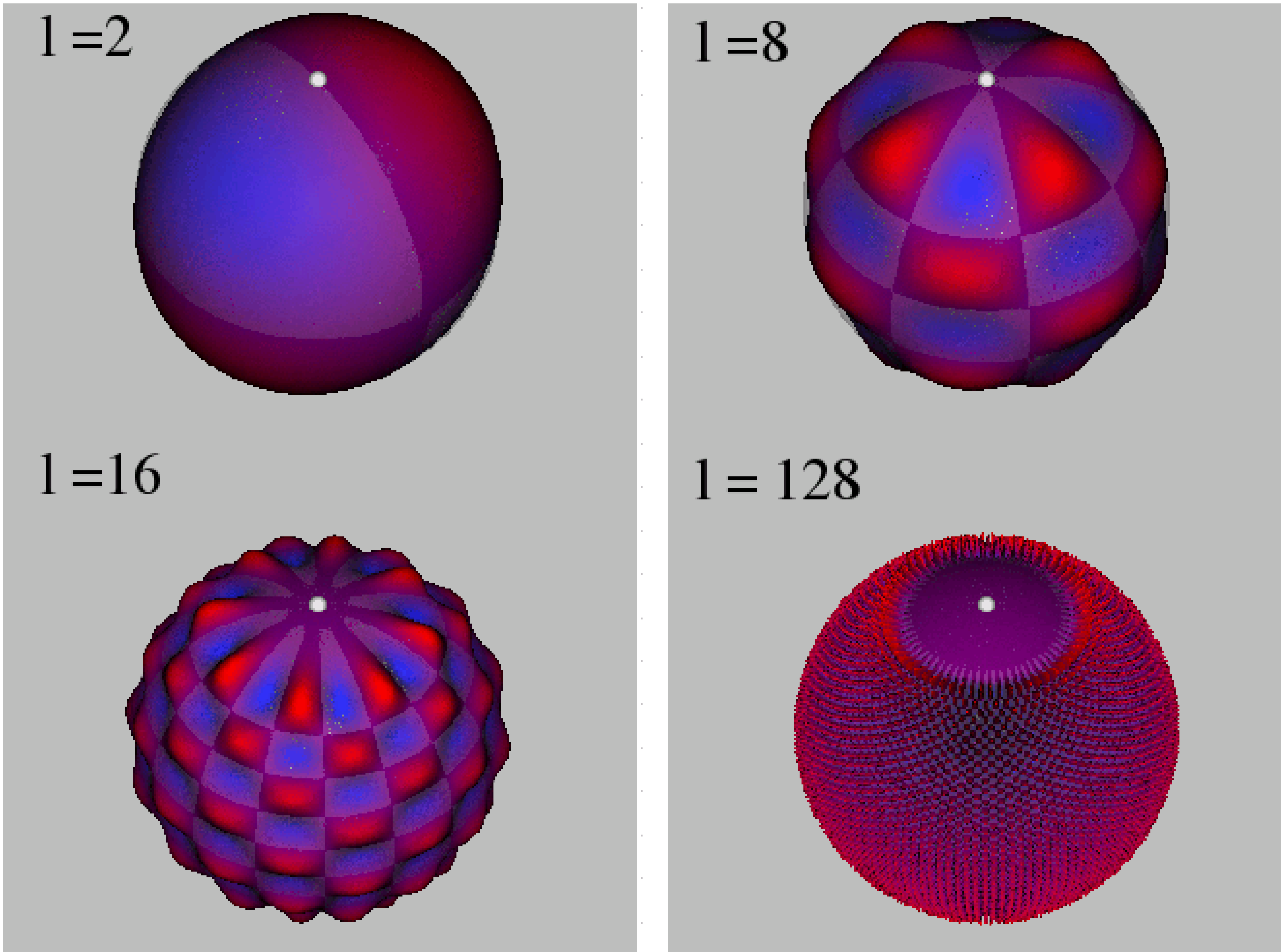

Power spectra

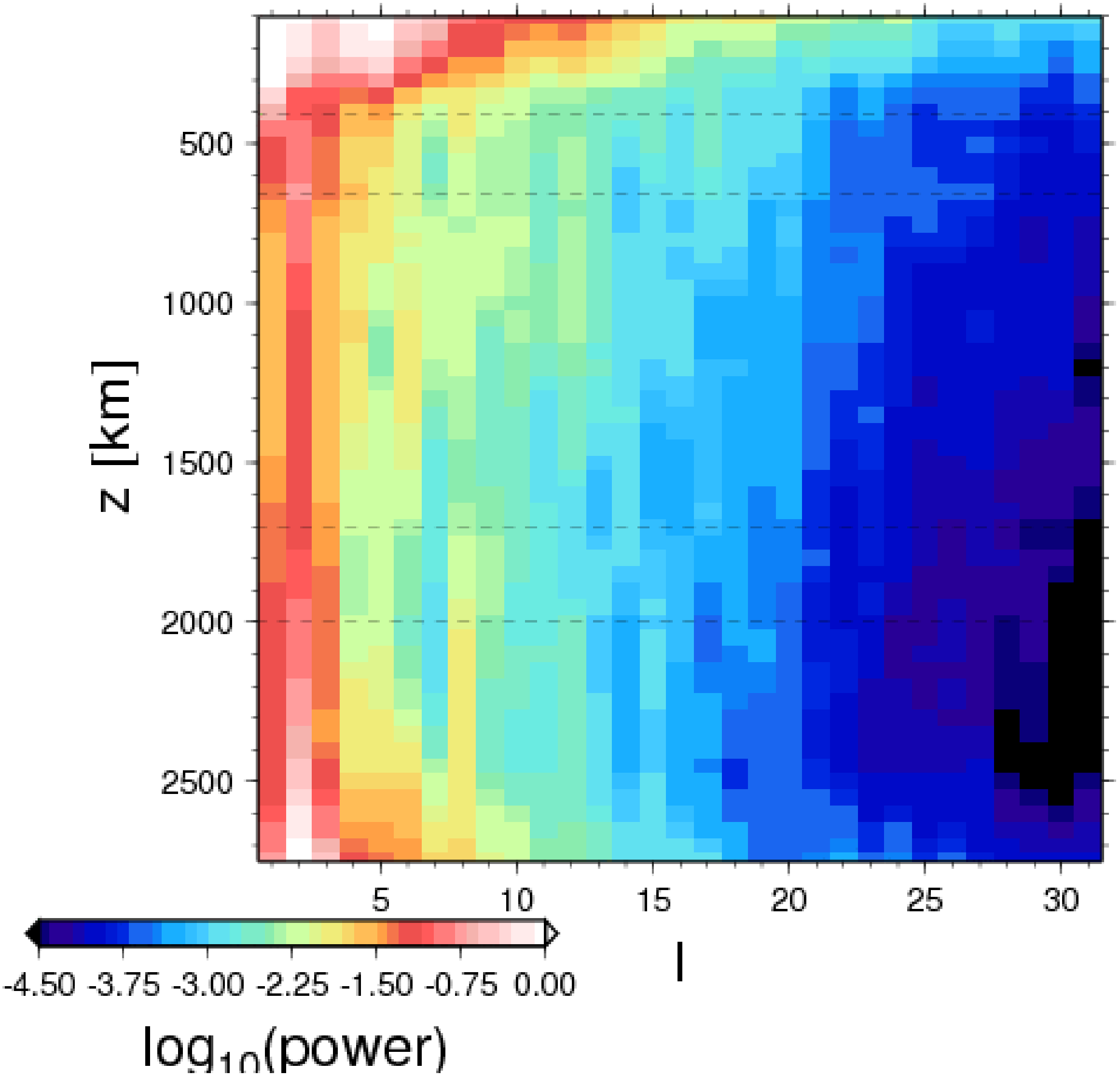

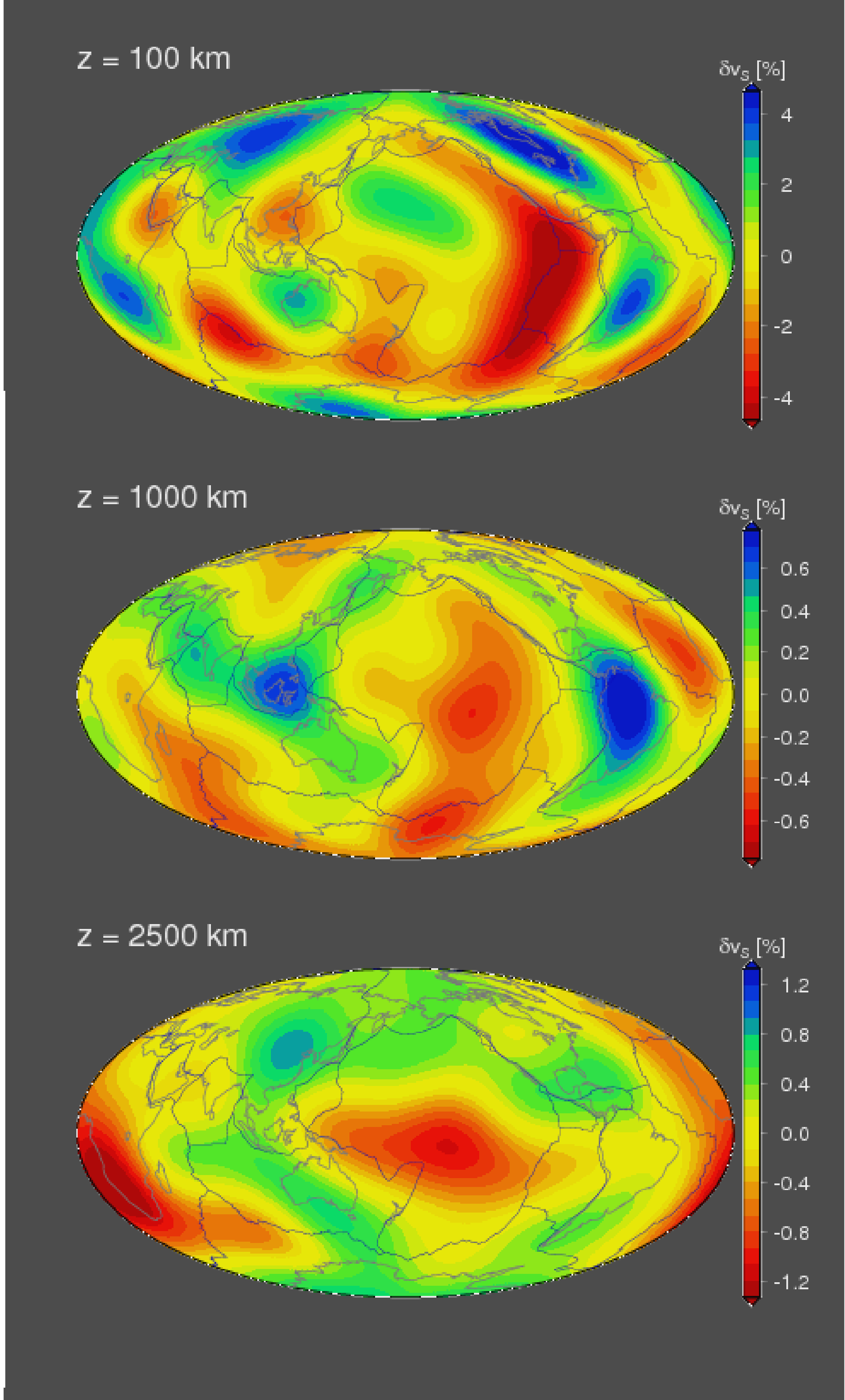

P-HVD
(ISC - P, pP,..)
(Boschi et al.)

P-(ISC P,pP,…)
(Karason et al.)

S-(S, surface
waves, modes)
(Ritsema et al.)

S- (S, Love,
Rayleigh)
(Gu et al.)

dyn-slablet
(Steinberger)

dyn-convection
(Zhong et al.)

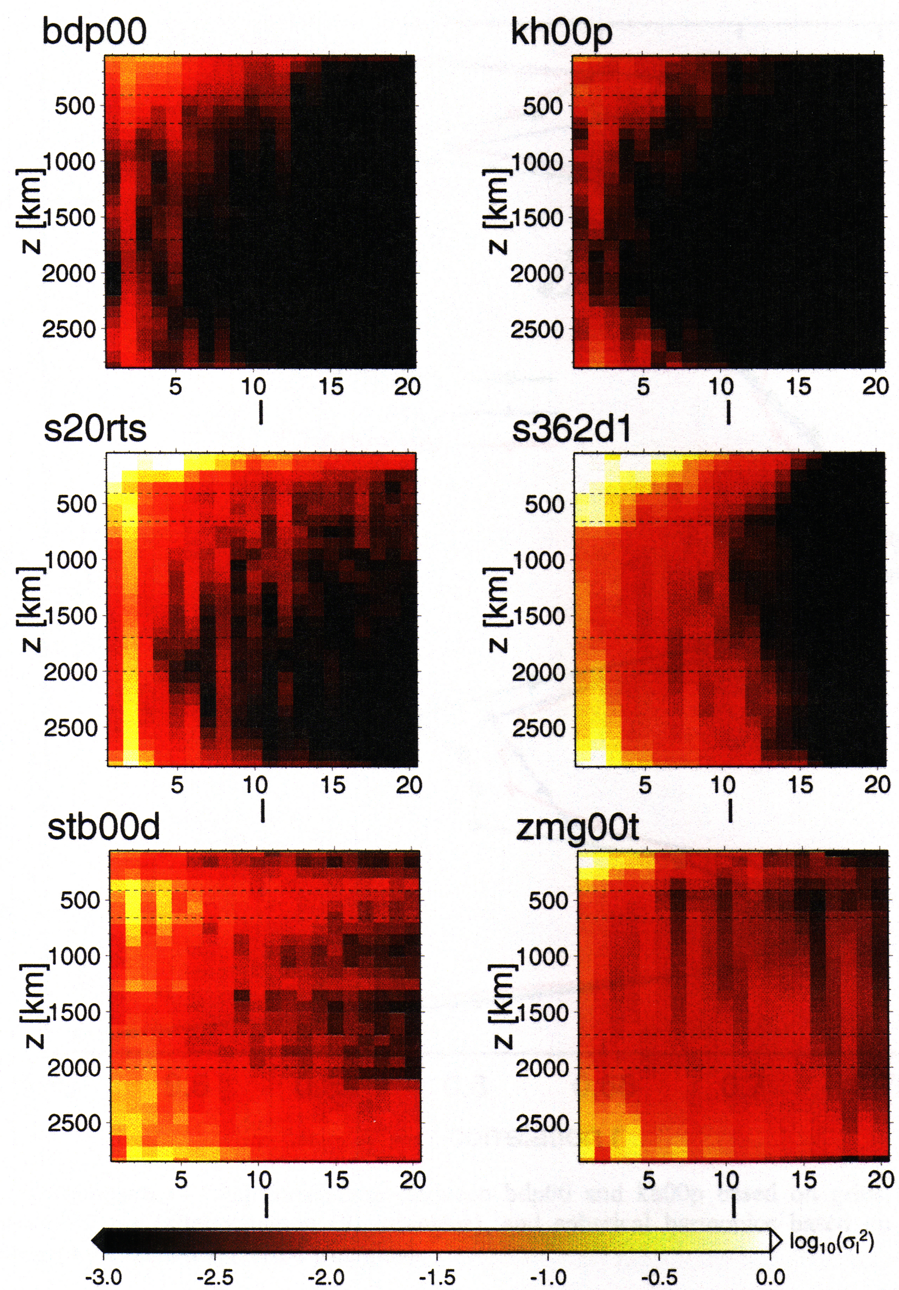

Figure C2. Absolute power per degree and unit area on a logarithmic scale, $\log_{10}(\sigma_\ell^2)$, for *P*, *S*, and geodynamic models (compare Figure 1 and additional online material).

Becker & Boschi (2002)